Viscoelasticity and Dynamics of Alignment in Side-Group Liquid Crystalline Polymers

Dissertation by

Susan Felicia Rubin

In Partial Fulfillment of the Requirements

for the Degree of

Doctor of Philosophy

California Institute of Technology

Division of Chemistry & Chemical Engineering

Pasadena, California

1996

(Defended June 10, 1996)

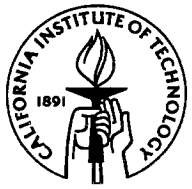

Dedicated to

my mother and father

for their love, constant support & encouragement

Acknowledgments

I would like to thank my advisor, Julie Kornfield, for her support; I hope to "inherit" some of her tenacity and drive as I embark on an independent career. I would like to thank the members of my candidacy/thesis committees – Professor Zhen-Gang Wang, Professor John Brady, Professor George Gavalas and Professor Jeff Hubbell. I am grateful for their helpful advice and suggestions in my pursuits of an academic career.

It has been a privilege to work with the fellow members of the Polymer Physics Group: R.M. Kannan, Geun-Cheng Chung, Barbara Arendt, Zhong-Ren Chen, Steve Paulin, Ramanan Krishnamoorti, Guru Kumaraswamy, and Weijun Zhou.

I am especially grateful that pursuing graduate studies at Caltech afforded me the opportunity to meet Vinay Gupta, my fiancé and co-worker. I look forward to the life we will share together.

One of the wonderful things about being at Caltech is the opportunity to work with some exceptionally talented – and exceptionally kind – individuals. In this spirit, I would like to thank Tom Dunn in the Chemistry Electronics Lab, who always answered my inane questions and helped kluge together all sorts of questionable-looking devices which always seemed to do the trick. I've always enjoyed my interactions with the fellows in the Chemistry and Mechanical Engineering shops – Ray Garcia, Tony Stark, Mike Roy, Guy Duremberg, Rodney Rojas, and John Van Deusen – for their kindness and understanding, and for taking my crazy designs seriously. I could never have graduated without the crisis-solving computer skills of Suresh Guptha. I would

also like to acknowledge Don Skelton for letting me so frequently borrow the Hall probe from the undergrad physics lab. I would also be remiss if I did not thank Kathy Bubash and Anne Hormann, and my good friends Lynn Russell, Sarah Ngola, Alison McCurdy, and Fay Peng for all their moral support.

I will forever be grateful for the constant support of my parents, Edward and Marcela Rubin, my sister, Brenda Rachel Rubin, and my grandmother, Martha M. Grace – for their guidance in my early years, and for their unwavering devotion and support. I thank my sister, Brenda, for providing much-needed comic relief. I look forward to seeing her succeed in college and follow her dreams.

I am especially grateful for the National Science Foundation for the Graduate Student Fellowship which supported me during my first three years in graduate school.

Abstract

Side-group liquid-crystalline polymers (SG-LCPs) consist of a flexible polymeric backbone and rigid mesogens (molecules forming LC phases), attached laterally to the backbone via flexible spacers. Since the dynamics of the mesogen field and polymeric backbone are partially decoupled, uniformly-aligned SG-LCP materials show promise in a variety of applications such as non-linear optical materials, optical data storage media, and stress sensors, which require switching of the mesogen orientation. Recent work has shown that uniform alignment of SG-LCP materials can be accomplished using flow-fields. However, the mechanisms of alignment, which are essential for the development of effective and rational processing strategies for the SG-LCP materials, remain poorly understood. To address this need, we focus on the viscoelastic properties of nematic and smectic SG-LCPs and the dynamics of field-induced alignment of SG-LCPs.

We have investigated the dynamic mechanical response of SG-LCPs having methacrylate backbone, hexamethylene spacer, and phenyl benzoate mesogens as a function of molecular weight in the isotropic, nematic, and smectic phases ($3 \times 10^5 \leq M_w \leq 3 \times 10^6$), and have discovered a unique molecular-weight dependence of the sensitivity of the dynamic modulus to nematic order of the melt. Nematic order produced a profound change in the dynamics of the entangled SG-LPCs relative to the isotropic phase; however, this effect was absent in the unentangled SG-LCPs. In SG-LCPs with smectic order, there was increase in the elastic character of the fluid with smectic ordering, but the incremental effect in a system that was entangled was relatively small. Oscillatory shear with large amplitude ($\gamma_o \geq 40\%$) induced macroscopic alignment in the nematic phase for all the SG-LCPs studied and could be used to alter the microstructure in the smectic liquid. Shearing the smectic phase produced a decrease in modulus, whereas shearing in the nematic phase followed by cooling into the smectic phase produced an increase in modulus.

To assess the effect of the coupling between the mesogen and the backbone on field-

induced orientation of nematic SG-LCPs, we have compared magnetically aligned and flow-aligned nematic SG-LCPs. Magnetic forces act primarily on the mesogens, and the backbone conformation changes to accommodate the torques on its pendant mesogens. In contrast, oscillatory shear can couple to the relaxation modes of both the director field and backbone. We have discovered that while the flow-aligned material exhibits distinct low-frequency relaxation dynamics, the relaxation of magnetically-aligned monodomains is indistinguishable from that of polydomain nematic melts. This suggests that flow alignment and magnetic alignment produce qualitatively distinct changes in the fluid miscostructure. We have further compared the processes of shear- and magnetic-alignment by monitoring the evolution of director orientation in nematic SG-LCP melts, *in-situ*, through visible transmittance (related to the liquid-crystalline domain size) and visible birefringence (related to the molecular orientation).

Contents

List of Figures

List of Tables

Chapter 1

Introduction

1.1 Liquid-Crystalline Polymers: Introduction

The chemistry and physics of polymers is an area at the frontiers of science and engineering. The ubiquitousness of polymers is brought about, to a great extent, by the capability to prepare highly oriented materials with useful mechanical, optical and electrical properties. In other words, the usefulness of polymers depends critically on our ability to orient the long polymer chains. Generally, this orientation is imposed through flow-processing of the polymer in its melt or liquid state, followed by subsequent solidification by cooling into a glassy or crystalline solid state. However, the natural tendency of the long flexible polymer chains to assume a statistical coil conformation and randomize their orientation often makes prolonged retention of the order in polymeric materials a challenge.

Polymer liquid crystals are a class of polymeric materials that optimize this orientation process, and thereby the material properties, by combining the self-ordering nature of the liquid-crystalline mesophase with the mechanical advantages associated with the macromolecular nature of the material [6–9]. In comparison to typical flexible polymeric chains, the macromolecules in liquid-crystalline polymers (LCPs) respond, strongly, not only to flow fields but also to electric and magnetic fields. To realize technological applications involving polymeric liquid crystals, an understanding of the processing–structure–property relations in these materials is essential.

1.2 Liquid-Crystals: A Self-Organizing System

The liquid crystalline (LC) state is a mesophase with a state of aggregation intermediate between an ordered crystalline solid (in which there is long-range orientational and positional order) and an amorphous liquid (in which positional and orientational correlations persist over a few molecular lengths) [10–13]. In liquid–crystalline systems, orientational order is always present, but only limited positional order exists. Formation of this mesophase requires the participating molecules to be rigid and geometrically anisotropic. Such *mesogenic* species may be discoidal, lath-like, cylindrical, etc. The ability of the molecules to aggregate in the LC state can be influenced by their concentration or the system temperature. Solvent effects induce ordering of *lyotropic* LCs, whereas *thermotropic* LCs undergo phase transitions due to changes in temperature. Thermotropic systems are the focus of the present work.

Above a certain temperature, the mesogens of thermotropic systems possess enough thermal energy to overcome the enthalpic driving force toward mesophasic order, and retain entropically-favored isotropy (Figure 1.1a). Below this transition temperature, many different liquid-crystalline phases are possible, depending on the chemical structure of the molecules involved. In the simplest LC phase, the *nematic* (Figure 1.1b), the orientation distribution of the mesogens is biased toward one direction, described by an apolar unit vector known as the *director*, $\mathbf{n}$.

The degree of alignment is characterized by the orientation distribution of the mesogens, $f(\theta)$, where θ is the angle between the director, $\mathbf{n}$, and the symmetry axis of a mesogen [12]. The strength of orientation of the mesogens is described using a

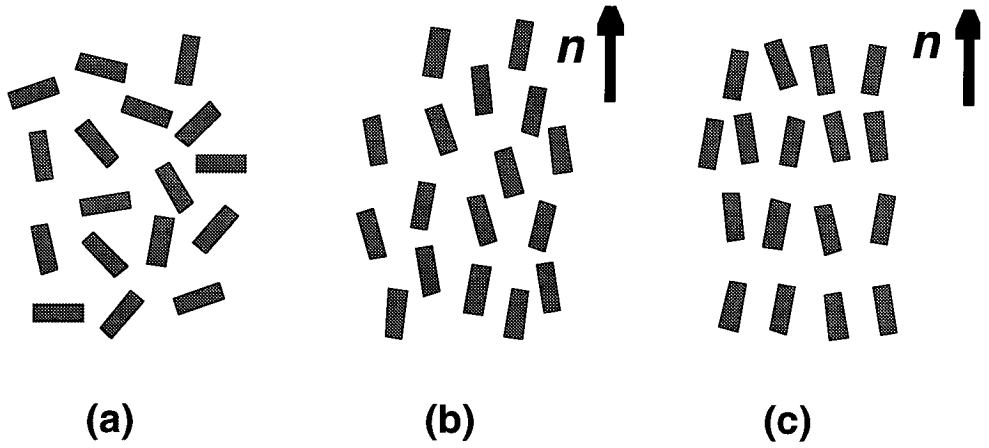

Figure 1.1: Schematic representations of the molecular arrangements in (a) isotropic, (b) nematic, and (c) smectic liquid–crystalline phases.

scalar order parameter

$$S = \frac{3\langle \cos^2 \theta \rangle - 1}{2}, \tag{1.1}$$

where the brackets denote an average over the mesogen orientation distribution.

$$\langle \cos^2 \theta \rangle = \int \cos^2 \theta f(\theta) \sin \theta d\theta. \tag{1.2}$$

S lies between 0 and 1, where 0 indicates an isotropic medium and 1 indicates perfect nematic order. In general, due to thermal fluctuations, the mesogens are only on average oriented along the director and S is less than 1.

The *cholesteric* phase is equivalent to a nematic that has been twisted periodically about an axis perpendicular to the director. This liquid-crystalline phase is possible only when the mesogens have a chiral structure.

The *smectic* phase (Figure 1.1c) resembles the nematic, except that the ends of the mesogens segregate into common planes, and the fluid forms a layered structure. A

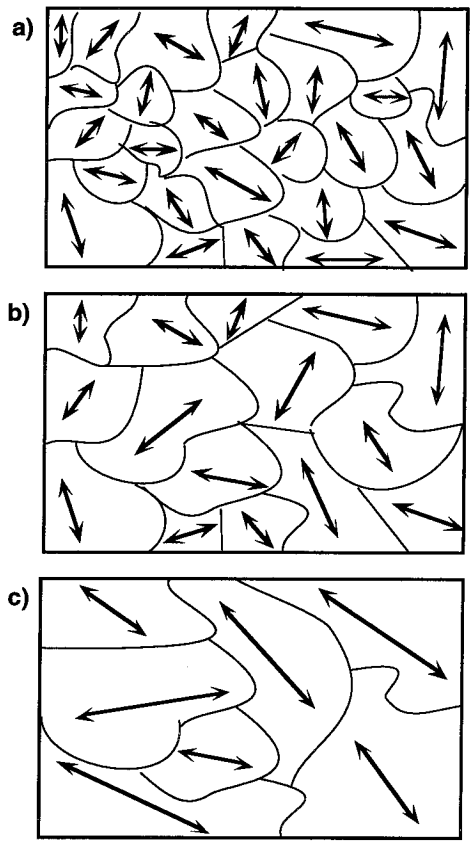

Figure 1.2: Macroscopic nematic ordering from a polydomain [(a)] towards a more aligned state [(b)-(c)] under the action of an external field. Each arrow corresponds to a local director and is drawn as an apolar vector.

common example of a lyotropic smectic system is found in the lipid bilayers forming cell membranes. Several variants of the smectic mesophase exist. The director is oriented perpendicular to the layers in the *smectic-A* phase, whereas it is tilted with respect to these planes in the *smectic-C* phase. Two-dozen additional classes and subclasses of smectic LC phases have been identified [14].

In lyotropic systems (surfactant systems, etc.) other more exotic mesophases, such as hexagonal and "blue" phases are found. Since the focus of this work is thermotropic nematic and smectic systems, the details of these more unusual structures will not be presented here.

In the absence of an external aligning field or surface effects, LC systems exist as textured materials (Figure 1.2a) in which the orientation of the local director meanders throughout the sample. A region in which the orientation is uniform is called a *domain*. Under the action of an external field a few domains grow at the expense of others (Figures 1.2b & 1.2c) and the material exhibits increasing degree of alignment on macroscopic scales. Since the mesogens possess anisotropic electric or magnetic susceptibility, macroscopic alignment can be induced under the action of an external field, such as external electric or magnetic fields. Surface effects, such as from substrates with a variety of physico-chemical treatments (e.g., surfactant or polymer coating followed by rubbing) can also induce substantial global ordering in LC thin films [10, 15].

1.3 Molecular Architecture and Applications of LCPs

1.3.1 Main-Chain and Side-Group LCPs

By covalently linking mesogens to polymeric strands, one can expand the usefulness of liquid crystals in engineering applications by combining the self-organizing, optical and field-responsive properties of liquid-crystalline systems with desirable mechanical properties of polymeric materials [6, 8, 9]. The resulting macromolecules, termed liquid crystalline polymers may offer many advantages over small-molecule liquid crystals. In particular, if an aligned LCP material is rapidly quenched below its glass

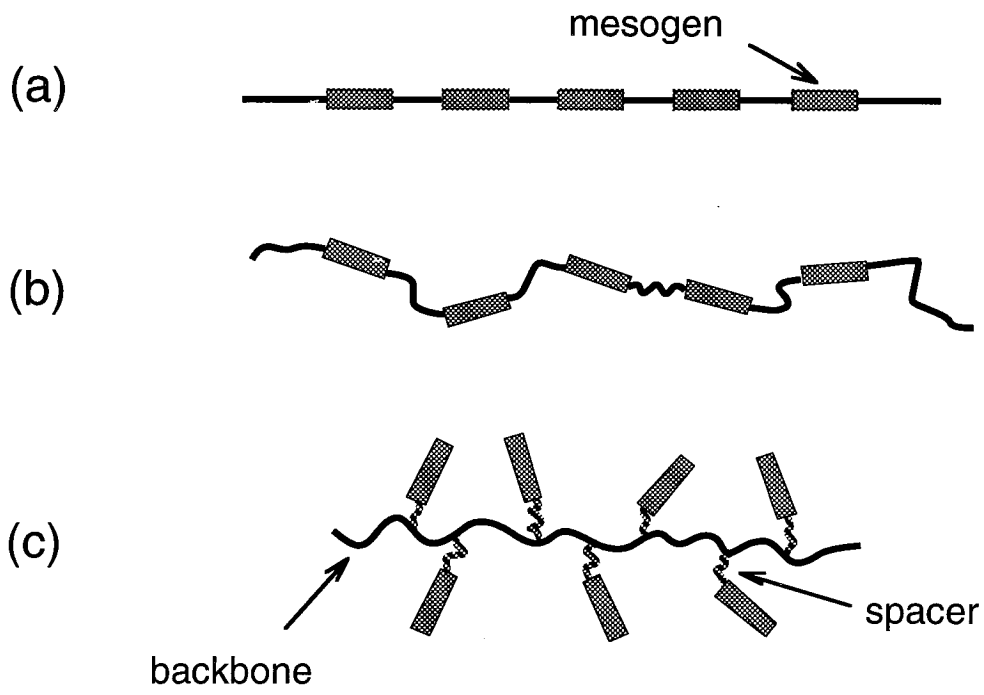

Figure 1.3: Schematic representations of (a) rigid-rod LCP, (b) main-chain LCP, and (c) side-group LCP molecular architectures.

transition temperature, macroscopic order may be preserved in the solid state.

A wide array of LCP molecular architectures are possible. Rigid-rod polymers, such as the polyglutamate and the DuPont aramid Kevlar^{TM}, consist solely of covalently-bonded mesogenic groups with no flexibility along the length of the molecule (Figure 1.3a). When mesomorphic Kevlar^{TM} polymer solutions are spun into a fiber, the pre-existent molecular alignment in the nematic domains encourages a high degree of molecular orientation during spinning, thus leading to the formation of ultra high strength fibers. Thermotropic mesophase transformations in polymeric systems can be evidenced only when the temperature at which they melt is lower than that at which they decompose. Whereas the relatively small entropy gain accompanying the melting process of extended rigid structures leads to relatively high melting

points, a thermally stable mesophase may be obtained by modifying the molecular architecture by incorporating mesogens into a flexible polymer backbone. An example of such a *main-chain LCP* is the melt-processable Hoechst-Celanese Vectra^{TM} polyester copolymer, in which polymer spacers of varying degrees of flexibility link the rigid subunits (Figure 1.3b). Like their rigid-rod counterparts, main-chain LCPs are particularly well-suited for materials in which a high tensile strength is desired, since nematic ordering of the mesogens facilitates the extensional alignment of the polymer that can be achieved through processing flows. However, in applications where it is desirable to switch the orientation of the mesogens (see below), such macromolecules are ill-suited, since re-orientation of the mesogens requires distortion of the entire polymer backbone.

To circumvent this problem, Finkelmann, Ringsdorf, and co-workers in 1978 [16, 17] suggested attaching mesogens as pendant groups to a flexible "backbone" using a short spacer chain (often a methylene or siloxane oligomer). In such macromolecules, termed *side-group liquid-crystalline polymers* (Figure 1.3c), the dynamics of the mesogens are partially decoupled from those of the backbone, thus allowing for more facile mesogen reorientation.

1.3.2 Applications of SG-LCP Materials

Since SG-LCPs were first synthesized in 1978, researchers in both industry [7, 18, 19] and academia [6–9] have been intrigued by the potential scope of applications for these novel materials, which potentially combine the functionality of conventional

LCs with the properties of macromolecules. Although most studies of SG-LCPs to date have focused on their synthesis and phase behavior, various attempts to exploit the structural and electro-thermo-optical properties of these unique materials have shown promise for a wide variety of technological applications.

The combination of polymeric and liquid-crystalline attributes allows SG-LCPs to function as effective compatibilizers for preventing phase separation in mixtures of conventional, flexible polymers with low molar-mass liquid-crystals [20]. Similarly, SG-LCPs can stabilize the interfacial boundaries of LC droplets suspended in solid polymeric matrices in the commonly-used polymer-dispersed liquid-crystal displays [21].

SG-LCPs have also found limited applicatons to various specialized separations technologies. Fused silica beads coated with a polysiloxane SG-LCPs exhibit excellent efficiency, polarity, and selectivity as gas-chromatography stationary phases [22]. Using electric fields to modulate the degree of macroscopic alignment of the mesophasic textured SG-LCP film, one can control the permeability over a 28-fold range to form membranes with an electrically-tunable permeability [23]. Such membranes have proven effective for the controlled permeation of gases and simple drugs [24, 25]. In a related application, smectic SG-LCPs have been proposed for use in capacitive chemical sensors [26].

Liquid crystals have long been used in electro-optic display devices. Although the high viscosity of polymeric LC systems makes SG-LCPs a somewhat impractical alternative to low molar-mass LCs in such applications, Langmuir-Blodgett films of

azobenzene SG-LCPs have proved effective as photo-switchable command layers in liquid-crystal displays [27–29].

Perhaps the most promising arena in which SG-LCPs may be utilized is in optical data storage media. Many of the proposed optical data storage applications of SG-LCPs [7, 30, 31] rely on a variant of the following technique for information recording: a laser heats a small ($\sim 10\mu$m across) spot of a magnetically- or electrically-aligned SG-LCP, allowing the chosen region to become isotropic. Upon cooling through the glass–transition, the vitrified defect–ridden spot appears opaque against the transparent "monodomain" background. This information can be erased by reheating the spot in the presence of an external aligning field. Using this technique, SG-LCPs may be used to produce a variety of erasable optical media storage devices, such as compact discs.

Alternative schemes for SG-LCP electro-optic displays [32, 33] employ smectic materials containing azobenzene mesogens or doped with trace amounts of dichroic light-sensitive azo dyes. When impinged upon with polarized UV laser light, the azobenzene chromophores cis-trans photoisomerize, thus altering the birefringence of the medium. Applying this holographic digital data recording technique to an SG-LCP polyester film, resolutions of over 5000 lines/mm and diffraction efficiencies of about 40% have been achieved. Data-storage lifetimes exceed 30 months, and the film may be erased (through heating) and re-written many times without loss of performance. Other similar schemes, detailed in a review article by Attard [30], have been devised to make WORM (write once, read many times) archival data storage media,

including three-dimensional holographic images, and non–linear optical devices.

A large percentage of the proposed applications to display technologies and optical data storage applications require pre-alignment of a mesophasic SG-LCP monodomain. Therefore, to realize these data recording schemes, uniformly-aligned SG-LCP materials must be produced. Surface effects may be used to impart global order to SG-LCP nematics of up to 10μm in thickness (see chapter by Noel in [7]). However, the resulting thin films are fragile and not thick enough for three-dimensional holographic optical data storage. Furthermore, surface-mediated macroscopic orientation often requires annealing several hours at a temperature just below the mesophasic-isotropic transition temperature [34]. High electrical or magnetic fields have been successful in inducing bulk orientation to systems of small–molecule LCs. However, the high viscosity of SG-LCPs frustrates the ability of strong external fields to macroscopically align mesogens, thus rendering such techniques prohibitively expensive and time-consuming for most commercial applications.

Fortunately, the polymeric nature of SG-LCPs can provide alternative means of achieving alignment. In particular, flow has been shown effective in aligning certain anisotropic macromolecular materials, such as main-chain LCPs. Until recently it was believed that flow could not be used to align SG-LCPs [35]. Recent results [36] have demonstrated that this is, indeed, possible and that large amplitude oscillatory shear can macroscopically align SG-LCP materials. One practical motivation for this work was to determine the extent to which flow can be used to macroscopically align SG-LCPs. In a broader sense, it is necessary to understand the rheological

behavior of SG-LCPs in order to devise intelligent processing strategies for these novel and promising materials. To provide context for understanding the dynamics of alignment of SG-LCPs, a portion of this study was devoted to understanding the linear viscoelastic response of SG-LCP melts. Building on that understanding, our goals were to elucidate the dynamics during flow-induced alignment and to compare the physics of flow-alignment to magnetic alignment. The techniques employed in our experiments are summarized in Chapter 2, and the linear viscoelastic properties of nematic and smectic SG-LCPs are discussed in Chapter 3. Chapters 4 & 5 are devoted to a discussion of alignment of SG-LCPs using large-amplitude oscillatory shear and high magnetic fields.

Chapter 2

Experimental Methods: Characterization and Alignment of SG-LCPs

2.1 Introduction

Although the large variety of properties of polymeric materials, and indeed of all materials, are ultimately rooted in the details of the local chemical structure, the polymeric nature and/or the topological organization of the macromolecules is directly responsible for many distinct and unique properties of polymeric materials. For example, properties such as rubber elasticity can be successfully studied both in theory and experiment in a unified way, *i.e.* independent of specific chemistry. Many fabrication processes rely on this idea and manipulate the way in which polymer molecules organize themselves into specific microstructures. Generally, these processes involve flow-processing of polymeric melts. Successful design of these processes requires a fundamental understanding of the relationships between the relaxation dynamics within a polymeric material (at both molecular and microstructural levels) and the bulk properties of the polymer. Typically, the relaxation dynamics in polymer melts are characterized by applying a sufficiently small deformation (*i.e.*, one that does not perturb the fluid microstructure) and measuring the viscoelastic stress response.

Such characterization is, indeed, essential for realization of the potential applications of side-group liquid-crystalline polymers. Since the mesophasic nature of the polymer introduces multiple levels of molecular and macroscopic structure in SG-LCP systems, viscoelastic characterization can reveal rich rheological behavior. To characterize and understand the stress-relaxation behavior of SG-LCPs and to elucidate the molecular and microstructural processes during their macroscopic alignment, we have

employed a variety of techniques. The following sections provide a brief discussion of (a) the mechanical properties of SG-LCPs, their relevance to characterization of the relaxation dynamics and the experimental tools used to measure them, (b) the optical properties of SG-LCPs, their use in characterizing the microstructure during macroscopic alignment of SG-LCPs, and (c) the experimental apparatuses used during shear-alignment and magnetic alignment.

2.2 Characterization of Relaxation Dynamics in SG-LCP Polymers

2.2.1 Rheology: A Background

Characterization of the mechanical properties of materials is done through measurement of the stress-strain behavior of the material. Typically the stress response to shear, extension, and/or bulk deformation is measured [37]. This response is either elastic or viscous or a combination of a viscous and an elastic response.

When a Hookean elastic solid is subjected to strain, the stress response (σ) is proportional to the strain and independent of the rate of strain. The constant of proportionality is either the elastic modulus E (for normal strain) or the shear modulus, G (for shear strain). In contrast, for a Newtonian viscous liquid, the stress is proportional to the rate of strain (at low rates of strain) and independent of the strain. The constant of proportionality is the viscosity of the liquid.

For viscoelastic materials, such as polymer melts, the stress has both viscous and

elastic components. At low temperatures and high rates of strain polymers display an elastic behavior whereas at high temperatures and low rates of strain they behave in a viscous manner. The exact nature of the time dependence of the mechanical properties of a polymer depends on the type of stress (creep testing) or strain cycle (stress relaxation) used. Since the work done in this dissertation is exclusively on the effects of shear flow, the discussion in this section focuses exclusively on shear stress-relaxation.

Under sufficiently small shear strains, a linear viscoelastic model can be used to describe the time-dependent stress response of a polymer, $\sigma(t)$. For a constant strain γ_o imposed at $t = 0$,

$$\sigma(t) = G(t)\gamma_o \tag{2.1}$$

where $G(t)$ is called the shear stress relaxation modulus. Deformation of a polymer melt distorts the conformation of the polymer chains, and recovery from these distortions is accompanied by a stress-relaxation response which varies in its behavior over the many different lengthscales inherent in polymeric fluids (*i.e.*,, from the segmental level to the level of the entire polymeric chain). This complex response is reflected in the form of the stress relaxation function $G(t)$.

For nearly monodisperse linear polymer melts, the function $G(t)$ consists of four regions: the glassy region, the transition zone, the rubbery plateau, and the terminal region (Figure 2.1a). On very short time scales, the response of the polymer chains to a deformation is glassy, and is characterized by a high modulus (typically 10^{11} dyn/cm^2). $G(t)$ then falls rapidly as the chains relax locally, and then over progres-

sivly longer chain distances. For chains that are sufficiently short, the relaxation process then procedes smoothly toward completion ($G(t) = 0$). When the chains are so long that they must disentangle from one another before conformational relaxation is complete, the relaxation rate is slowed down, and is manifested by a modulus that remains relatively flat in what is known as an entanglement (or "rubbery") plateau.

The complete relaxation curve or the viscoelastic spectrum can be measured using an oscillatory (e.g., sinusoidal) shear strain. Under the linear viscoelastic assumption, the shear stress can be described as being proportional to the shear strain but with a phase lag.

$$\gamma(t) = \gamma_o \sin \omega t \tag{2.2}$$

$$\sigma(t) = \sigma_o \sin(\omega t + \delta) \tag{2.3}$$

$$= \gamma_o [G'(\omega) \sin \omega t + G''(\omega) \cos \omega t] \tag{2.4}$$

The term $G'(\omega)$ is the *dynamic rigidity* or *storage modulus*, because, like the modulus of an elastic solid, it is an indication of how much energy is stored and recovered over each successive cycle of strain. Similarly, $G''(\omega)$, the factor accompanying the portion of the stress response that is proportional to the rate of strain, is termed the *loss modulus*, because it is related to the amount of energy dissipated over each cycle of strain. The complex sum $G^*(\omega) = G' + iG''$ is referred to as the *dynamic modulus*, and is related to the shear stress relaxation modulus by:

$$G'(\omega) = \omega \int_0^\infty G(t) \sin \omega t \, dt \tag{2.5}$$

$$G''(\omega) = \omega \int_0^\infty G(t) \cos \omega t \; dt. \tag{2.6}$$

As shown above, the stress response of macromolecular fluids is frequency-dependent; *i.e.*, the response depends on the timescale of molecular relaxation relative to that of the deformation. Typically, polymeric melts display storage and loss moduli similar to those sketched in Figure 2.1b. Deformations applied with a rapid characteristic frequency will lead to a glassy-like response characterized by a high modulus plateau (Figure 2.1b). Very slow deformations will allow the molecular conformations of the polymer coils to relax before the fluid is "aware" of the deformation, and the response will be liquid-like, as shown in the terminal regime of the viscoelastic spectrum (at long times in Figure 2.1a or at low frequencies in Figure 2.1b).

For polymer chains that are sufficiently short, the viscoelastic spectrum will be comprised almost entirely by the glassy-like and liquid-like (terminal) regimes alluded to above. However, once the chains become long enough that they become topologically entangled in one another, an intermediate regime, known as the viscoelastic plateau (Figure 2.1a) begins to emerge. The breadth of entanglement plateau is related to the number of entanglements the average chain experiences (and hence is an increasing function of molecular weight). The height of the entanglement plateau in either the storage modulus or the relaxation modulus is $G_N^\circ \sim \rho RT/M_e$, where ρ is the density, R is the gas constant, T is temperature, and M_e is the average molecular weight of the length of polymer strand between entanglements.

The complete relaxation spectrum, from the glassy state (short-time response) to

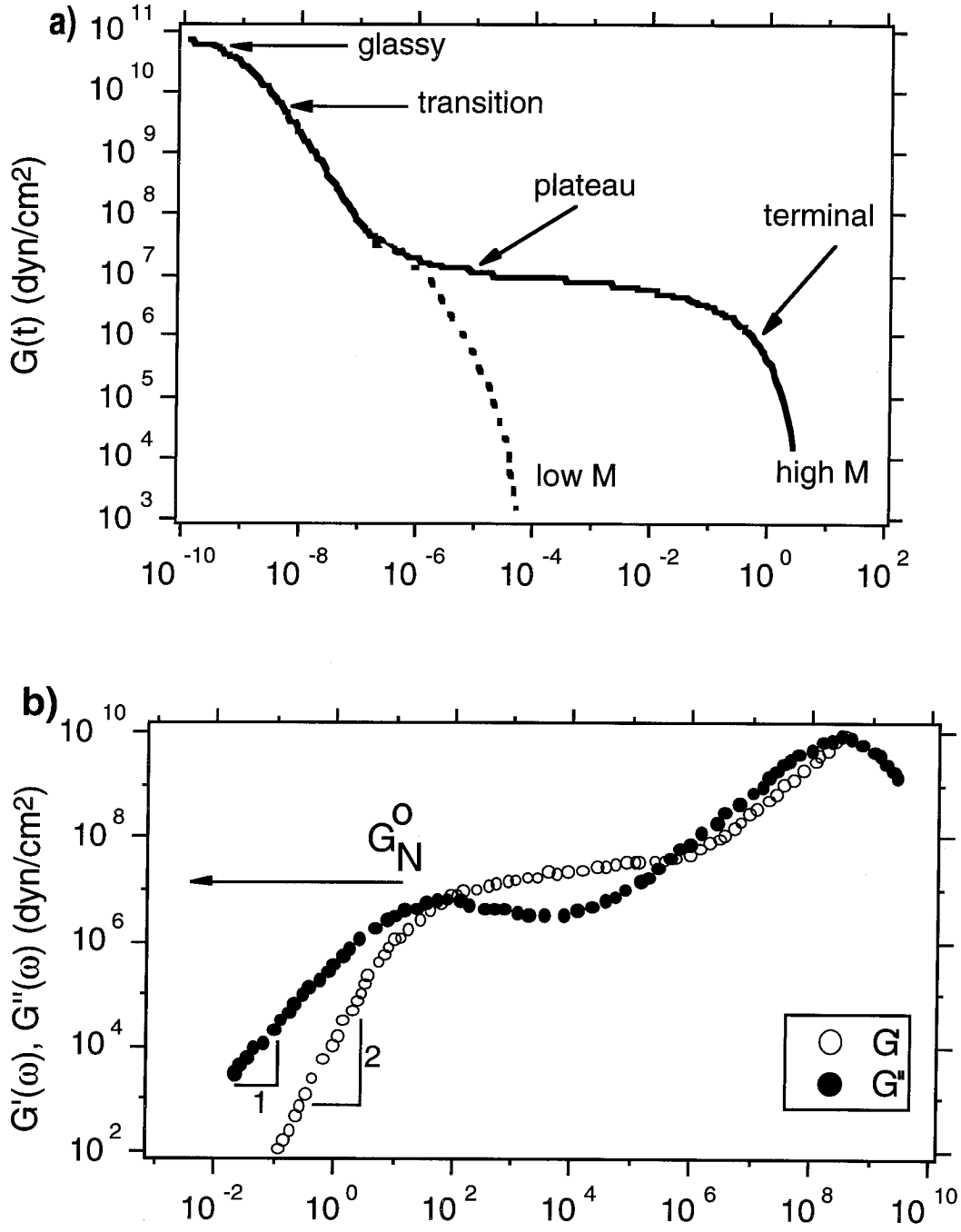

Figure 2.1: Shear stress relaxation for a typical polymer melt plotted as (a) dynamic modulus G(t) as a function of time (b) dynamic moduli $G^*(\omega)$ against frequency.

the terminal regime (long-time response), of a polymer melt typically encompasses many orders of magnitude in time (or frequency). However, no single experiment can cover this entire range and so composites of data measured at different temperatures are used. Higher temperatures shift the response to smaller times (or higher frequencies), since on molecular levels the rate of Brownian motion is increased but the molecular organization remains unchanged. Thus, temperature shifts the viscoelastic functions along the time (or frequency) scales without changing their shapes. Most polymer liquids obey this principle of *time–temperature superposition* [5] by which measurements at different temperatures can be reassembled (using "shifted" frequency ($a_T\omega$) to create a master curve of the viscoelastic spectrum.

Thus, the mechanical response as observed by the dynamic moduli (Figure 2.1 b) is a macroscopic reflection of the dynamic processes occurring at the molecular level in a typical polymer melt. Since, in SG-LCPs the material undergoes transition from glassy state to a liquid state through nematic (smectic mesophases) that exhibit distinct microstructures, these dynamics have to be understood within each phase. Results of such characterization and a discussion of the results are provided in Section 3.

2.2.2 Characterization of Linear Viscoelasticity

To characterize the rheological behavior of SG-LCP melts, oscillatory shear was applied to the samples using an RSA-II (Rheometrics^{TM} Solids Analyzer) rheometer. The sample is held in a shear cell (Figure 2.2) fitted with CaF_2 windows to permit

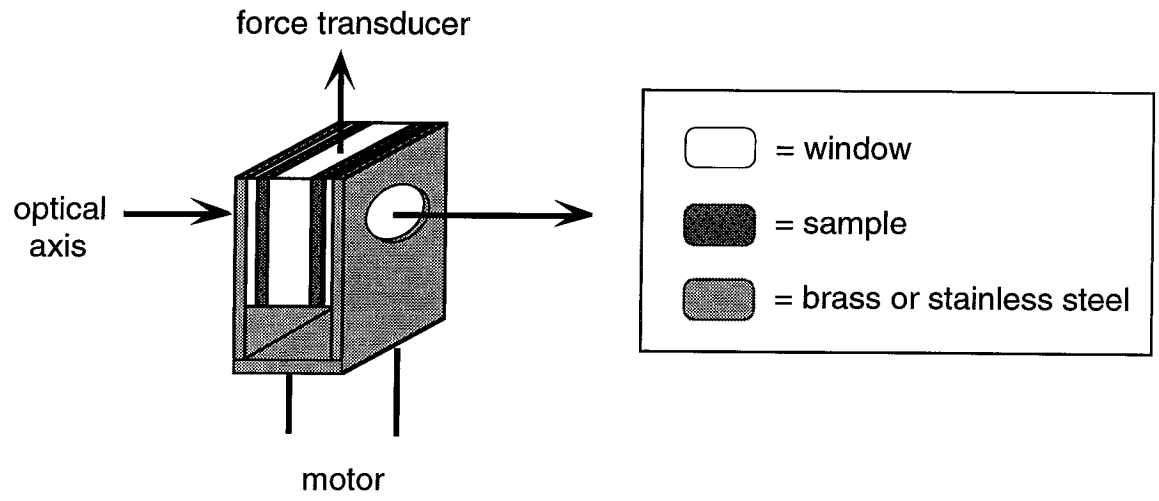

Figure 2.2: Rheometer flow cell used in RSA-II rheometer for characterization of viscoelastic response of SG-LCP melts.

passage of light for visual observation and *in-situ* optical measurements. The two outer plates of the "shear sandwich" cell are driven by a motor interfaced with an IBM computer equipped with the RHIOS software package (Rheometrics, Inc.). Sinusoidal deformations may be applied at frequencies of 100 to 0.001 rad/s, with strain amplitudes of 0.1 to 100%. A transducer measures the force exerted by the fluid on the center plate. Stresses in the range of 250 to 250,000 dyn/cm^2 are calculated by dividing this force by the tool area ($\approx$ 2 cm^2). Data is acquired using LabView^{TM} (National Instruments, Inc.) virtual instrument programs (written by R.M. Kannan; see [38]). A convection oven surrounds the flow cell, and a thermocouple-feedback to the control computer allows for temperature control to within $\pm$0.5°C uniformity over the range of -150°C to 500°C.

In order to analyze the linear viscoelastic response by extracting a valid dynamic modulus (*i.e.*, one accurately described by equation 2.4) from the measured stress,

strain amplitudes used to probe the linear viscoelasticity generally did not exceed 10-20%. Larger shear strains were employed to shear-align the SG-LCP materials in accord with the protocols developed in previous work [36]. A description of these procedures is also provided in the discussion on flow induced alignment in later chapters.

2.3 Optical Characterization of the Alignment Process in SG-LCPs

Insight into the process of macroscopic alignment of SG-LCPs requires one to correlate — and establish the relationships between — macroscopic properties and the underlying microstructure. Towards this goal, observation of the changes in the state of orientation at a molecular level are necessary. Several different techniques exist to characterize molecular orientation (for example, methods based on optical anisotropy, scattering, NMR, diffraction). Since the mesogens in the SG-LCPs possess a high degree of birefringence, we can use optical methods based on the transmission of polarized light to characterize molecular orientation.

2.3.1 Optical Examination of Oriented Materials

The refractive index probed by polarized light along the long axis of a mesogen ($n_{\parallel}$) is significantly different than the refractive index along a direction perpendicular to the long axis ($n_{\perp}$) (Figure 2.3), and the mesogen is said to be optically anisotropic with

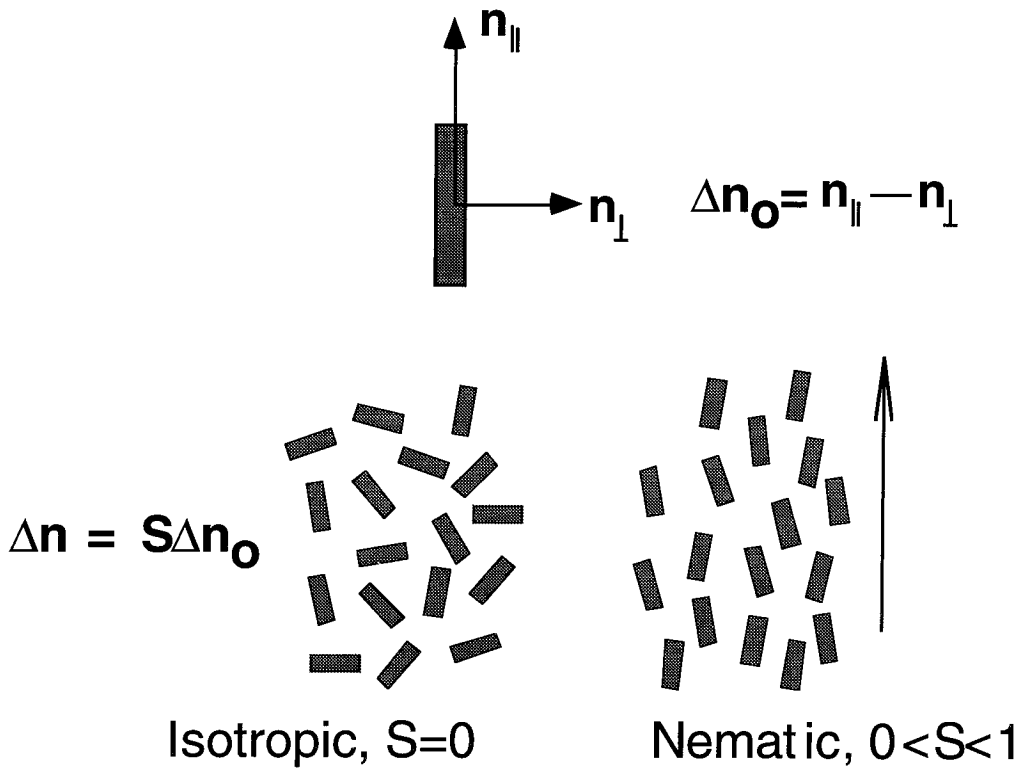

Figure 2.3: Optical anisotropy associated with the mesogen and the isotropic and nematic phases.

a birefringence, $\Delta n_o = n_{\|} - n_{\perp}$.[1] The effective birefringence (Δn) of a collection of such mesogens depends on the degree of orientational order and can be written simply as $\Delta n = S\Delta n_o$, where S is the scalar order parameter (defined in chapter 1). Thus, the isotropic phase ($S = 0$) is associated with zero birefringence, while the nematic phase exhibits a non-zero birefringence which, ideally, reaches a maximum value upon perfect ordering of the mesogens parallel to each other ($S = 1$).

When a birefringent material is placed between crossed polars (a linear polarizer-analyzer pair with their axes of polarization orthogonal), one observes transmission

[1]Typically, the birefringence Δn_o is fairly large (~ 0.2) for the moieties that form liquid crystalline phases

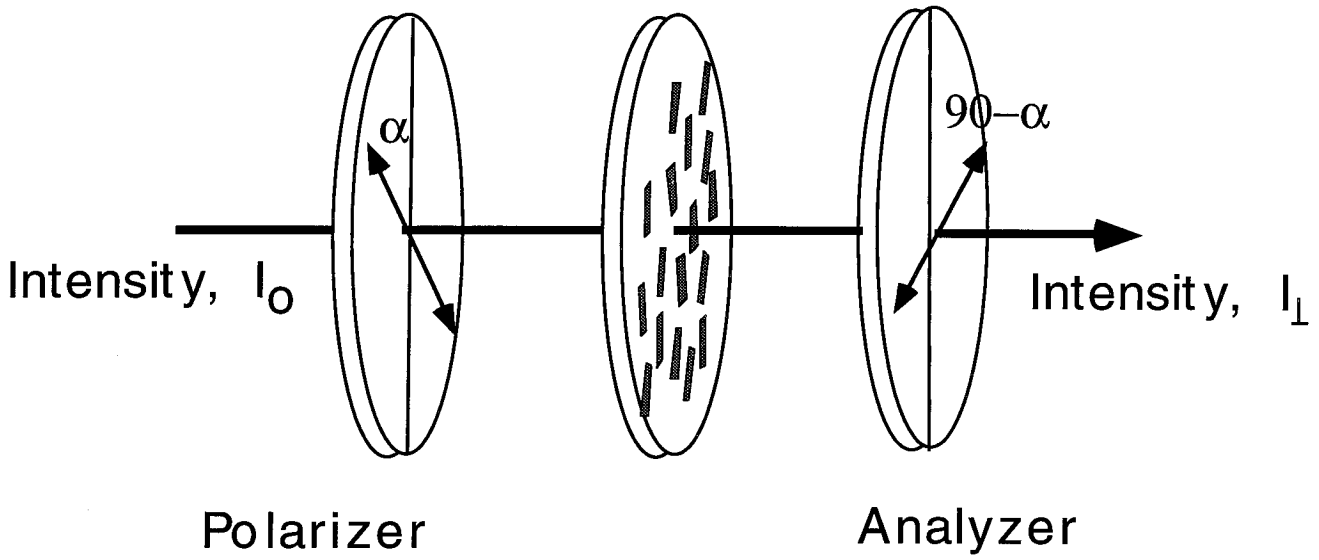

Figure 2.4: Typical set-up for a crossed-polar experiment.

of light (Figure 2.4). The fractional intensity of light ($I_\perp/I_o$) transmitted is a function of the amount of phase retardation experienced by the polarized light, and this retardation depends on the effective birefringence (Δn), the path-length the polarized light has to traverse (d), and the angle (α) between the polarization direction of incident light and projection of the optical axis of symmetry of the material (e.g., the director **n** for a nematic) in the plane normal to the direction of propagation of light. In particular, for illumination with monochromatic light of wavelength λ

$$\frac{I_\perp}{I_o} \propto \sin^2\left[\frac{\pi\Delta n d}{\lambda}\right]\sin^2 2\alpha \tag{2.7}$$

If the analyzer is rotated by 90° such that it is parallel to the polarizer then $I_\parallel/I_o = 1 - I_\perp/I_o$ (in the absence of any depolarization scattering or absorption).

This expression allows us to understand a few important considerations for exam-

ination of a sample under crossed-polars:

1. If the sample is uniformly oriented, then the intensity will be constant across the sample and extinction can be achieved by rotation of the sample to a position where the optical axis of symmetry is either parallel or perpendicular to the polarizer ($\alpha = 0°$ or $90°$). The intensity will be maximum when the optical axis is at a $45°$ angle to the polarizer.

2. For a polydomain sample (as shown in Figures 1.2a-c), the director orientation, and hence α, varies from point to point. An image formed from $I_\perp$ will thus reflect this variation.

3. For a uniformly oriented sample, by setting $\alpha = 45°$,[2] the retardation ($\mu = \frac{\pi \Delta n d}{\lambda}$) can be measured. From this retardation and a known d, one can estimate the effective birefringence and thus, the degree of order or S.

4. The angle α indicates the orientation of the optical axis of symmetry or the average orientation in a sample relative to the polarizer. Because the intensity is proportional to $\sin^2 2\alpha$ and is independent of the sign of α, it is not possible to unambiguously determine the optic axis using monochromatic illumination. However, the phenomenon of interference colors can permit the determination of the direction of the optic axis. This is explained below.

5. Illumination with white light (which is comprised of light of different wavelengths) and crossed polars causes, in general, the formation of interference

[2]Since $\sin^2 2\alpha$ is multivalued function, α can be any odd integer multiple of $45°$.

colors. These colors result from unequal transmission by the analyzer of the light of different wavelengths. The extent to which the analyzer transmits (or absorbs) each wavelength depends on the retardation (Δnd) of light. The resulting interference colors (given by a Michel-Levy chart) are divided into "orders" according to whether they result from retardations of 0 to 550nm (first-order colors), 550-1100nm (second-order), 1100-1650nm (third order), and so on [39]. Interference colors corresponding to 560nm can be readily discriminated by the eye. Very high retardations (in excess of 2000nm) cause the interference colors to appear washed-out and pale. This results from the overlapping of extinction bands from different parts of the spectrum of incident white light.

6. When the optical axis of symmetry, *e.g.* the director of a nematic phase, is parallel to the axis with high refractive index (or the slow axis), orientation of the director relative to the polarizer can be inferred from measurement of the orientation of the slow axis. The slow axis can be determined by observing the direction of shift of interference colors produced by the sample when an additional retarder (or "accessory") of known Δnd is inserted in the optical path. When the slow axis of the sample and the accessory coincide, the net retardation increases and the interference colors shift towards higher retardations in the Michel-Levy chart; when the slow axis of the sample and the accessory are orthogonal to each other, the interference colors shift to lower retardations.

Thus, characterization of the material between crossed polars is a convenient tool for characterization of long-range molecular orientational order.

2.3.2 Determination of Director Alignment for High-Retardation Samples

As discussed in the preceding section, observation of the shift of interference colors can be a useful method for determining the optical axis of symmetry of a sample. However, this method is limited to samples that have low enough retardations to permit discrimination of the colors by observation between crossed polars. At retardations exceeding many orders, the interference colors appear nearly white to the observer's eye and can no longer yield information about director orientation.

In such cases, quantitative measurement of the birefringence is possible by a spectrographic technique [40]. The optical train is essentially the same as the one shown in Figure 2.4 (parallel polarizers can also be used). The sample is illuminated with white light and instead of determining the birefringence by visually observing interference colors, a diode-array spectrograph is used to quantitatively characterize the "color" by detecting intensity as a function of wavelength. For this situation:

$$I_{\perp} = A\, I_o \sin^2\left(\frac{\pi \Delta n d}{\lambda}\right) \sin^2 2\alpha \tag{2.8}$$

$$I_{\parallel} = A\, I_o [1 - \sin^2\left(\frac{\pi \Delta n d}{\lambda}\right) \sin^2 2\alpha] \tag{2.9}$$

where A is a factor which takes into account the attenuation of light due to scattering and absorption. Normalized ratios for the intensities can also be defined as

$$N_{\perp} = \frac{I_{\perp}}{I_{\perp} + I_{\parallel}} \tag{2.10}$$

$$N_{\parallel} = \frac{I_{\parallel}}{I_{\perp} + I_{\parallel}} \tag{2.11}$$

The shearing-direction is fixed to be at 45° to the polarizer. A plot of intensity versus wavelength will have periodic minima (I_{min}) whenever the the condition $\Delta nd = k\lambda$ is fulfilled (k is an integer). If a quarter-wave plate or a full-wave plate with known slow-axis is inserted between the crossed polars, then the net retardation is changed, and I_{min} shifts along the wavelength axis. If the shift is towards higher values of wavelengths, the sample element has a slow axis with a strong projection parallel to that of the added retarder. Similarly, if the shift is towards lower wavelengths, the sample's slow axis lies primarily perpendicular to that of the known retarder. In general, by fitting the spectra of intenisty as a function of wavelength, the birefringence Δn may be evaluated. This value of Δn along with the birefringence for a perfectly aligned sample allows the estimation of a macroscopically averaged scalar order parameter S. The spectrographic birefringence measurements discussed in this dissertation were conducted in the laboratory of Professor Burghardt at Northwestern University (Evanston, Illinois).

2.4 Shear Alignment of SG-LCP Melts Simultaneous With Optical Characterization

Examination of a sample under crossed-polars allows one to deduce the uniformity of orientation in a sample as well as the orientation of the director. Therefore, opti-

cal examination, *in-situ*, during large amplitude shear alignment can yield valuable information about the evolution of alignment and the orientation of the director. To perform shear-alignment simultaneous with optical characterization, three different shearing-devices were used; these are described below:

- Large amplitude oscillatory shear was performed to align the SG-LCPs macroscopically. The sample was sandwiched in the cell shown in Figure 2.2 and mounted in the RSA-II rheometer described in the preceding section. Quantitative measurements of the small-strain dynamic moduli (G' and G'') were made before and after the alignment process to characterize the changes in the viscoelasticity of the SG-LCPs due to macroscopic shear alignment. The effective dynamic modulus (ratio of stress to strain) was also measured during the alignment process. The sample was viewed between crossed-polars using a long distance microscope and the images recorded using a video camera.

  In the rheometer, the large optical path length d ($\sim$ 0.7mm) led to retardations of many orders. Consequently, only the uniformity of the orientation could be measured by observing the uniformity of intensity under monochromatic illumination. When illuminated with white light, the high orders of retardation produced washed out interference colors which did not permit determination of the director orientation. However, even though the exact magnitude of the birefringence remains ambiguous for materials with a thick optical path-length, one can still gain valuable information about the rate of coarsening of the domain structure by measuring the transmittance of the sample during its strain

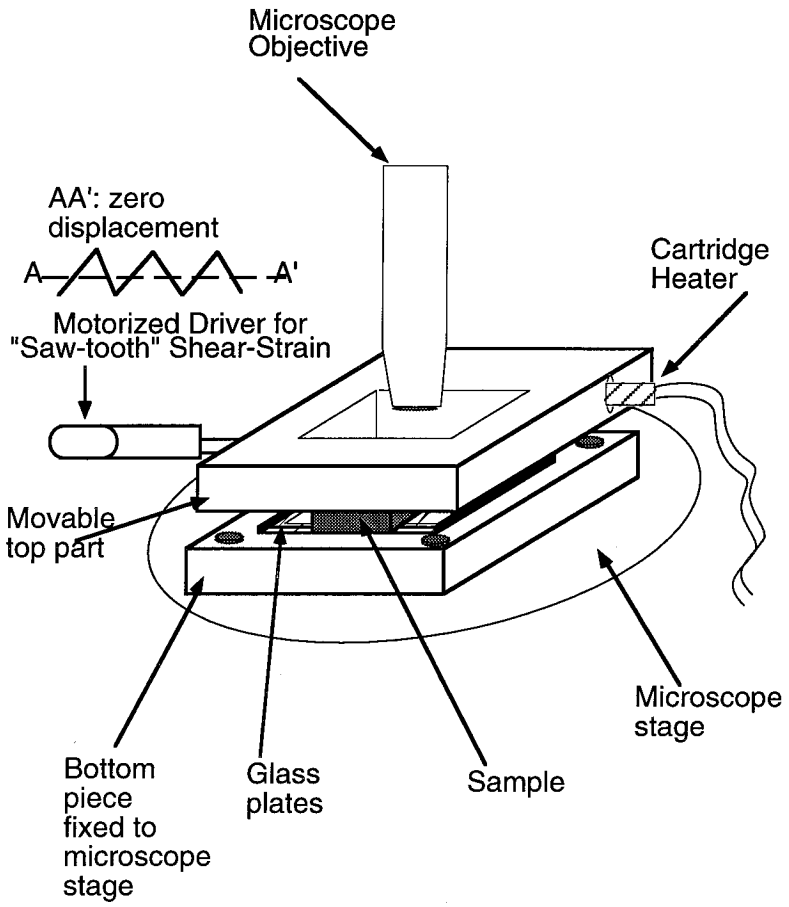

Figure 2.5: Schematic of a shear cell used to examine the sample during shear-alignment on polarizing microscope.

history.

- To circumvent this problem, a shearing device was constructed (Figure 2.5) where oscillatory shear could be applied to a thin slab of the sample at an elevated temperature within the nematic liquid crystalline phase. The cell-gap could be maintained at 0.28mm. We used a motorizer, interfaced with a controller (Newport 860-C2) and a MacIntosh computer, to obtain a desired displacement of the top plate bounding the sample. The motorizer was driven in a saw-tooth oscillatory manner at frequencies of approximately 0.1-1.0 rad/s. The

displacement of the upper plate was chosen to correspond to strain amplitudes of about 100-300%.[3] Under limited conditions, observation of the interference colors was possible in this simple shearing device using a standard polarizing microscope. The results obtained using this device are discussed in Chapter 4. This device allowed us to study the director alignment during the shearing at points close to the zero-displacement position AA' (Figure 2.5). At the extremes of the oscillatory shear cycle, the images obtained under crossed-polars still showed appreciable retardation and the retardation colors appeared pale-white, thus, not allowing us to discern the director alignment at these points.

To measure the optical axis direction under high retardation we constructed a portable, compact shearing-device (Figure 2.6) that could be used in the spectrographic birefringence apparatus at Northwestern University (Evanston, Illinois). Detailed description of the design and the mechanical drawings are provided in the Appendix.

2.5 Magnetic Alignment of SG-LCPs Melts

2.5.1 Macroscopic Alignment Using an External Magnetic Field

Mesogenic molecules tend to orient under the influence of an external magnetic or electric due to an anisotropy in their magnetic ($\Delta\chi = \chi_{\parallel} - \chi_{\perp}$) or electric suscepti-

[3]The strain was not measured using a transducer; instead the displacement of the upper plate was monitored visually under the microscope.

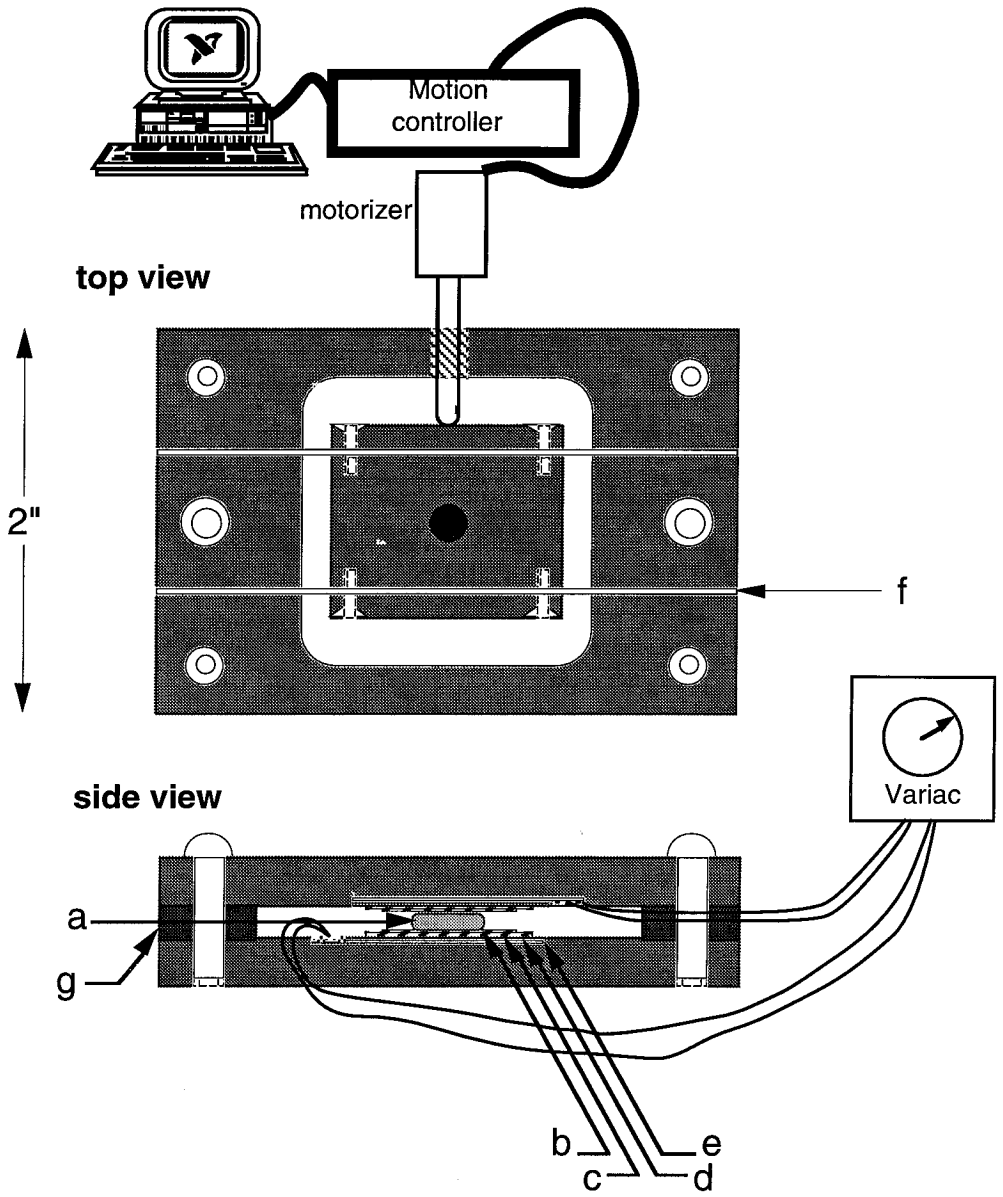

Figure 2.6: Schematic of a shear cell used to examine the SG-LCP sample ('a') during shear-alignment with a spectrographic birefringence technique. The SG-LCP melt is sandwiched between glass plates ('b') attached to thin copper sheets ('c') and heated by thin, annular-shaped Kapton-insulated heater ('d'). Beryllium-copper or stainless steel leaf springs ('f') constrain the motion of the plate to achieve uniaxial shearing motion and thermally isolate the sample. Different spacer bars ('g') maintain a gap width of typically 0.3 - 0.1mm. See Appendix for design drawings.

bility ($\Delta\epsilon = \epsilon_{\parallel} - \epsilon_{\perp}$), respectively. The orientation of the long axis of the molecules relative to the field vector depends on the sign of the anisotropic susceptibility - a positive sign leading to alignment parallel to the field vector and a negative sign to alignment perpendicular to the field vector. Since paramagnetic molecules (molecules with permanent magnetic dipoles) are fairly uncommon, and in general, molecules are diamagnetic, $\Delta\chi$ is a result of induced magnetic dipoles. Consequently, a magnetic field almost always induces an alignment of molecules parallel to the field vector. A magnetic field is also safer and more practical than an external electric field for macro-ordering of bulk samples (though, practical considerations limit the maximum field strength to $\approx$ 1-5 Tesla). Furthermore, during induced ordering associated with a magnetic field, extensive hydrodynamic perturbation due to motion of charges species is also absent.

Past studies have shown that side-group liquid crystalline polymers exhibit macroscopic alignment under the action of a magnetic field [7]. While long times and high field strengths are required to align the material, the study of magnetic alignment has been very useful towards an understanding of the field-induced motion of the mesogenic side-group and its subsequent influence on the conformation of the polymer backbone. Most past studies have employed the method of nuclear magnetic resonance (NMR) to follow the molecular motions of the mesogens [7, 8]. The polymer backbone conformation has been studied by freezing oriented materials into a glassy state with subsequent characterization by small-angle neutron scattering (SANS).

We utilized the ability of a magnetic field to orient mesogens parallel to the field

vector and studied the mechanical properties of SG-LCP samples aligned along chosen directions by annealing in a strong magnetic field. The goal of our magnetic alignment studies of SG-LCP melts was to elucidate the origins of the rheological behavior of polydomain and monodomain SG-LCPs and isolate out the potentially anisotropic contributions of the mesogen field. Furthermore, to compare and contrast the kinetics of alignment resulting from shear flows to those produced under the action of a magnetic field, we performed an *in-situ* optical study of the process of magnetic alignment, which is to our knowledge the first study of its kind for SG-LCPs.

2.5.2 Preparation of Magnetically Aligned Samples for Rheological Characterization

To study the rheology of magnetically-aligned samples using the RSA-II rheometer, it is important that the alignment induced by the magnetic field is not perturbed. Since the process of loading a sample cell (Figure 2.2) generally involves significant deformation of the sample, we annealed in a magnetic field a sample which had been already loaded in the appropriate testing cell. The cell was sheathed in Teflon^{TM} "jacket" to maintain the integrity of the gap and to prevent sample leakage when the polymer was heated above its glass transition temperature (magnetic alignment is done in the liquid crystalline phase, which is typically at temperatures exceeding 100°C). The jacketed, loaded cell was encased in aluminum heat-sink chamber that was affixed to the end of an aluminum rod. The sample could be then inserted in the narrow bore of a 7 Tesla superconducting NMR magnet. While in the magnet,

the temperature of the complete assembly (flow-cell with the SG-LCP melt and the aluminum encasing) was controlled to within $\pm 1°C$ using an Omega^{TM} CN-2011 controller and Kapton^{TM} flexible heaters. The heaters were wrapped around the exterior of the aluminum chamber. The temperature was monitored using a type T (copper-Constantin^{TM}) thermocouple.[4]

After alignment, the cell-assembly was cooled below the glass -transition temperature of the melt, removed and mounted in the rheometer for rheological testing. The results of this testing are discussed in Chapter 4.

2.5.3 In-Situ Optical Study of Magnetic Alignment of SG-LCP Melts

Since the optical properties of SG-LCP materials in their unaligned and aligned states form the basis of a number of potential applications, it is essential to understand how properties such as birefringence and transmittance are affected by the degree and direction of orientation within SG-LCP materials. Our use of optical methods to study alignment and realignment processes during the application of a magnetic field permits us to compare the response of the SG-LCP melt under shear flows and magnetic fields as well as to provide information on the transient optical properties of SG-LCP materials as they align.

To perform an *in-situ* study of magnetic alignment, we used a Varian 100-XL NMR electromagnet that could produce a maximum field of 2.5 Tesla. We set-up an

[4]A type T thermocouple is necessary because it is not constructed from any magnetic materials.

optical train around this magnet that would permit optical examination of the sample during the alignment process (Figure 2.7). For each beamsplitter (PBS-1 or PBS-2), the light emerging through the beamsplitter is of orthogonal polarization to the light split to the side (Figure 2.7). The polarizing axis of PBS-1 is rotated (out of the plane of the paper) anticlockwise by 45° relative to **B**, while the polarizing axis of PBS-2 is rotated (out of the plane of the paper) clockwise by 45° relative to **B**. Therefore, the light reaching detector D1 is in effect transmitted through crossed-polarizers ($I_{\perp}$) and the light reaching detector D2 is transmitted through parallel-polarizers ($I_{\parallel}$). Since magnetic alignment of extremely viscous LCPs may require annealing times exceeding 12-24 hours, an additional detector D3 measures the intensity of light before passage through the sample and provides a reference intensity (I_{ref}) to account for intensity drift. All intensities are recorded as a function of time using Labtech Notebook Software and a DAS-08/Jr data acquisition board (Computer Boards) on an IBM-PC 386. A helium-neon (HeNe) laser (Melles Griot) with wavelength (λ) of 633nm was used for all experiments described in Chapter 5. The SG-LCP melt can also be viewed through either crossed or parallel polarizers during the magnetic alignment process using a Javelin Chromachip II^{TM} MOS camera fitted with a 5X boroscope (Moritex^{TM} Econoscope, Edmund Scientific).

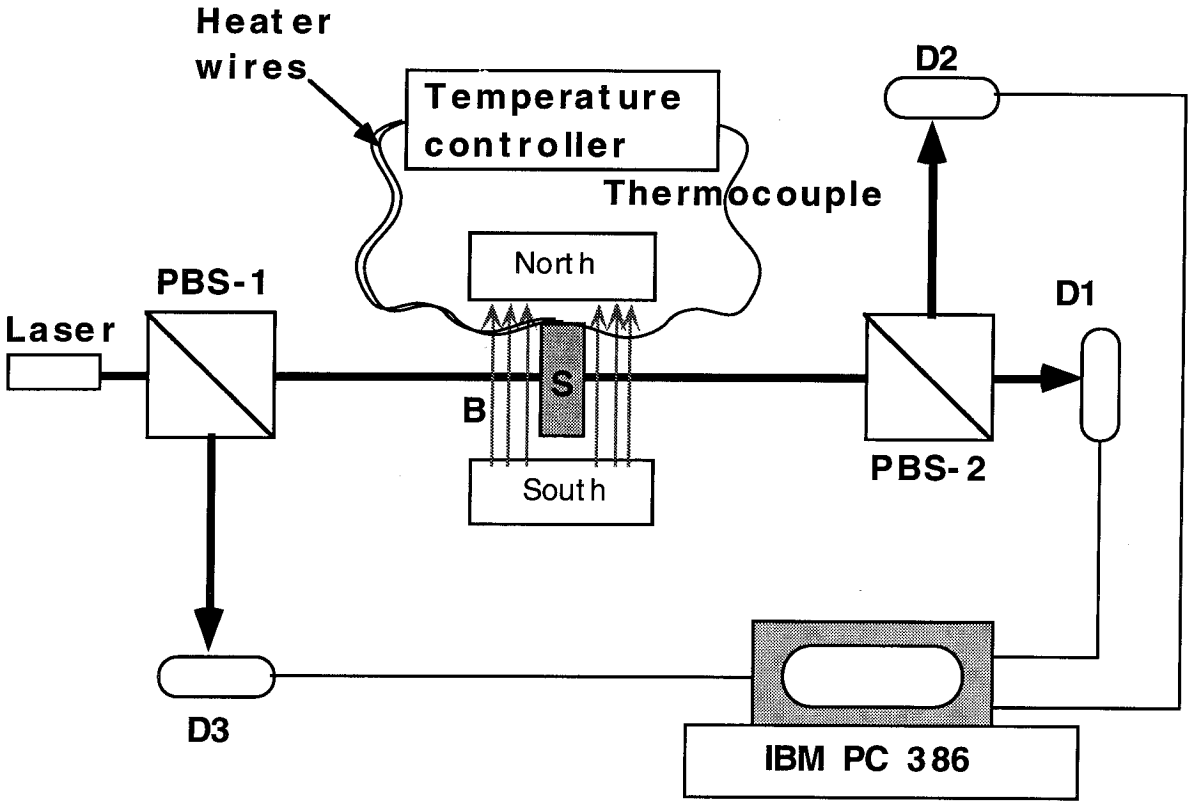

Figure 2.7: Schematic of the optical set-up around the electromagnet. The poles of the electromagnet are marked as south and north and the sample (S) is placed between the poles. The magnetic field vector, **B** is in the plane of the paper and shown by dashed arrows. PBS-1 and PSB-2 are polarizing beam splitters (Melles Griot). D1, D2, and D3 are Si-pin photodetectors (DET-S1 type, Thor Labs) that measure the intensity of light and relay it to an IBM-PC. See Appendix for design drawings.

Chapter 3

Relaxation Dynamics of Nematic and Smectic Side-Group Liquid-Crystalline Polymers

3.1 Introduction

Side-group liquid-crystalline polymers (SG-LCPs) consist of a flexible polymeric backbone to which rigid, anisotropic chemical groups, termed mesogens, are attached via flexible spacers. SG-LCPs show promise in a variety of applications [7], such as nonlinear optical materials, optical data storage media, and stress sensors. Most of the research on SG-LCPs to date has been devoted to their chemistry, particularly the effect of molecular structure on their mesophases and optical properties. The few studies of the flow behavior of SG-LCP melts have shown that the multiple levels of molecular and microscopic structure in SG-LCP systems give rise to rich rheological consequences [1, 41, 42]. Flow also provides a powerful means to manipulate molecular alignment in SG-LCPs [42]. To develop effective processing strategies for these materials it is necessary to understand the effects of molecular structure on their steady and dynamic rheological behavior.

Some of the previous investigations of the viscoelastic behavior of side-group liquid-crystalline polymeric materials have produced intriguing results. Steady-shear experiments on SG-LCP melts revealed that although the viscosity increased sharply at the nematic–to–smectic transition [35], it remained continuous through the isotropic–to–nematic transition [35, 43]. This indifference to the isotropic–to–nematic transition is surprising, since thermotropic main-chain LCPs [44], small-molecule liquid crystals [45], and lyotropic rigid-rod systems [46, 47] show an abrupt drop in viscosity upon cooling from the isotropic to nematic state.

Two recent oscillatory shear studies of SG-LCPs led to apparently contradictory

results. Colby et al. [41] reported that the shape of the relaxation spectrum — the very signature of a viscoelastic material's dynamic response — is unaffected by the transition from the isotropic to the nematic phase. Their results are in accord with previous studies that concluded that the change from isotropic to nematic order does not affect the viscoelasticity of SG-LCPs. In contrast to previous researchers, Kannan et al. [1] found that the nematic and isotropic branches of the relaxation spectrum of an SG-LCP are distinct at low frequencies. They studied materials with much higher molar masses (20 to 150 times larger) than the SG-LCPs used in previous studies [35, 41, 43]. This suggests that molecular weight may influence the effect of the isotropic–to–nematic transition on the relaxation dynamics of SG-LCP melts. To determine the origin of this discrepancy in the literature, we characterize nematic SG-LCPs with molar masses that bridge the gap between those used in the two disparate groups of studies.

Another facet of SG-LCP melt rheology about which contradictory conclusions have been reported is whether or not macroscopic orientation of the director can be achieved by shearing nematic SG-LCPs. On the basis of the observation that the viscosity remained continuous through the isotropic–to–nematic transition, Zentel and Wu concluded that flow could not be used to macroscopically align nematic SG-LCPs [35]. In contrast, Kannan et al. [1] observed that shear not only induces alignment of the nematic phase, but does so extremely rapidly relative to other means of producing the macroscopic alignment required for many of the proposed optical applications of SG-LCPs. Here, we probe the molecular-weight dependence of flow-

induced alignment in nematic SG-LCP melts.

Based on the efficacy of flow in aligning other layered liquids [48, 49], we also examine the the linear and non-linear viscoelastic behavior of smectic SG-LPCs. We compare the behavior of the nematic and smectic phases, focusing on the interplay between molecular weight and mesophase order in determining their flow behavior.

3.2 Experimental Section

Materials. The SG-LCPs used in this investigation have a methacrylate backbone, a hexamethylene spacer, and a 4-hydroxy phenyl-benzoate mesogen terminated with either a methoxy (PM6**M**) or butoxy (PM6**B**) moiety (Figure 3.1). [1] Molecular weights, polydispersities and transition temperatures of these materials are summarized in Table 3.1. Multiple fractionation was used to achieve relatively low polydispersities. The synthesis and characterization of these samples is described elsewhere [1].

Apparatus. Oscillatory shear experiments were performed on a Rheometrics RSA-II dynamic mechanical testing system (described in Chapter 2). A shear-sandwich flow fixture was equipped with CaF_2 windows to permit observation during mechanical testing. The tool area was 2 cm^2. Gap thickness varied from sample to sample and ranged from 0.32 mm to 0.55 mm. The flow cell is described in more detail in a previous publication [1].

[1] These SG-LCPs were synthesized by Christine Boeffel and U. Pawelzik at the Max-Planck Institüt fur Polymerforschung, Mainz, Germany.

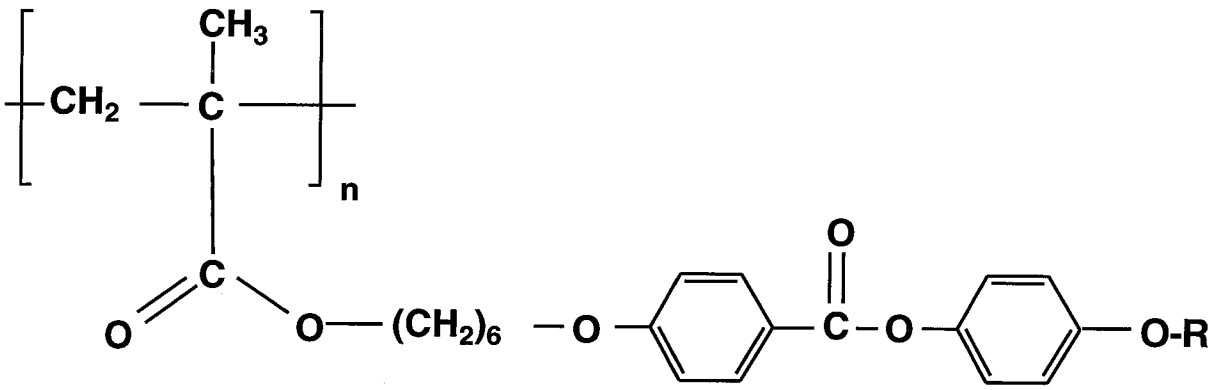

pM6M: $R = CH_3$
pM6B: $R = C(CH_3)_3$

Figure 3.1: Chemical structure of the side-group liquid crystalline polymer.

R	sample	M_w (kg/mol)	M_w/M_n	T_g(°C)	T_{sn}(°C)	T_{ni}(°C)
CH_3	PM6M-11	1130	1.54	46	–	115
	PM6M-3	312	1.34	41	–	113
C_4H_9	PM6B-32	3180	1.59	48	111	115
	PM6B-5	487	1.42	43	109	113

Table 3.1: Chemical structure and phase transition temperatures for SG-LCPs used in this study. R denotes the mesogen terminal group (see text). Molecular weights and polydispersities measured by GPC; Transition temperatures detected by DSC.

Methods. Three types of oscillatory shear experiments were performed: (1) "Frequency sweeps" using sufficiently low strain amplitude to probe linear dynamic response over up to five decades of applied frequency, (2) "single cycle" shearing experiments to determine the strain-dependence of the dynamic moduli at a given frequency, and (3) "prolonged shearing" to manipulate the alignment of the liquid crystal using

large-amplitude (40 - 110%) oscillatory shear at a fixed frequency for an extended period of time (hours).

To provide a reproducible initial condition, samples were heated well into the isotropic phase ($\approx T_{ni} + 10°\mathrm{C}$) and held there for at least 20 minutes just before each set of shearing experiments to erase any previous strain history. To determine the effects of mesophase order and molar mass on SG-LCP relaxation dynamics, frequency sweeps were performed in the isotropic, nematic, and (if applicable) smectic phases of each sample. The response was taken to be within the linear viscoelastic regime when a 2– to 6–fold increase in the strain amplitude produced no discernible change in the dynamic moduli.

To determine the effect of prolonged shearing on SG-LCP relaxation dynamics, frequency sweeps were conducted at a fixed temperature within the nematic phase before and after prolonged large-amplitude shear. For the PM6B series, which exhibits both nematic and smectic–A phases, frequency sweeps in the smectic phase were coordinated with prolonged shearing experiments in two modes: (1) Frequency sweeps were conducted at a fixed temperature within the smectic phase before and after prolonged large-amplitude shearing at that temperature; (2) Frequency sweeps were performed at a single temperature within the smectic phase before and after subjecting the sample to prolonged large-amplitude oscillatory shear at a temperature in the *nematic* state.

3.3 Results

3.3.1 Linear Viscoelastic Response

The storage and loss moduli (G' and G'') of the four PM6M and PM6B polymers listed in Table 3.1 were measured at temperatures from 75 to 135°C. Some data sets were omitted from the Figures shown in this section for clarity.

Isotropic *vs.* Nematic Phases. Within either the isotropic or nematic phase, all four SG-LCPs obeyed time-temperature (t-T) superposition. However, the isotropic and nematic phases have qualitatively different relaxation spectra for samples with sufficiently high molecular weights ($M_w \geq 1 \times 10^6$ g/mol) (Figures 3.2a, 3.2b, 3.4a and 3.4b), manifested by distinct curves in a Cole-Cole plot of G'' *vs.* G' (Figure 3.8). The two families of curves converge at high modulus values. Therefore, the distinct isotropic- and nematic-phase master curves were shifted to superimpose at high frequency, corresponding to the high values of G' and G'' where the two families of curves converge on a Cole-Cole plot. Loss modulus master curves showed trends similar to storage modulus master curves (as is evident in Figures 3.2a & 3.2b). A reference temperature of $T_o = 118$°C, in the isotropic phase for all materials, is used throughout this chapter.

When shifted in this way, the dynamic moduli of all four SG-LCPs are indistinguishable at high reduced frequencies, ωa_T, above a critical value ω_c ($\omega_c' \approx 300$ rad/s, $\omega_c'' \approx 30$ rad/s), regardless of molecular weight, mesogen terminus, or phase (Figures 3.2a- 3.5). This commonality of the high frequency relaxation signature is not

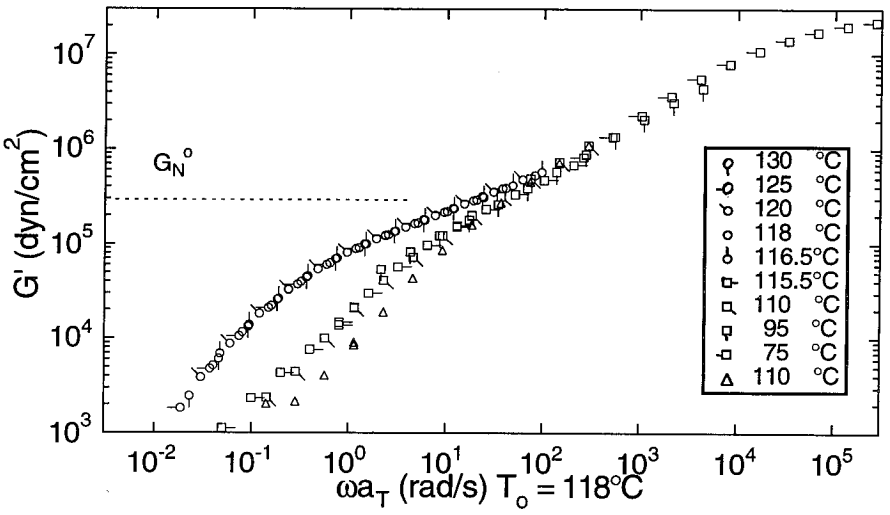

Figure 3.2a: Storage modulus, (G') master curves [$T_0 = 118°$C] for isotropic, nematic and "aligned" nematic PM6M-11 [$M_w = 1.13 \times 10^6$ g/mol]; Throughout this dissertation, all data gathered on a particular SG–LCP sample at a given temperature are horizontally shifted by the same amount, regardless of sample flow history. The term "aligned" refers to material that has been sheared to produce a transparent, highly birefringent nematic.

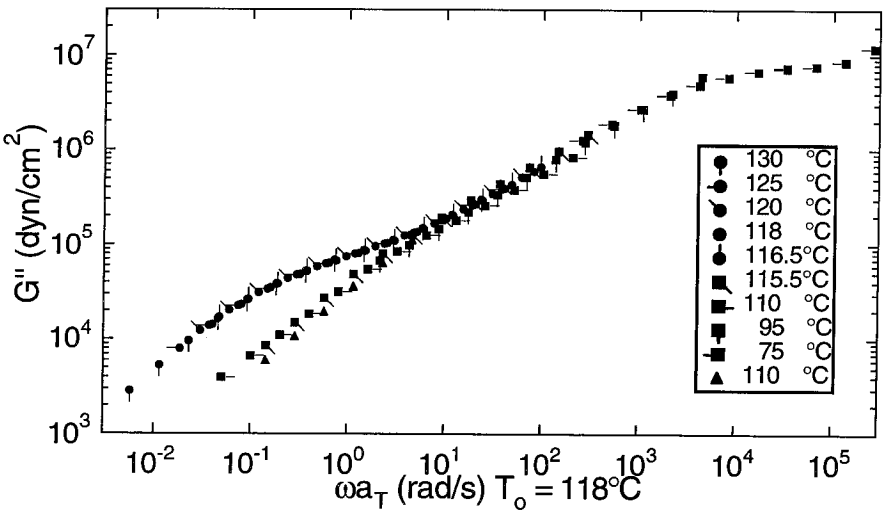

Figure 3.2b: Loss modulus, (G'') master curves [$T_0 = 118°$C] for isotropic, nematic and "aligned" nematic PM6M-11 [$M_w = 1.13 \times 10^6$ g/mol]

surprising, since (1) the short-range internal (Rouse–like) modes probed by these quick oscillations should be independent of the length of the polymer chain, and (2) the difference between methoxy and butoxy terminal moieties on the mesogen are unlikely to profoundly influence SG-LCP dynamics at the level of Rouse-like modes. In addition, this common portion of the relaxation spectrum indicates that the Rouse-like modes are insensitive to mesophase order (isotropic *vs.* unaligned nematic).

The effects of liquid-crystalline order and molecular weight are manifested in the linear viscoelastic spectrum only at frequencies below ω_c' or ω_c''. For the higher molecular weight fractions of both PM6M and PM6B (Figures 3.2a, 3.2b, 3.4a and 3.4b), the nematic branch falls below the isotropic branch at low frequencies ($\omega < \omega_c'$ or ω_c''). This behavior is consistent with that observed previously in an entangled PM6M ($M_w \approx 3 \times 10^6$ g/mol), referred to here as PM6M-30 [1]. A weak plateau emerges in the isotropic phase, and from the plateau modulus $G^0_{N,iso} \approx 1.2 \times 10^5$ dyn/cm^2 (estimated using the value of the storage modulus at the frequency where $\tan\delta$ is at its minimum value [50]), we calculate an entanglement molecular weight of $M_{e,iso} \approx 2.7 \times 10^5$ g/mol in the isotropic phase. No plateau was observed for the lower molecular weight PM6M (Figures 3.3a and 3.3b), consistent with its molecular weight ($M_w < 1.5 M_{e,iso}$). In the nematic phase even the higher molecular weight material PM6M-11 has no plateau, making it impossible to determine the entanglement molecular weight of nematic PM6M.

Although the terminal loss modulus of PM6M-11 was not accessible over the temperature and frequency range of our measurements, based on the lowest fre-

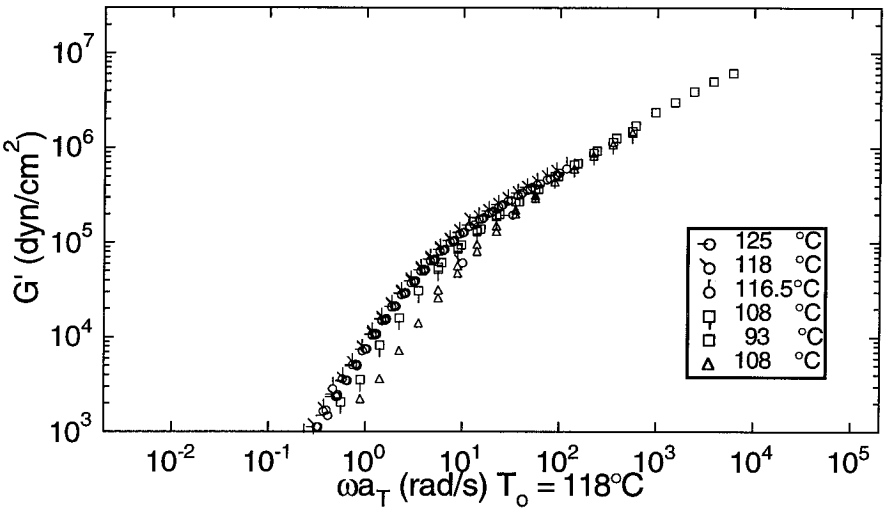

Figure 3.3a: Storage modulus master curves [$T_0 = 118°C$] for isotropic, nematic and "aligned" nematic PM6M-3 [$M_w = 3.12 \times 10^5$ g/mol]

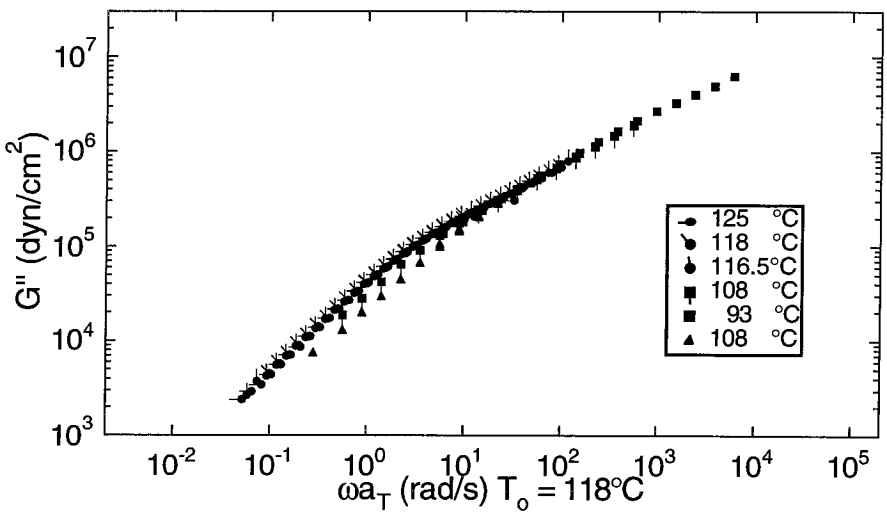

Figure 3.3b: Loss modulus master curves [$T_0 = 118°C$] for isotropic, nematic and "aligned" nematic PM6M-3 [$M_w = 3.12 \times 10^5$ g/mol]

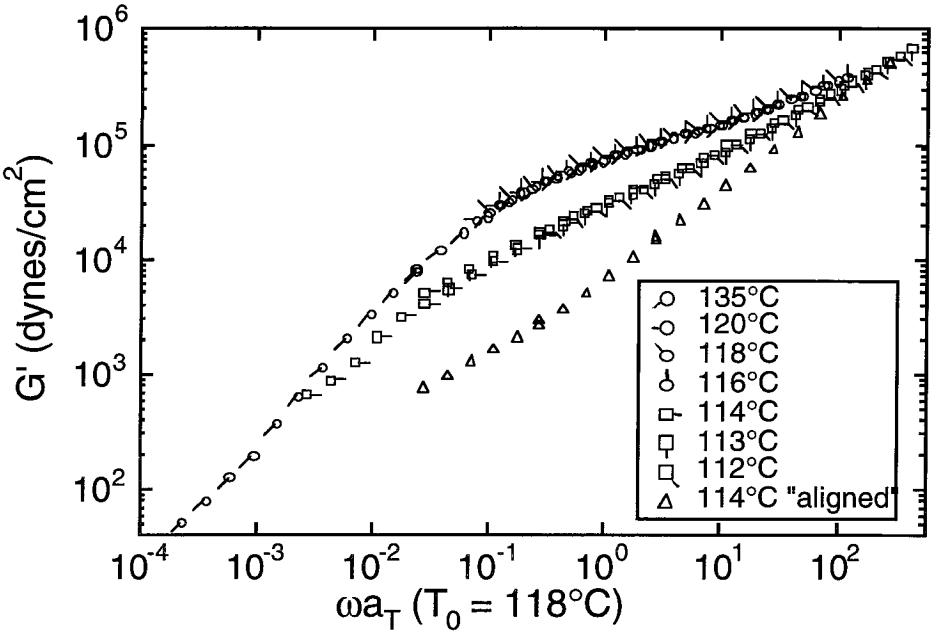

Figure 3.4a: Storage modulus master curves [$T_0 = 118°C$] for isotropic, nematic and "aligned" nematic PM6B-32 [$M_w = 3.18 \times 10^6$ g/mol] The high-frequency end of the viscoelastic spectrum can be seen more fully in Figure 3.6a.

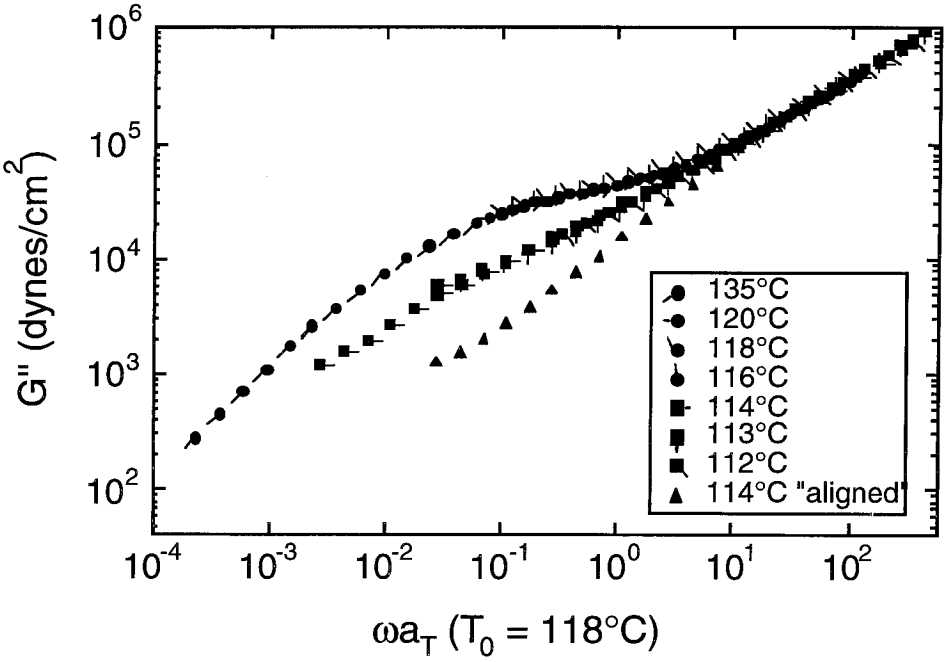

Figure 3.4b: Loss modulus master curves [$T_0 = 118°C$] for isotropic, nematic and "aligned" nematic PM6B-32 [$M_w = 3.18 \times 10^6$ g/mol] The high-frequency end of the viscoelastic spectrum can be seen more fully in Figure 3.6b.

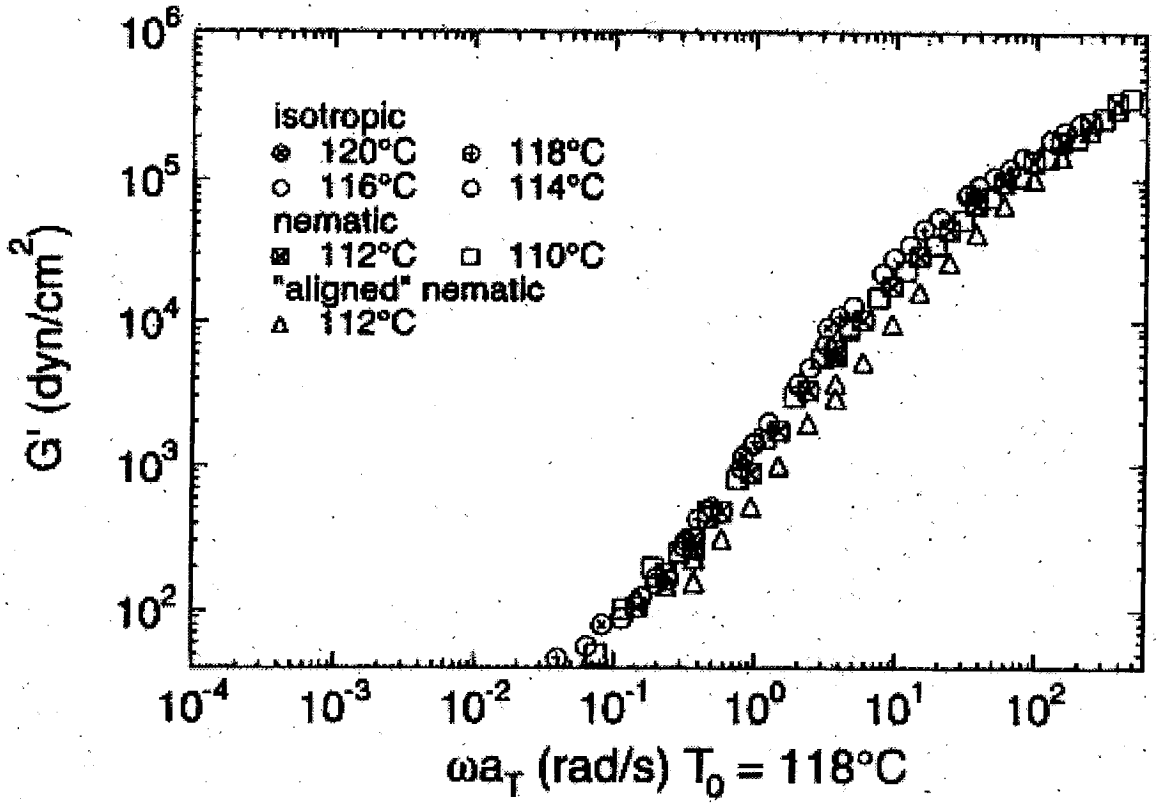

Figure 3.5: Storage modulus master curves [$T_0 = 118°C$] for isotropic, nematic and "aligned" nematic PM6B-5 [$M_w = 4.87 \times 10^5$ g/mol]; The high-frequency end of the viscoelastic spectrum can be seen more fully in Figure 3.7.

quency we could measure, we estimate a 2.6–fold drop in the zero–shear viscosity η_0 [$\eta_0 = \lim_{\omega \to 0} \frac{G''}{\omega}$] upon cooling through T_{ni}. While consistent with the behavior of small-molecule liquid crystals [45] and main-chain liquid-crystalline polymers [44], this behavior contrasts with previous reports that showed no abrupt change in the viscosity of dynamic moduli of SG-LCPs at the onset of nematic liquid-crystallinity [35, 41].

For PM6B, the viscoelastic response of the higher molecular weight fraction showed a considerable plateau in the isotropic phase (Figure 3.4a) of about $G^0_{N,iso} \approx 9.2 \times 10^4$ dyn/cm^2, corresponding to $M_{e,iso} \approx 3.5 \times 10^5$ g/mol. This is in reason-

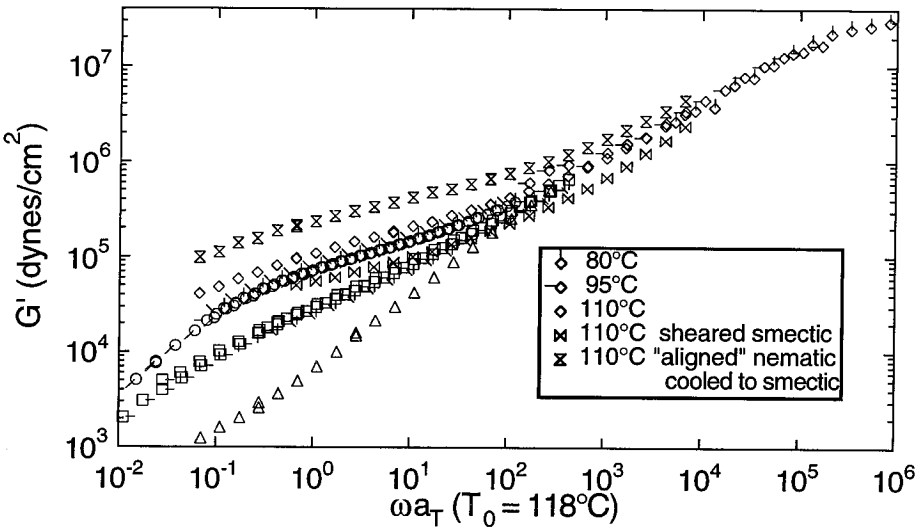

Figure 3.6a: Storage modulus master curves [T_0 = 118°C] for ordinary smectic and sheared smectic PM6B-32. Also shown are data from smectic PM6B-32 that has been shear–aligned in the nematic. Isotropic, nematic, and shear–aligned nematic data from Figure 3.4a are shown for comparison.

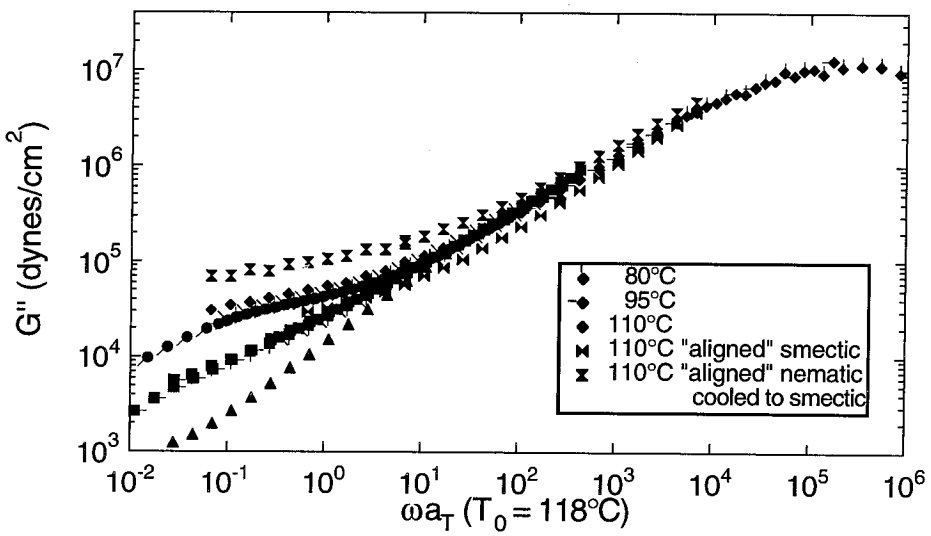

Figure 3.6b: Loss modulus master curves [T_0 = 118°C] for ordinary smectic and sheared smectic PM6B-32. Also shown are data from smectic PM6B-32 that has been shear–aligned in the nematic. Isotropic, nematic, and shear–aligned nematic data from Figure 3.4b are shown for comparison.

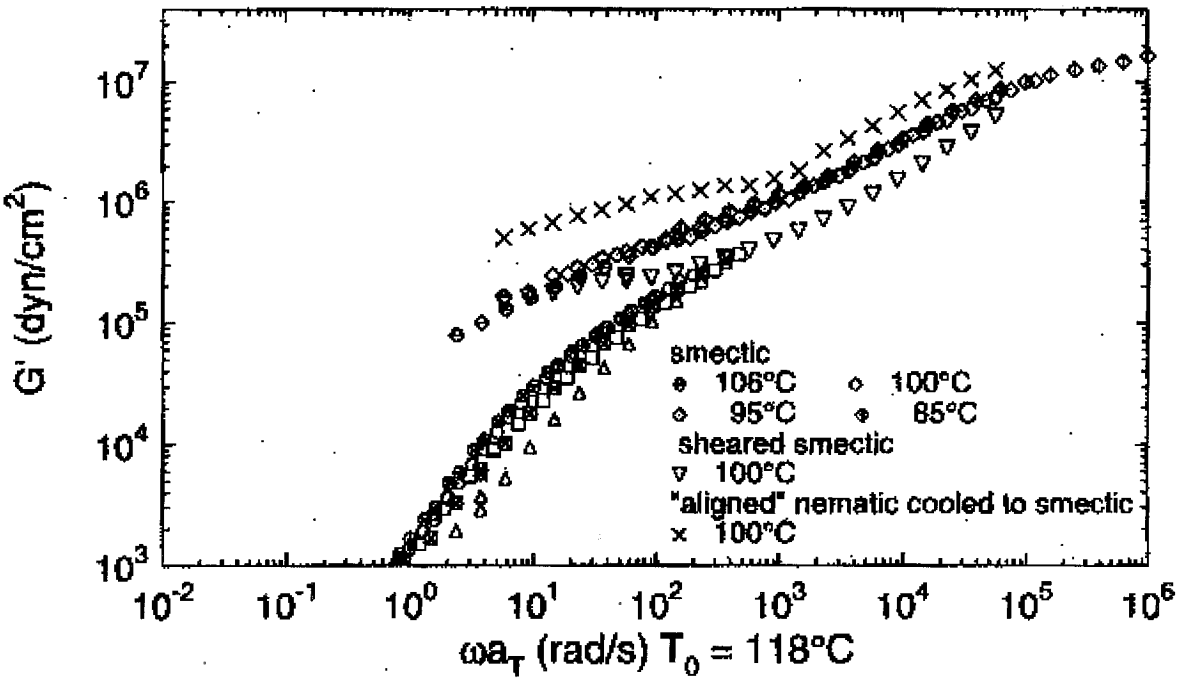

Figure 3.7: Storage modulus master curves [$T_0 = 118°C$] for ordinary smectic and sheared smectic PM6B-5. Also shown are data from smectic PM6B-5 that has been shear–aligned in the nematic. Isotropic, nematic, and shear–aligned nematic data from Figure 3.5 are shown for comparison.

able agreement with the estimate of $M_{e,iso}$ we obtain for PM6M-11. Because only a slight plateau is discernible in the nematic phase, the value of $M_{e,nem}$ is more difficult to extract. To obtain a rough estimate of its value, we approximate $G^0_{N,nem}$ in two ways: (1) by the value of G'_{nem} at the same frequency used for the isotropic phase (i.e., $\omega a_T \approx 2$ rad/s), leading to $M_{e,nem} \approx 8 \times 10^5$ g/mol $\approx 2.3 M_{e,iso}$, and (2) by the value of G'_{nem} at the minimum in $\tan\delta_{nem}$ ($\omega a_T \approx 0.2$ rad/s), which gives $M_{e,nem} \approx 2.1 \times 10^6$ g/mol $\approx 6 M_{e,iso}$. In either case, the rheological evidence (Figure 3.4a) indicates that the polymer is less entangled in the nematic phase than it is in the isotropic phase. Possible explanations for this change in G^* at the isotropic–nematic transition are addressed in the Discussion. In the smectic phase the plateau

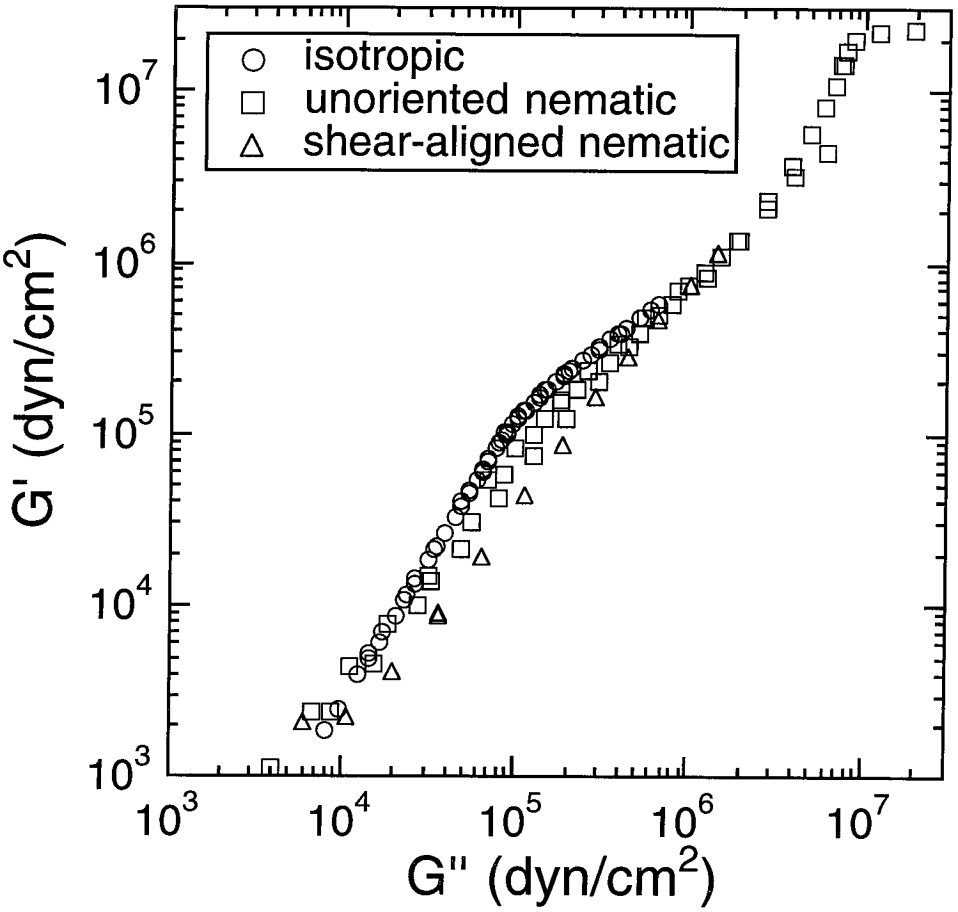

Figure 3.8: Cole-Cole plot for PM6M-11. Storage modulus is plotted against loss modulus in the isotropic (130 – 116.5°C), unoriented nematic (115.5 – 75°C and "shear-aligned" nematic (110°C) phases.

is dominated by the layered morphology rather than chain entanglements [49]; therefore, we cannot determine the effect of smectic order on entanglement based on the plateau modulus.

Smectic Phase. As in the nematic phase, the linear viscoelastic spectra of both molecular weight fractions of PM6B in the unaligned smectic state converge for $\omega \geq \omega_c$. Frequency sweeps in the smectic phase obeyed time-temperature superposition for both PM6B-32 and PM6B-5. As has been observed earlier in SG-LCPs [41], main-

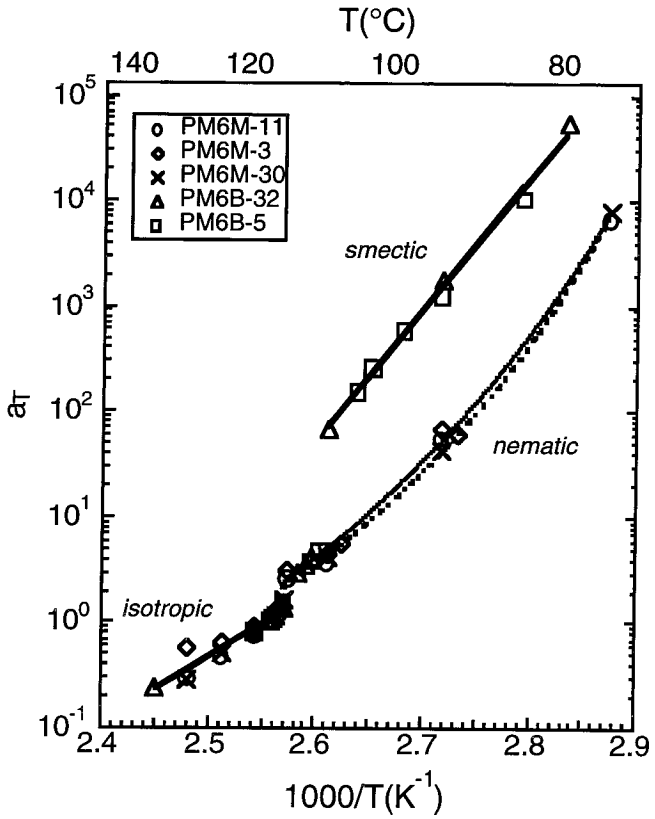

Figure 3.9: Shift factor (a_T) *vs.* inverse temperature for PM6M and PM6B. Also shown for comparison are shift factors for PM6M-30 ($\times$), and corresponding WLF dependence (dashed curve) [1].

chain LCPs [51] and small-molecule liquid crystals [49] the storage and loss moduli of the smectic phase exceed those of either the nematic or isotropic phases, and fail to reach terminal behavior even at the lowest accessible frequencies (Figures 3.6a, 3.6b & 3.7). It has recently been shown that such behavior is characteristic of unaligned layered liquids [49].

Cole-Cole plots were examined to determine whether or not the smectic arm converges with the isotropic and nematic branches of the relaxation spectrum. This appears to occur, but at higher modulus levels (and correspondingly higher frequency) than the convergence of the isotropic and nematic branches. We use the overlap region

of the Cole-Cole plot to identify the modulus range at which the smectic data should superpose with the nematic and isotropic data on a reduced frequency plot. The shift factors obtained show an abrupt jump at the nematic-smectic phase transition (Figure 3.9). For a given temperature, the shift factor determined for the unaligned smectic sample is applied to all data taken at that temperature, regardless of flow history (see below).

Temperature-Dependence of Shift Factors. The temperature dependence of frequency shift factors for all fractions of PM6M and PM6B in the isotropic and smectic phases can be described by Arrhenius relationships, yielding apparent flow activation energies per backbone bond of 120 and 240 kJ/mol, respectively (Figure 3.9). The flow activation energies we observe in the isotropic and smectic phases are consistent with those reported earlier for lower-molar-mass PM6M and PM6B [35], although the present values are somewhat higher (15-40%). In the nematic phase, the shift factors obey a WLF temperature dependence, with $\log a_T = \frac{-C_1(T-T_0')}{C_2+(T-T_0')}$, where the reference temperature T_0' is treated as an adjustable parameter and found to be $T_0' = 396$K, with $C_1 = 4.78$ and $C_2 = 108$K. The WLF behavior we observe in the nematic phase agrees well with the previously reported WLF dependence of the high-molar-mass PM6M-30 [1] (Figure 3.9). Earlier studies have reported Arrhenius behavior for methacrylate–based nematic SG-LCPs with hexamethylene spacers [35, 41], including PM6M [35]. The Arrhenius activation energies of 159-175 kJ/mol, based on temparatures from 100-130°C, reported in these two previous studies are in good agreement with the nematic-phase temperature dependence of the present

samples over a comparable range in temperature.

3.3.2 Departure from Linear Response

In the isotropic phase, the effective dynamic moduli of PM6B-32 remain essentially independent of strain over the range of 0.1 - 100% and at ω = 100-0.1 rad/s. In the nematic phase, similar linearity is observed at high frequencies ($\geq$ 10 rad/s). However, at lower frequencies ($\leq$ 1 rad/s), strain-*hardening* is observed at strains of 10% or more (Figure 3.10a). The strain dependence of G'' (not shown) is similar to that of G'. Indications of strain-hardening in the nematic phase have been reported previously in PM6M [36, 42]. The present results are in accord with the dynamic moduli of PM6M at ω = 0.1 rad/s and T = 110°C reported both in the linear regime and in the first cycle of 100% strain used to induce alignment [36, 42]. Qualitatively similar non-linear behavior is observed in the nematic phase of for PM6B-5 (Figure 3.10b).

In the smectic phase, PM6B is strain-softening above $\gamma \approx 6\%$ for all frequencies at which the corresponding stress is measurable by our rheometer (Figures 3.11a & 3.11b). This strain-softening of the dynamic moduli in the smectic phase is qualitatively similar to the behavior of another layered system, lamellar diblock copolymers [52, 53].

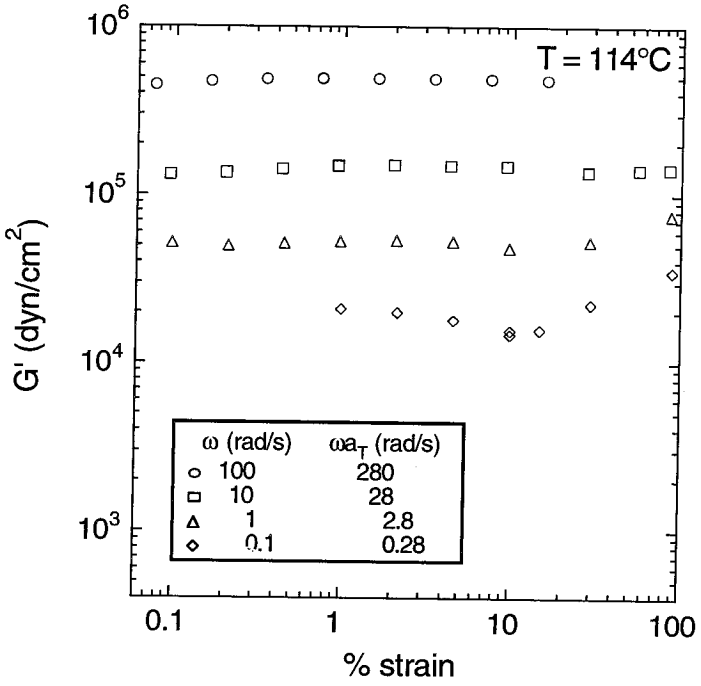

Figure 3.10a: Strain-dependence of storage modulus (G') for PM6B-32 ($T = 114°C$) in the nematic phase.

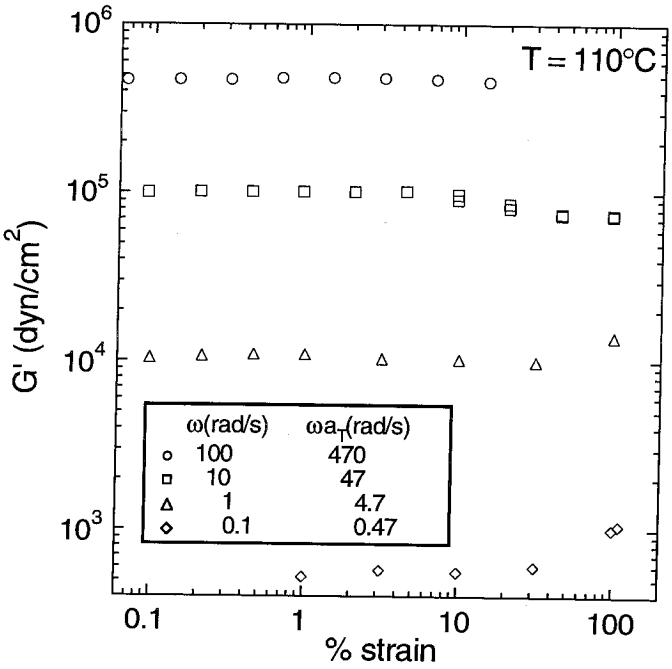

Figure 3.10b: Strain-dependence of storage modulus (G') for PM6B-5 ($T = 110°C$) in the nematic phase.

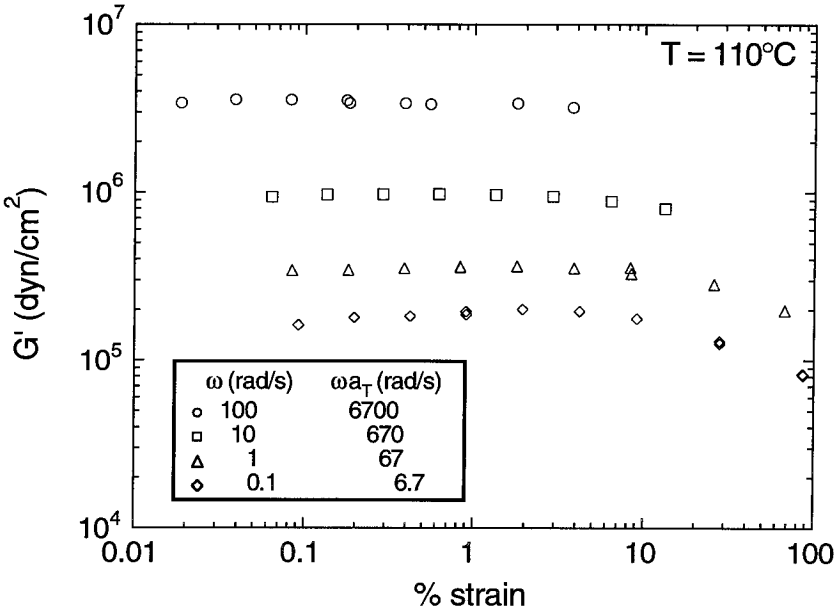

Figure 3.11a: Strain-dependence of storage modulus (G') for PM6B-32 ($T = 110°C$) in the smectic phase.

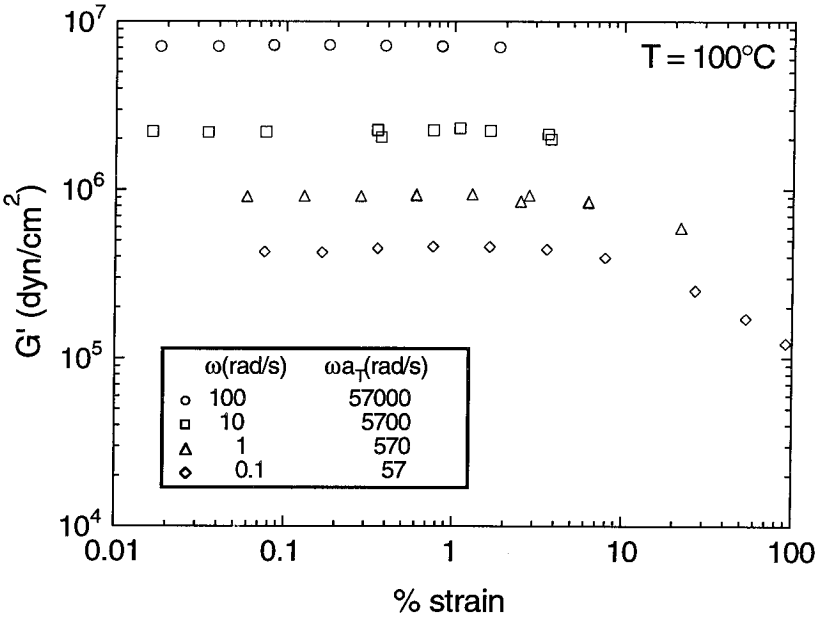

Figure 3.11b: Strain-dependence of storage modulus (G') for PM6B-5 ($T = 100°C$) in the smectic phase.

3.3.3 Consequences of Prolonged, Large-Amplitude Oscillatory Shear

Nematic Phase. Large-amplitude (100 - 110%) oscillatory deformations applied to polydomain nematic SG-LCPs cooled from an isotropic melt produced a dramatic change from an opaque, intensely scattering medium to a transparent and highly birefringent material [42]. This transformation was rapid, occurring within the first few cycles of shear. Shearing was continued for hundreds of cycles (typically 800). After cessation of large-amplitude shearing, the viscoelastic response of the material was probed with small-amplitude oscillations. The magnitudes of the low–frequency dynamic moduli ($\omega a_T < \omega_c$) of these shear-oriented materials were lower than those of the polydomain (unsheared) nematic (Figures 3.2a-3.5), as had been observed earlier in PM6M-30 [1].

Although the rheological consequences of prolonged shearing were more pronounced for longer chains (*cf.* Figures 3.2a & 3.4a *vs.* Figures 3.3a & 3.5), the effects of large-amplitude oscillatory shear on the turbidity and viscoelasticity of the nematic phase were observed for all samples studied, regardless of molecular weight or mesogen terminus. This demonstrates that, contrary to the conclusion reached by Zentel and Wu [35], the linear viscoelastic response of the nematic phase need not be markedly different from that of the isotropic phase in order for flow to be an effective means of inducing macroscopic orientation.

Smectic Phase. Prior to the application of large-amplitude oscillatory shear, the smectic-phase polymer appeared an opaque white, indicating a high concentration of

scattering defects. During sustained shearing, the polymer became slightly translucent, but never attained the clarity or high birefringence characteristic of the shear–aligned nematic materials. Prolonged large-amplitude oscillatory shearing (45% strain at 0.1 rad/s for 800 cycles at 110°C) of smectic PM6B-32 did significantly reduce both the storage and loss moduli. Assuming that the procedure for time-temperature shifting the smectic phase frequency sweeps with respect to the nematic and isotropic data is correct, the shear-induced change in G' was not confined to frequencies below ω_c (Figures 3.6a & 3.7), suggesting that large-amplitude shearing induces profound structural changes in the smectic phase on length–scales even shorter than those affected by shearing in the nematic phase.

Smectic SG-LCP Sheared in the Nematic Phase. After equilibrating at T_{ni} + 10°C for 20 minutes to erase any prior strain history, PM6B-32 was cooled to the nematic state (T = 114°C) and subjected to the identical large-amplitude shearing protocol described above (γ_o = 45%, ω = 0.1 rad/s, 800 cycles). Upon cessation of shear, the aligned material was cooled into the smectic state (T = 110°C) and allowed to equilibrate for 15 minutes. During this time the sample became progressively more turbid, suggesting the formation of defects. Nevertheless, the quenched smectic sample was still more translucent than the polydomain (unsheared) smectic material, which was completely opaque.

Immediately after temperature-equilibration, the sample was probed with small-amplitude oscillatory shear. Surprisingly, the magnitudes of the resulting dynamic moduli *exceeded* those of the polydomain smectic polymer probed at the same temper-

ature, frequency range, and strain amplitudes (Figure 3.6a). The effects of previous large-amplitude oscillatory shearing in the nematic phase again manifested themselves in the smectic phase at shifted frequencies both above and below ω_c. In fact, even at frequencies some 1.5–2.5 decades higher than ω_c'' or ω_c', respectively, the effects of the shearing history are evident in the viscoelastic behavior of the smectic phase polymer. Qualitatively similar behavior was observed for the lower molecular–weight fraction of PM6B (Figure 3.7). This is significant in that ω_c represents a critical frequency above which oscillatory shear probes such local dynamics that the phase transitions alone have no impact on the relaxation spectrum.

3.4 Discussion

3.4.1 Entanglement Molecular Weight in the Isotropic Phase

The number of repeat units per entanglement (N_e) in isotropic PM6M and PM6B is very similar (Table 3.2), with the somewhat higher N_e for the material with the bulkier side-group.

The values of $N_{e,iso}$ are roughly on par with experimental values [4] for methacrylate polymers with large non-mesogenic side groups (Table 3.2). The group-contribution method of Wu overestimates the number of repeat units per entanglement strand of isotropic PM6M and PM6B by 30-35% [3]. The method of estimating M_e by Fetters et al. [54] utilizing correlations between the plateau modulus, mean-square end-to-end distance, and density, leads to a value of $M_{e,iso}$ for PM6M within

5% of our experimentally-determined value of $M_{e,iso}$=2.7 $\times$ 10^5 g/mol.

Methacrylate polymer	M_e (kg/mol)	N_e
PM6B *isotropic*	**355**	**780**
PM6M *isotropic*	**270**	**660**
Poly(triphenyl methacrylate)	203[a]	618
Poly(4-*t*-butylphenyl methacrylate)	69.7[a]	320
Poly(diphenylmethyl methacrylate)	74.1[a]	278
Poly(*n*-hexyl methacrylate)	33.8[b]	200
Poly(*t*-butyl methacrylate)	28.1[a]	198
Poly(methyl methacrylate)	9.2[b]	92
	4.7[c]	47

Table 3.2: Number of repeat units per entanglement chain: comparison of PM6M and PM6B with other polymethacrylates. Sources: a - [3]; b - [4]; c - [5]

The fact that the entanglement molecular weight of PM6M and PM6B in the isotropic phase is an order of magnitude larger than that of conventional poly(methyl-methacrylate) discredits the recent assertion [55] that SG-LCP spacers behave as branches, increasing the entanglement density. Surprisingly, the chain contour length per entanglement appears to rise dramatically (by a factor between 2.3 and 6) upon cooling through the isotropic–to–nematic transition, as evidenced by a drop in the low–frequency modulus of the entangled materials (and an absence of any corresponding change in the relaxation dynamics of the unentangled polymer). This apparent increase in N_e in the nematic phase discredits the notion that the nematic mesogen field stabilizes entanglements [55]. Possible interpretations of the observed decrease in chain entanglement accompanying the isotropic–to–nematic phase change are addressed below.

3.4.2 Effect of Isotropic–to–Nematic Phase Transition

Comparison of the dynamic moduli of higher molecular weight versus lower molecular weight SG-LCP melts (*cf.* Figures 3.2a & 3.4a *vs.* Figures 3.3a & 3.5) clearly indicates that manifestation of nematic liquid-crystallinity in the linear viscoelastic spectrum correlates with the emergence of a plateau in G' of the isotropic phase. We have considered various explanations for the molecular–weight–dependent drop in the dynamic modulus at the isotropic–to–nematic transition, such as (1) a decrease in the entanglement density due to an increase in the persistence length upon attaining nematic order; (2) a change in the friction coefficient of each repeat unit in the isotropic *vs.* nematic melt; and (3) the possibility that "soft modes" in the nematic phase lead to energetically–favorable deformations, thus leading to lower moduli than in the isotropic phase. These alternatives are explored, and refuted, below. Finally, we are left with a working hypothesis involving a tube dilation that occurs without changes in contour length per unit volume, but rather due to changes in the way polymer chains fluctuate among one another.

We consider the possibility that the constraints imposed by a locally-ordered mesogen field might effectively stiffen the chain, giving rise to a longer persistence length for the polymer backbone in the nematic phase. Based on this assumption, one would expect to observe an expansion of the radius of gyration as the material is cooled through the isotropic–nematic transition. However, SANS experiments on PM6M and PM6B [56] reveal that although the backbone assumes a slightly ellipsoidal rather than spherical shape in the nematic state, the overall mean dimension

of the polymer coil remains essentially unchanged.

One might also argue that with the onset of liquid–crystalline order, the viscosity experienced by the laterally attached mesogens might drop, as it does in small molecule liquid crystals. This could produce a drop in the monomeric friction coefficient. However, this explanation can also be ruled out because such a decrease in resistance to chain movement should lead to an abrupt drop in the shift factor at the isotropic–to–nematic transition (in contrast to the rise observable in Figure 3.9), without any change in the shape of the viscoelastic spectrum, regardless of the degree of chain entanglement.

Another explanation for the difference in the moduli of the isotropic and nematic phases draws upon the balances in free energy of the mesogen field and the backbone. In side-group liquid-crystalline polymers, the backbone's propensity to assume a random coil configuration is antagonistic to the mesogens' tendency to form an ordered microstructure. Although the flexible spacer serves to partially decouple these two opposing tendencies, orientational coupling between the backbone and mesogen still exists. It is possible that one consequence of the fact that the backbone spontaneously adopts an anisotropic conformation in the nematic phase might be that certain distortions of the chain might be nearly iso-free-energy ("soft") deformations [57]. If the free energy cost of a given conformational distortion is higher when the pendant mesogens are isotropic than when they have nematic order, then the modulus in the isotropic phase might exceed that of the nematic polymer. However, the primary weakness in this interpretation is that it fails to address the molecular–weight depen-

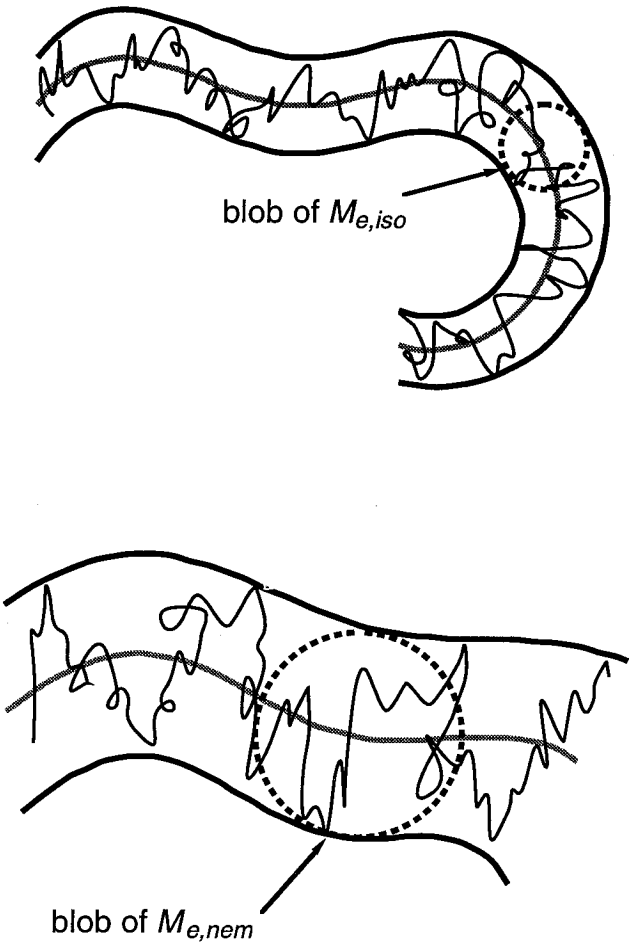

Figure 3.12a: The drop in the low–frequency modulus of entangled SG-LCPs at the isotropic–to–nematic transition suggests a tube dilation associated with enhanced mesogen mobility.

dence of the sensitivity of the linear viscoelastic spectrum to the isotropic–nematic phase transition (Figures 3.2a–3.5). That is, this hypothesis would lead to a drop in modulus not only in the plateau region, but also in the Rouse regime, contrary to what we observe. Furthermore, this hypothesis would lead to having a modulus that depends on the direction of mesogen alignment, in contradiction to recent results on magnetically-aligned nematic SG-LCP melts [42].

Alternatively, we propose that the distinct viscoelastic behaviors exhibited by

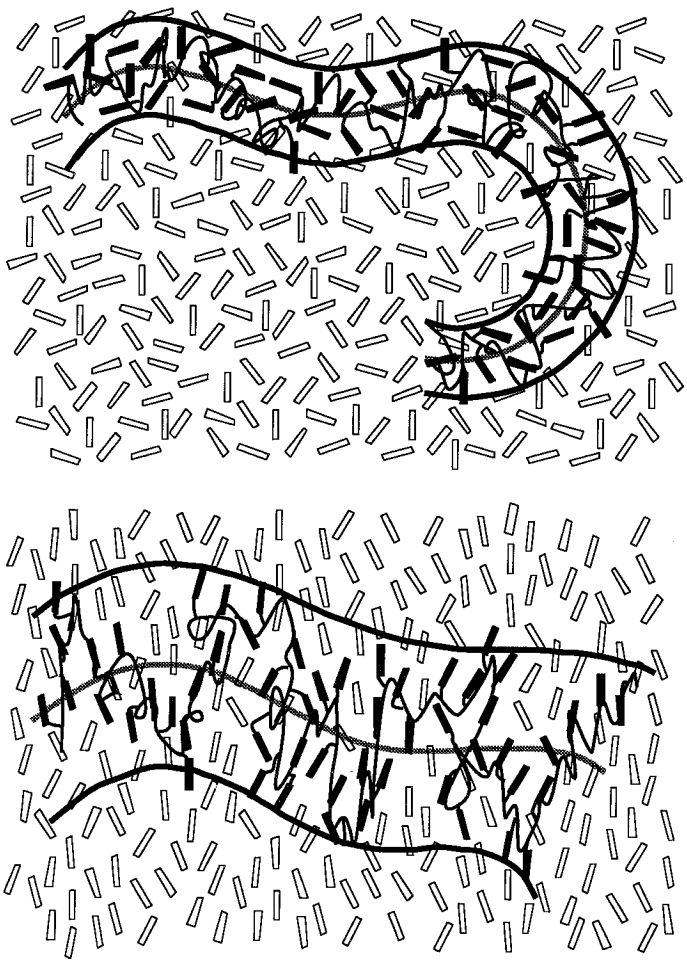

Figure 3.12b: As the material moves from the isotropic phase *(top)* to the nematic phase *(bottom)*, the mesogens may offer less hinderance to lateral fluctuations. The effect is somewhat exaggerated in this figure to illustrate the interpretation.

long SG-LCP chains in the nematic phase are related to an enhanced mobility of the mesogens in the nematic *vs.* isotropic states. Experiments have shown that many low molar mass nematic liquid crystals exhibit faster diffusion in the mesophase than in the isotropic phase, with the diffusivities along ($D_{\parallel}$) and perpendicular to ($D_{\perp}$) the director having relative magnitudes $D_{\parallel} > D_{iso} > D_{\perp}$ [58]. In SG-LCPs, such enhanced mesogen mobility might permit larger lateral fluctuations of the polymer backbone to which mesogens are covalently tethered, as illustrated schematically in

Figure 3.12a & 3.12b. In the context of the reptation model, this corresponds to a dilation of the confining "tube" *without* an increase in R_g. Such tube dilation would be manifested by a decrease in the plateau modulus and terminal relaxation time of the entangled SG-LCP, consistent with the effect of nematic ordering on the dynamic moduli of PM6M-11 and PM6B-32 (Figures 3.2a, 3.2b, 3.4a & 3.4b, Table 3.2). In particular, the increase in M_e of 2.3– to 6–fold suggested by our estimates of $M_{e,nem}$ and $M_{e,iso}$ would correspond to a 1.5– to 2.4–fold increase in the tube diameter.

For non–entangled polymers (e.g., PM6M-3 and PM6B-5), lateral constraints imposed by neighboring chains do not limit conformational relaxation; therefore, increasing lateral freedom does not alter the shape of the relaxation spectrum, so the dynamic moduli are insensitive to the isotropic–nematic transition (Figures 3.3a & 3.5). We assume that the effective mobility of a Rouse segment is determined by the mean diffusivity, as is consistent with the observation that the isotropic–nematic transition has little measurable impact on the monomeric friction coefficient (Figure 3.9).

This physical picture complements one suggested by Hall et al. [59] to explain tracer-diffusion data that seemed to indicate a strong *decrease* in the constraining tube diameter upon cooling from the isotropic to the nematic state for *main–chain* liquid–crystalline polymers. In this situation, the mesogenic unit is incorporated directly into the polymer backbone, and therefore necessarily lies along the chain contour. Hence, the cage of surrounding mesogens in the nematic phase further confines movement transverse to the backbone relative to the isotropic phase. In contrast, the mesogens in PM6M and PM6B lie perpendicularly to the backbone;

nematic order thus facilitates movement normal to the backbone contour.

To test the physical interpretation suggested above, one might investigate the molecular weight-dependence of the viscoelasticity of a SG-LCP whose mesogens tend to be *parallel* rather than *perpendicular* to their local backbone segment. In such a case, if the directional diffusivities indeed follow the order $D_{\|} > D_{\perp} \simeq D_{iso}$, one might expect the low-frequency relaxation dynamics of the nematic to differ comparatively less from the isotropic phase. Since phenyl benzoate mesogens with six-carbon spacers are known to have such a parallel coupling to an acrylate backbone [56], the viscoelastic response of nematic and isotropic P**A**6M and P**A**6B should be characterized to see if the drop in modulus is absent in that system.

3.4.3 Strain-Hardening in the Nematic Phase

The strain-dependence of G^* in the isotropic and smectic phases is in accord with the behavior expected of amorphous melts and layered liquids, respectively. However, the nematic phase shows strain-hardening behavior which is not expected to arise from either the flexible backbone or the nematic liquid structure. This anomalous strain dependence at low frequencies and strains above 10% (Figures 3.10a, 3.10b, 3.11a & 3.11b) may be due to the tendency of the mesogens to orient perpendicular to the backbone in the present SG-LCP, since the mesogens attached to a given strand may be forced to adopt an intermediate orientation between that dictated by the backbone segment and that dictated by the local orientation of the director.

This compromise (which may involve a reduction in the order parameter or a

distortion of the spacer conformation or both), gives rise to a higher energy state for the local fluid structure. This increase in energy would be associated with an additional contribution to the modulus. If this contribution grows non-linearly with strain, it could explain the observed strain-hardening behavior. A more detailed discussion of this mechanism for strain-hardening and its relationship to a mechanism for flow-induced alignment of nematic SG-LCPs is given in the next chapter.

3.4.4 Effect of Shear History on the Smectic Phase

As has been found in other studies of the effect of shear on smectic phases, the modulus of the present SG-LCPs decreases when the smectic phase is subjected to shearing. That this does not produce a well–aligned material is also in accord with previous studies [49]. Surprisingly, we observe an *increase* in the dynamic modulus of the smectic phase produced by a history of shear in the nematic phase. The partial transparency of the smectic sample upon cooling from the aligned nematic state indicates a residual degree of alignment. A bias in the orientation distribution of the smectic could lead to the observed increase in the modulus, as has been established for other layered systems. In particular, when lamellae are oriented edge-on to the flow (layers tangent to the flow direction), lamellar block copolymers exhibit a lower modulus than the unaligned material; when the layers are broad-side to the flow (i.e., lamellae normal to the flow direction), the modulus is higher than that of the unaligned material [48]. If the smectic SG-LCP has a similar dependence of G^* on the orientation of the lamellae, then the increase in modulus would indicate that

shearing in the nematic and cooling into the smectic leads to formation of layers biased such that the lamellae tend to lie normal to the direction of flow. However, the relationship between layer orientation and modulus in smectic SG-LCPs has not yet been established. Since the backbone in the smectic phase is in a highly distorted state ($R_{\parallel}$:$R_{\perp} \approx 4$) [56], its contribution to the modulus may be anisotropic. This could have the consequence that layers normal to the vorticity axis may have the highest modulus. To resolve these issues we must 1) determine the lamellar orientation distribution in a smectic obtained from a previously sheared nematic, and 2) establish the effect of orientation on the dynamic modulus of smectic SG-LCPs.

A second possible explanation of the increase in modulus of the smectic phase obtained by cooling a shear-aligned nematic is that this flow and thermal history profoundly changes the microstructure of the smectic relative to the polydomain smectic SG-LCP. Instead of merely changing the orientation distribution of the layered structure, the process of heating to the nematic state, shearing, and re-quenching to the smectic phase may induce changes in the detailed organization of the fluid at the molecular level. Indeed, this is suggested by the fact that this treatment alters the relaxation signature of the smectic at *all* accessible frequencies.

3.5 Conclusions

By examining a series of PM6M fractions with molecular weights ranging from 3×10^5 to 3×10^6 g/mol, we have determined that the effect of the isotropic–to–nematic transition on the flow behavior of the melt has a strong molecular-weight

dependence. At high molecular weights ($M_w \geq 3 \times 10^5$ g/mol), the dynamic moduli at low reduced frequencies are significantly lower in the nematic than in the isotropic state. For lower molecular weight samples the nematic and isotropic phases have virtually identical rheological behavior. Because rheological consequences of liquid-crystallinity are observed only for entangled chains, we formulate a preliminary explanation within the context of the reptation model. We hypothesize that the decrease in plateau modulus indicates that nematic order increases the effective tube diameter relative to that in the isotropic phase; the enhanced mobility of the mesogens parallel to their long axis may lead to this increase in the amplitude of lateral fluctuations of the polymer backbone.

An unusual strain-hardening phenomenon is observed in the nematic phase of these SG-LCPs, which we attribute to a combination of (1) a strain-induced distortion of the polymer backbone which drives an energetically unfavorable disruption of the mesogen field, and/or (2) nematic hinderance of the preferred perpendicular orientation between the backbone and mesogen, thus leading to energetically unfavorable relative orientations.

We find that flow-induced alignment of the nematic phase is possible for all the molecular weight fractions of the SG-LCPs used in this study. Contrary to assertions presented in the recent literature [35], the linear viscoelastic response of the nematic phase need not be markedly different from the isotropic phase in order for flow to be an effective means of producing aligned materials. Shear can, plausibly, induce alignment by perturbing the conformation of the backbone and biasing the orientation

of the mesogens due to coupling through the spacer.

We find an appreciable drop in the modulus of the smectic phase after many cycles of large–amplitude oscillatory shear; however, the sample remains turbid throughout the shearing process, indicating that a high density of defects remains. A smectic material heated into the nematic phase, shear-aligned, and cooled to the smectic phase shows an *increase* in modulus. We have put forth two possible explanations: one hypothesis attributes the sample's increased modulus to a change in the orientation distribution of the smectic layers; the second attributes the increase in modulus to change in the local organization of the fluid structure in the smectic SG-LCP melt. To discriminate between possibile explanations of this phenomenon, we propose that it may be useful to determine both the lamellar orientation and backbone conformation in sheared smectic SG-LCPs, and to characterize the effect of lamellar orientation on the dynamic moduli of smectic SG-LCPs.

Chapter 4

Alignment of Side-Group Liquid-Crystalline Polymers Using Large-Amplitude Oscillatory Shear

4.1 Flow-Induced Alignment in Liquid-Crystalline Polymers: Introduction

Macroscopically oriented materials are essential for many of the technological applications of side-group liquid crystalline polymers. Towards this goal, the use of flow fields can form the basis of a simple, economical method to obtain macroscopically anisotropic materials, which in turn necessitates a knowledge of the dynamics of alignment of SG-LCPs together with their rheological properties.

Past studies have shown that shear flow can be used to align mesophasic polymeric materials such as block copolymers [60] and main-chain LCPs [44]. Even exceptionally small deformations ($\leq 10\%$) can align SG-LCP elastomers [17]. Until recently, it was believed that nematic SG-LCP melts could not be aligned using flow [43] and as discussed in Chapter 3, this conclusion was based on the observation that for nematic SG-LCP melts the viscoelastic properties were dominated by the flexible backbone [35, 41, 43]. However, Kannan and coworkers [1, 42] have shown that oscillatory shear can induce macroscopic alignment in nematic SG-LCP melts. The earlier discussion in Chapter 3 shows that the linear viscoelastic response of the nematic phase need not be markedly different from the isotropic phase in order for flow to be an effective means of producing aligned materials. While shear can, plausibly, induce alignment by perturbing the conformation of the backbone and biasing the orientation of the mesogens due to coupling through the spacer, it can, with arguably equal plausibility, induce alignment on account of the anisotropic flow properties of liquid crystals.

Past studies of the conformation of the backbone of magnetically aligned SG-LCPs have shown that the backbone of a macromolecule with a repeat unit similar to that of the SG-LCPs studied in the present investigation (Figure 3.1) is perturbed slightly from a random coil configuration when the melt is in the nematic phase [56]. In particular, one can describe the "ellipsoid of gyration" of the backbone as oblate with axis of rotation oriented parallel to the director. This implies that in PM6M and PM6B, the mesogens and the backbone tend to orient perpendicularly to each other [7, 61]. The analogous SG-LCP networks show the same relative orientation under extensional deformation [62]. The time required to align SG-LCPs in magnetic fields depends significantly on the coupling between the mesogen orientation and that of the backbone, and appears to be limited by the overall conformational relaxation time of the polymer chain [55]. Such a coupling between the mesogens and the backbone suggests a mechanism of flow-induced alignment that originates with the distortion of the backbone and propagates out to the director due to the correlation between the mesogen and backbone orientation. Under the mild flow conditions that produce shear-induced alignment, the backbone conformation is expected to be biased along an axis close to the extensional axis and tipped toward the flow direction. In analogy to SG-LCP networks [17, 62, 63], this may drive the director field to align perpendicular to the extensional axis of the shear flow. To test the feasibility of this mechanism, we characterize the direction of mesogen alignment induced by flow. In addition, we consider how a change in the relative orientation of the backbone with respect to the mesogens during shear may also explain the observed strain hardening of SG-LCPs.

Alternate mechanisms might be proposed based on the flow behavior of other liquid crystals or other intrinsically anisotropic polymer melts. In shear flow of small molecule LCs and of LCPs, there are numerous regimes of flow behavior; in regimes in which shear biases the orientation of the director, it generally favors the flow direction [64]. Therefore, if a similar mechanism were responsible for the alignment observed in SG-LCPs it would lead to a different orientation of the mesogens than the preceding mechanism.

Liquid crystals possess anisotropic viscosity coefficients termed *Miesowicz viscosities* [10]; in the most extreme situations, the viscosity ratios vary from 4 for small molecule LCs [11] to about 100 for lyotropic rod-like LCP solutions [65]. If the present SG-LCP has such an anisotropy in viscoelastic properties, this could provide a mechanism for flow-induced alignment, and could cause the drop in the modulus of SG-LCPs upon alignment [1]. To further support this hypothesis, we note that other intrinsically anisotropic macromolecular media, such as ordered block copolymers (BCPs), also become aligned during oscillatory shear. In BCPs, anisotropy in the viscoelastic properties appears to play an important role, with the microstructure aligning along a direction characterized by a lower viscosity than the unaligned material [66]. To ascertain whether a similar alignment mechanism could cause a reduction in the modulus of ordered SG-LCP melts, we measure the mechanical properties of SG-LCP samples aligned along a chosen direction by annealing in a strong magnetic field. To our knowledge, these are the first measurements of the dynamic mechanical properties of magnetically-aligned aligned SG-LCP melts.

The drop in the dynamic moduli during large-amplitude shearing [42] may possibly be attributed to melt fracture: a phenomenon not uncommon in conventional homopolymer melts. Such materials often exhibit shear instabilities which result in a significant drop in the shear stress during large amplitude oscillatory shear [67–70]. These instabilities can also be manifested by stress oscillation becoming non-sinusoidal at longer times, and by the sample appearing severely cracked and crumbled [70]. Melt fracture has been shown to occur at strain levels comparable to those used in our study [53, 70]. In light of these findings, we investigate the possibility that melt fracture may be occurring in the present SG-LCP sample causing the drop in the modulus observed during large amplitude shearing.

The following sections describe experiments that characterize the direction of alignment induced by flow and the effect of director orientation on the dynamic moduli. We will present the first results on the mechanical properties of magnetically aligned SG-LCPs. We will discuss the implications of our results regarding the mechanism of shear-induced alignment in SG-LCP melts.

4.2 Materials, Apparatus and Methods Used to Study Flow Alignment

Materials The side-group liquid-crystalline polymers chosen for the this portion of the current investigation were two PM6M samples named PM6M-11 and PM6M-8. The properties of PM6M-11 have been listed in the experimental section of

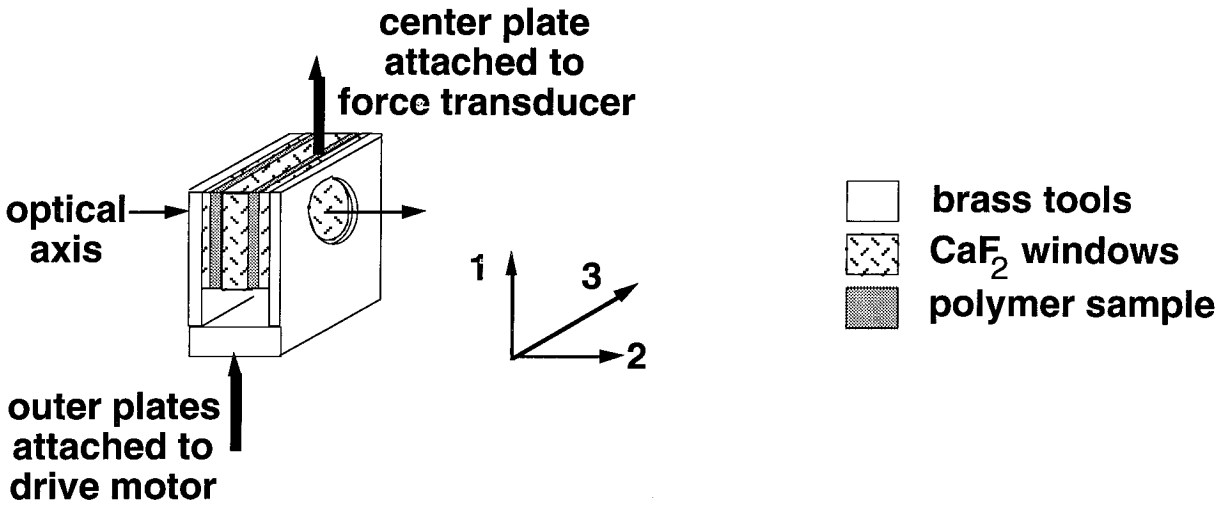

Figure 4.1: Shear sandwich flow cell for measuring transmittance in the 1,3-plane and the mechanical properties of shear-aligned and magnetically aligned samples.

Chapter 3. PM6M-8 has the sample repeat unit structure as PM6M-11, with $M_w \approx 7.8 \times 10^5$ g/mol with $M_w/M_n = 1.41$ (phase transitions: g 315K (44 ± 2°C) n 383K (110°C) i, where g =glassy, n = nematic and i =isotropic).

Apparatus Shear alignment and mechanical characterization of the sample were performed using a Rheometrics Solids Analyzer (RSA II). All the rheological experiments were conducted under oscillatory shear, in the shear sandwich geometry (Figure 4.1). The sample dimensions were 15.95 mm × 12.6 mm × 0.35 mm, giving an optical path length of 0.7 mm. Windows were used to permit transmittance measurements, and to view the sample through crossed polarizers during the alignment process using a long distance microscope (magnification 10X). For transmittance measurements, we use a visible (HeNe) laser source ($\lambda = 633$ nm), collect the transmitted light using a lens and monitor the intensity using a photodetector.

In the rheometer, the optical path length is ≈ 0.7 mm, which leads to a retardation

of many orders when the nematic sample becomes aligned during shear. To determine the direction of mesogen orientation upon flow-induced alignment, the gap must be sufficiently thin that the retardation is less than a few orders. Therefore, we also performed experiments in the two flow cells described in Chapter 2 (Section 2.4).

Methods To erase any effect of previous history, the sample is heated well into the isotropic state (130°C) and equilibrated at that temperature for 20 minutes. The sample is then cooled to the desired temperature with a 20 minute equilibration time. Two types of oscillatory shear protocols were used: (1) frequency sweep measurements, where a small strain ($\leq$ 3%) is used to characterize the dynamic response and (2) prolonged, large amplitude (typically 100%) oscillatory shear at a chosen frequency. We study the response of the sample to a sinusoidal strain: $\gamma = \gamma_o \sin \omega t$, where γ_o is the magnitude of strain. The stress in the linear viscoelastic regime is described by $\sigma = \gamma_o\{G' \sin \omega t + G'' \cos \omega t\}$. During shear at large strain, the shear stress still oscillates with the frequency of the applied strain, but with amplitude and phase that change with time. Hence, σ can be described using effective moduli, $G'_{eff}(t;\omega,\gamma_o)$ and $G''_{eff}(t;\omega,\gamma_o)$.

To study the mechanical properties of the magnetically aligned sample, we annealed the samples in a 7 Tesla superconducting magnet prior to dynamic mechanical measurements. The magnetic field aligns the mesogens along the direction of the field due to the positive anisotropic diamagnetic susceptibility of the mesogens. The sample was loaded in the flow cell (Figure 4.1), and placed in the magnetic field so that the mesogens can be aligned along a chosen direction. The sample temperature of the

flow cell while in the magnet was controlled to within ±1°C (Omega^{TM} controller CN 2011 with Kapton^{TM} flexible heaters and a Type T thermocouple). Once mounted in the magnet, the sample is heated to 125°C (isotropic) at a rate of 1°C/min and held at 125°C for 20 minutes so that any previous history is erased. It is then cooled to 110°C (nematic state) at a rate of 0.15°C/min, and held at 110°C for 12 hours. After this long annealing period, the sample is brought to room temperature (to the glassy state) at 0.5°C/min. In contrast to the opaque, unaligned polydomain nematic glass, after magnetic alignment the sample has considerable transmittance (typically 30% of that in the isotropic state), indicating that although the magnetic field did not produce a perfect monodomain, it was effective in aligning the sample, since, there must be a significant enhancement in alignment and a decrease in the number of defects for such a thick sample (d=0.7 mm)to appear translucent. Once the sample is removed from the magnetic field, the flow cell is loaded into the RSA II and tested at temperatures above T_g but below $T_{ni} - 7°C$ with small strain frequency sweeps.

4.3 Results

4.3.1 Optical Characterization During and After Shear Alignment

A sample that is cooled from the isotropic (Figure 4.2a) into the nematic phase in the absence of an applied field or surface effect is a macroscopically unaligned polydomain material. It appears turbid due to the large density of defects (Figure 4.2b). When

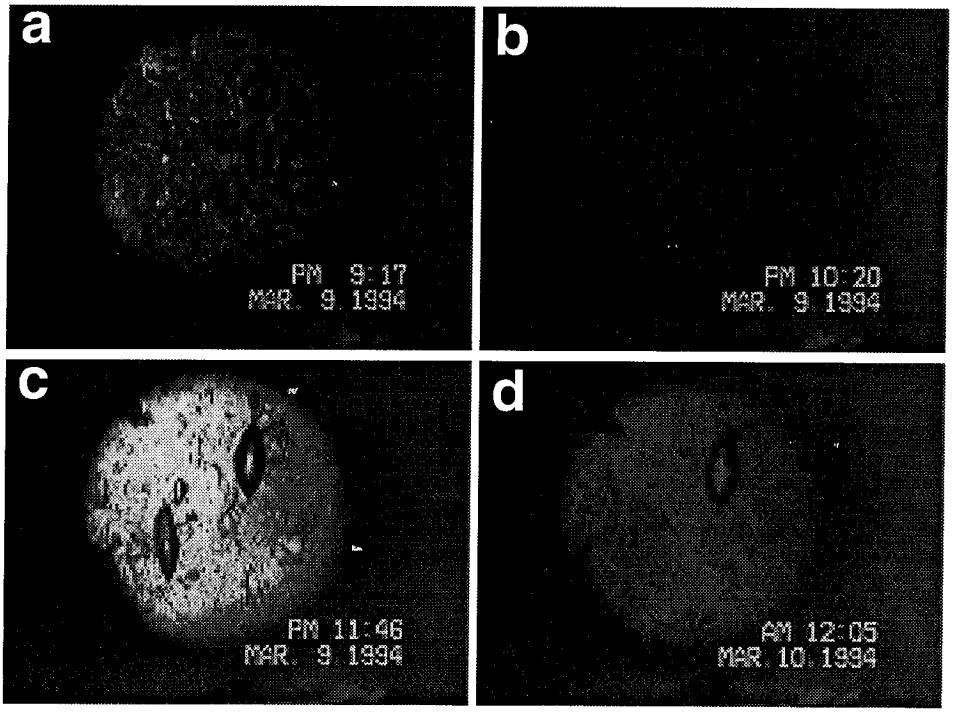

Figure 4.2: 10X magnification of PM6B-5 between crossed-polars [$\pm 45°$ w.r.t. flow direction (vertical)]: **(a)** isotropic, **(b)** nematic, **(c)** "flow–aligned" nematic ($T = 110°C$, after 90 cycles at $\omega = 0.1$ rad/s, $\gamma = 90\%$), **(d)** "flow–aligned" nematic cooled to smectic ($T = 100°C$).

we apply large amplitude shear to PM6M-11 in an initially polydomain nematic state, it becomes translucent (Figure 4.3a) and highly birefringent (Figure 4.2c) within the first 2-3 cycles of shear at 0.1 rad/s with 100% strain at 110°C. The transmittance (T) reaches a value of more than 80% within the first two minutes (Figure 4.3a, inset). Further prolonged shearing does not change the transmittance appreciably. Upon cessation of large amplitude shearing, there is a decrease in the transmittance of the sample (Figure 4.3a). It falls to about 73% within the first few minutes, followed by a more gradual decrease to approximately 40% over a period of 10 hours.

To determine the sign of the birefringence upon flow-induced alignment, we observed PM6M-8 during shear in the parallel plate device that could be mounted on a

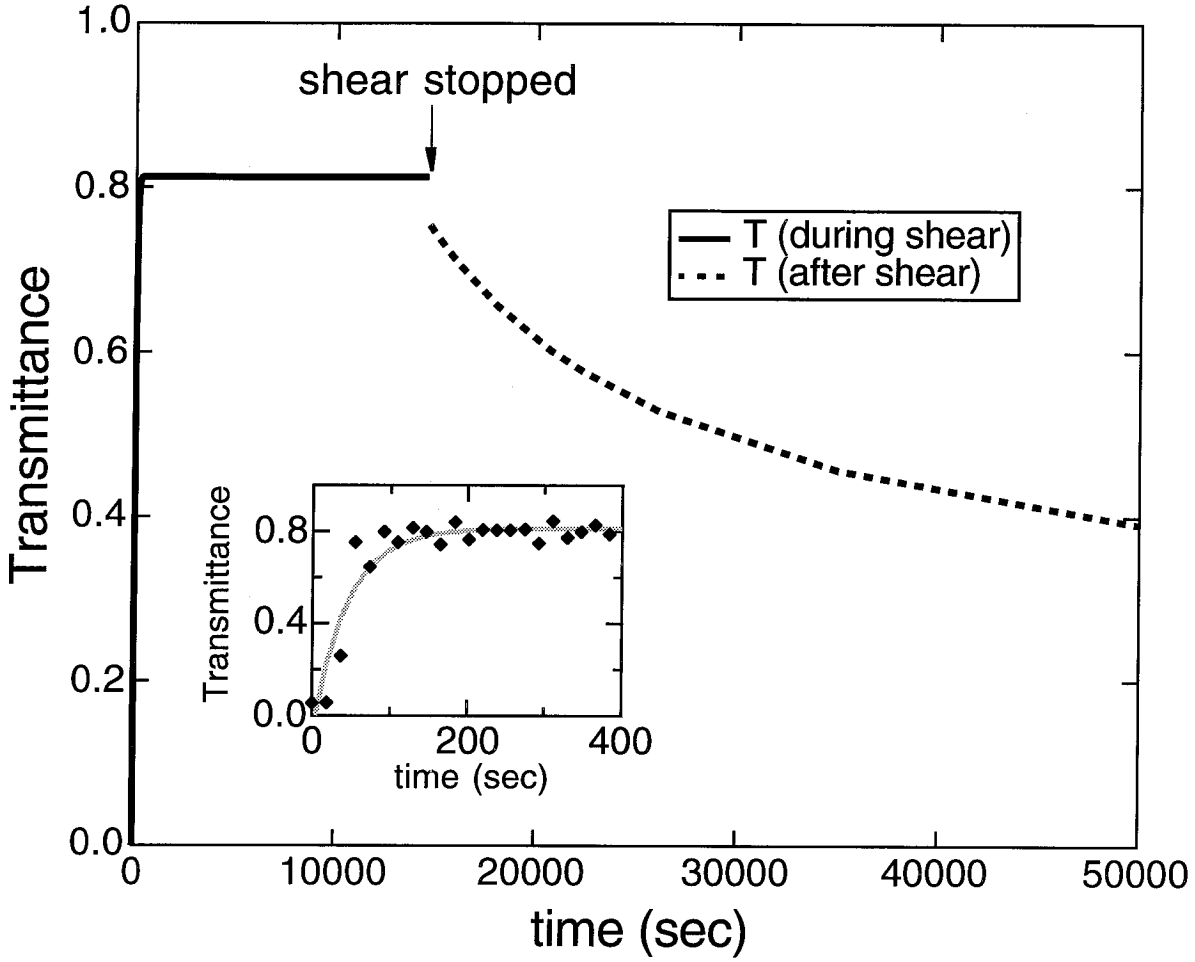

Figure 4.3a: Transmittance during and after shear-induced alignment at 0.1 r/s with 100% strain at 110°C for 4 hours ($T = \frac{I}{I_{iso}}$, where I is the average of the dc component of the transmitted intensity over one shearing cycle and I_{iso} is the transmitted intensity in the isotropic state).

polarizing microscope (described in section 2.4). The sample was first heated to the isotropic state ($T = 120°C$) for 20 minutes to erase any effects of the flow history associated with sample loading. No transmission of light was observed when the sample was viewed between cross-polars (Figure 4.4a). As earlier, the sample became turbid and highly scattering (Figure 4.4e) upon cooling to the nematic phase ($T = 95°C$).

The sample was then sheared at approximately 0.25 rad/s and at a strain of ap-

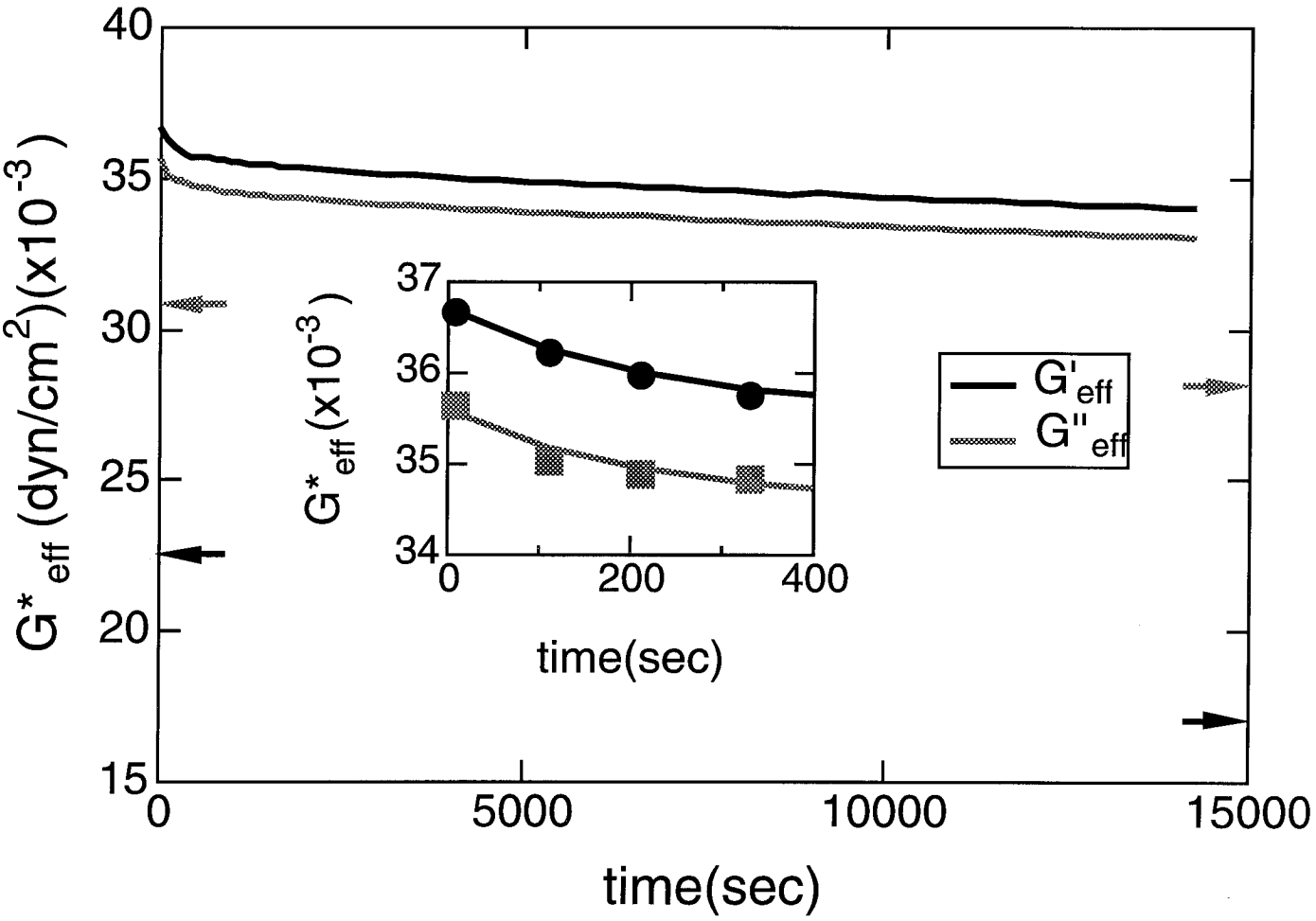

Figure 4.3b: Evolution of the effective storage and loss moduli (G'_{eff} and G''_{eff}) during the same shearing process as in Figure 4.3a. Arrows indicate the modulus measured at small strains before and after the alignment process.

proximately 100%. When viewed between crossed polarizers and illuminated with white light, the initially opaque, unaligned nematic became transparent to the eye after one cycle of shear ($\gamma_0 \approx 100\%, \omega \approx 0.25$ rad/s, $T \approx 95°$C). The sample was observed between crossed polarizers during one half of the shearing cycle *i.e.* from the point of maximum displacement in one direction to the point of maximum displacement in the opposite direction. For shearing direction at 45° with respect to the polarizer, both extrema of the cycle exhibited the highest intensity of transmitted

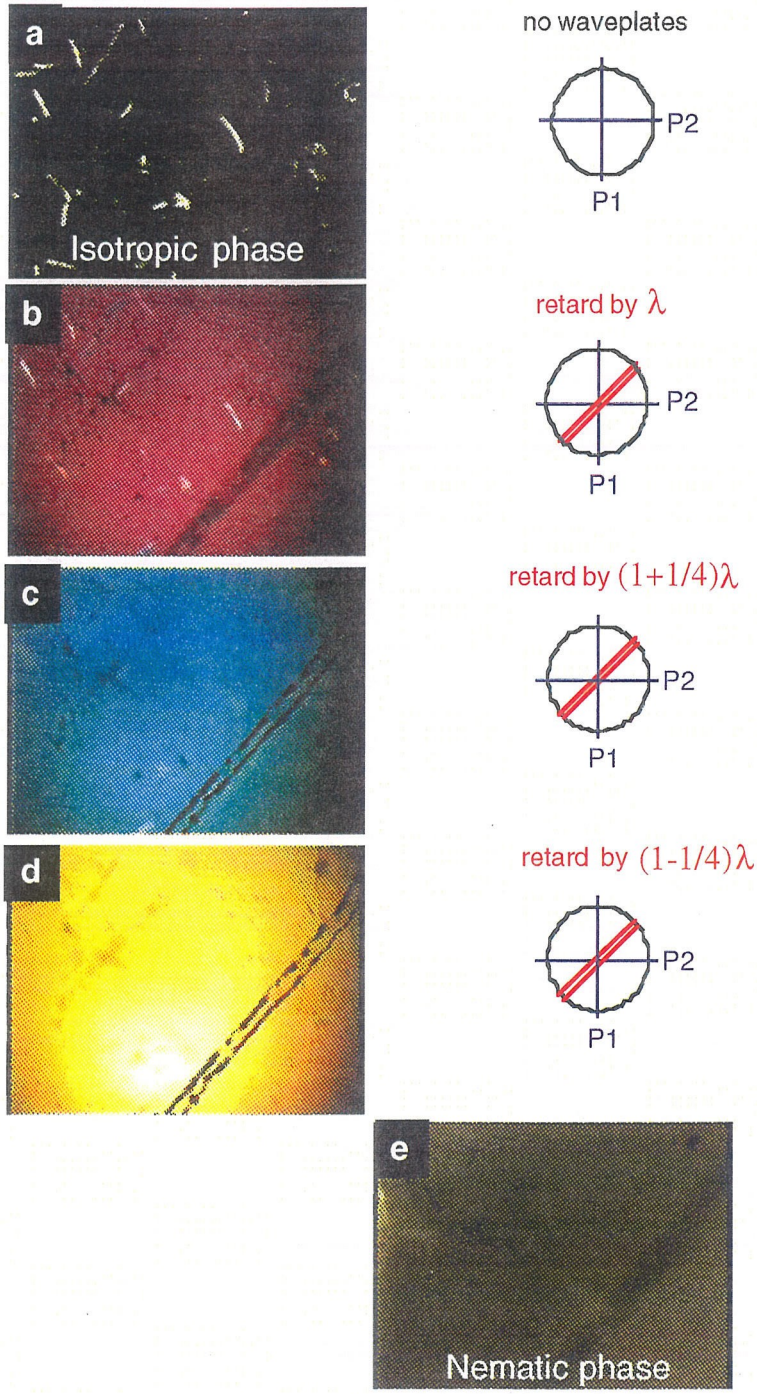

Figure 4.4: 2.5X magnification of PM6B-5 between crossed-polars (P1 and P2; vertical and horizontal) [±45° w.r.t. flow direction (vertical)]: **(a)** isotropic. Parts **(b)**-**(d)** show the intereference colors observed when an accessory (made up of by combinations of a full-wave plate with $\lambda = 530$nm and a quarter-wave plate) was inserted at 45° angle with respect to the polars (slow axis of the accessory is shown by the double line) **(e)** "poly-domain" nematic obtained by cooled the isotropic sample as shown in (a).

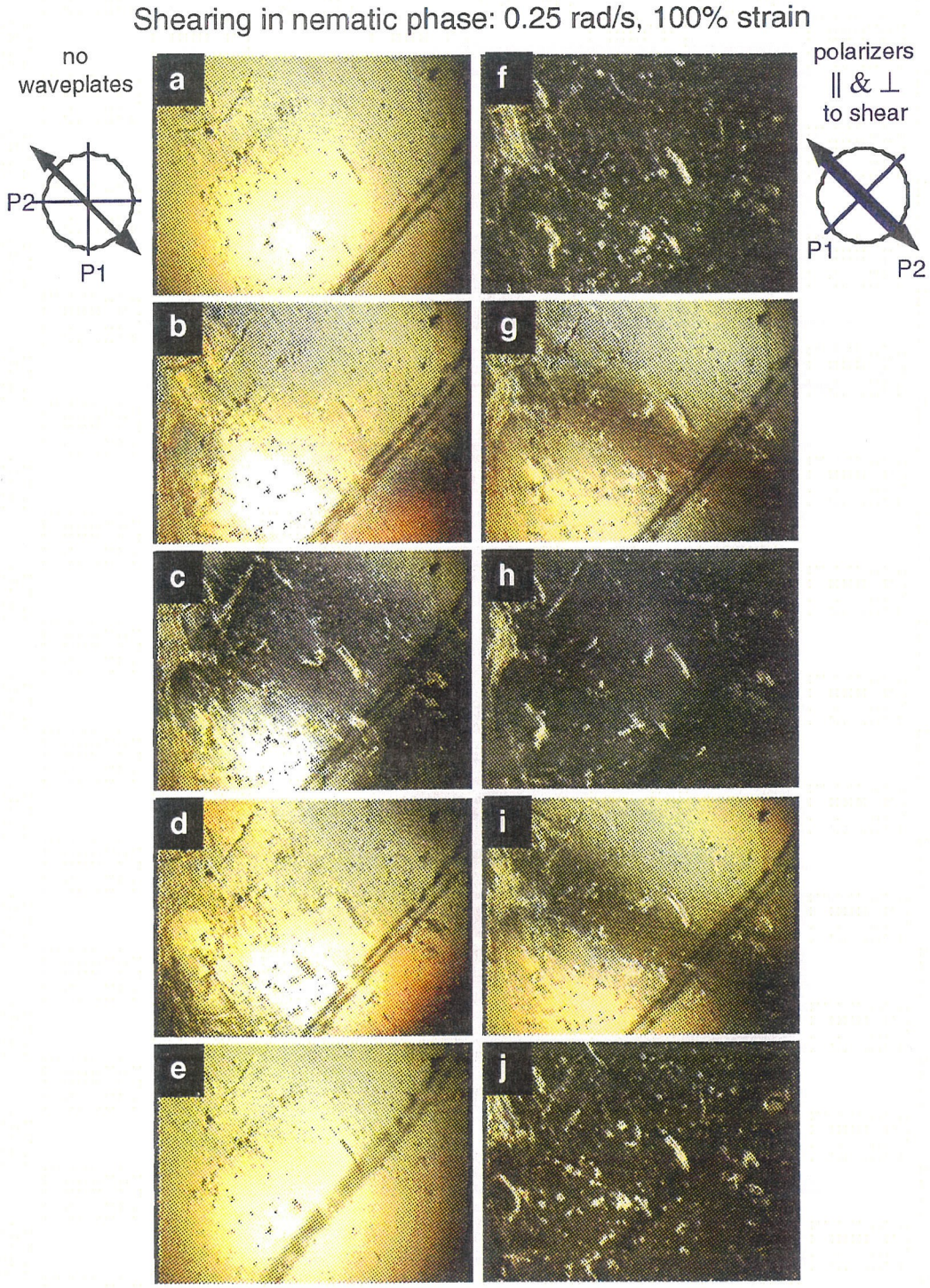

Figure 4.5: 2.5X magnification of PM6B-5 during shear and between crossed-polars. P1 and P2 (axes for the polars indicated by the blue lines). (a)-(e) shearing direction at 45° w.r.t. flow direction (indicated by the double arrow). (f)-(j) shearing direction parallel to flow direction. The double diagonal lines in the lower right hand corner were drawn on the glass slide to track the displacement during shear.

light (Figures 4.5a and 4.5e). At the point of zero displacement, the sample showed a range of colors. It was dark-grey in the center of the microscope view and became progressively lighter in areas away from the center (Figures 4.5c). Uniform extinction was not observed for any part of the cycle for a shearing direction that was at 45° to the polarizer. The polars were then rotated by 45° (keeping them crossed) such that they were parallel and perpendicular to the shearing direction. Now the sample exhibited uniform extinction at both extrema of the displacement cycle as well as at the point of zero displacement (Figures 4.5f, 4.5h and 4.5j). This suggests that the high transmittance observed when the sample is sheared at $\pm 45°$ to the polarizers is indeed due to a significantly uniform director orientation, and not a "depolarization" effect from a sample with decreased defect density but a low global order parameter.

When the shearing direction was at 45° to the crossed polarizers, a full-wave retarder plate was inserted into the light path between the cross-polars. The slow axis of the retarder plate was oriented perpendicular to the shearing direction (Figure 4.6). At the point of zero displacement, a shift in the intereference colors could be observed (Figures 4.6c and 4.6h). Large parts of the sample in the center of the view changed from dark and light grey to purple and deep blue. At the points corresponding to extrema in displacement, no shift in colors was observed upon insertion of the full-wave retarder plate. We also observed a shift in the intereference colors at the zero-displacement point when a retardation of $(1 - 1/4)\lambda$ or $(1 + 1/4)\lambda$ was introduced (Figures 4.7c and 4.7h). However, once again no shift in the colors was observed at the points corresponding to extrema in displacement indicating that here

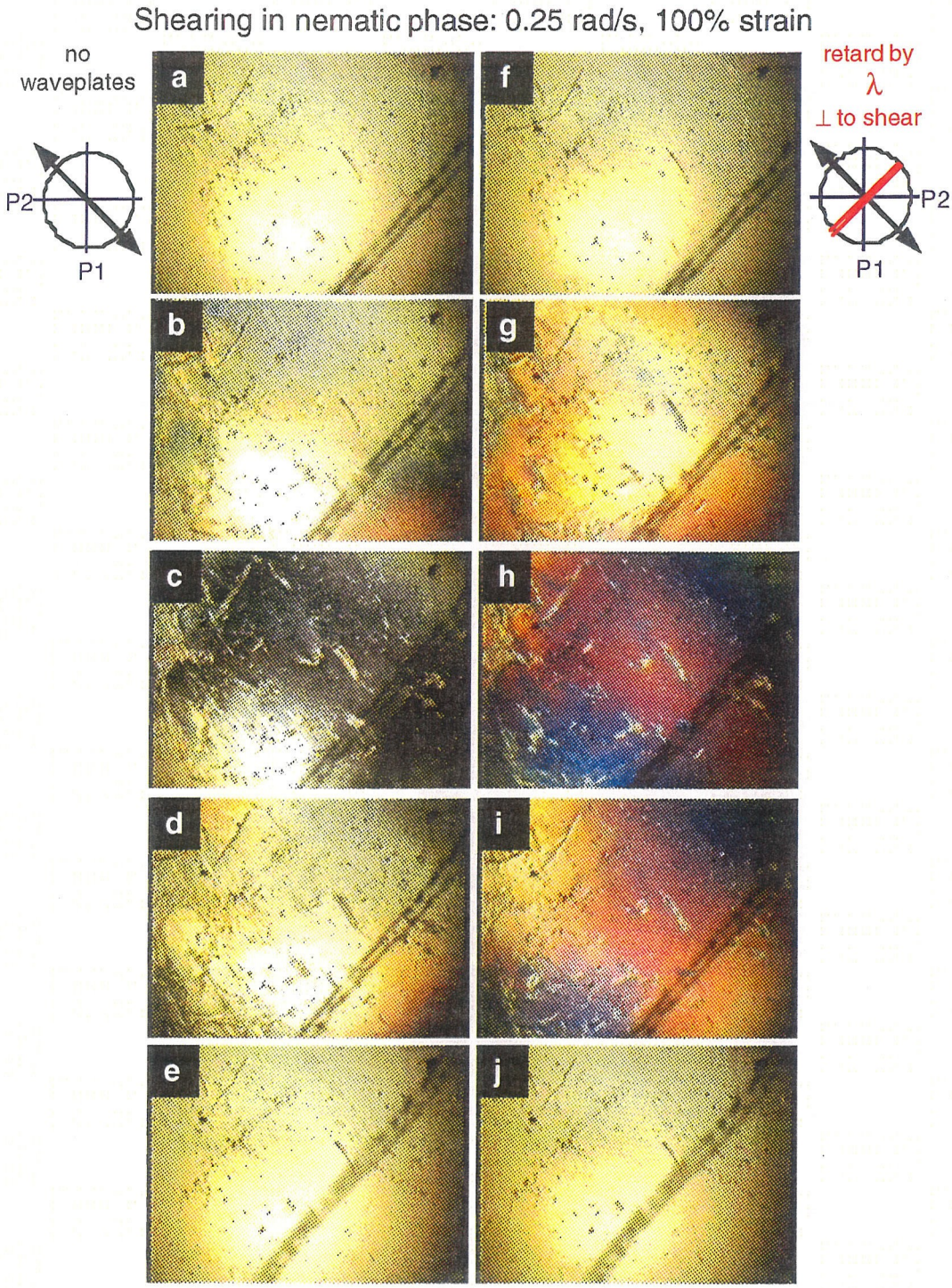

Figure 4.6: 2.5X magnification of PM6B-5 during shear and between crossed-polars. P1 and P2 (axes for the polars indicated by the blue lines) and shearing direction at 45° w.r.t. flow direction (indicated by the double arrow). **(a)-(e)** are reproduced from Figure 4.5 for comparison. **(f)-(j)** a full-wave retarder plate (retardation = $530nm$) has been inserted with its slow axis (indicated by the double red lines) perpendicular to the shearing direction.

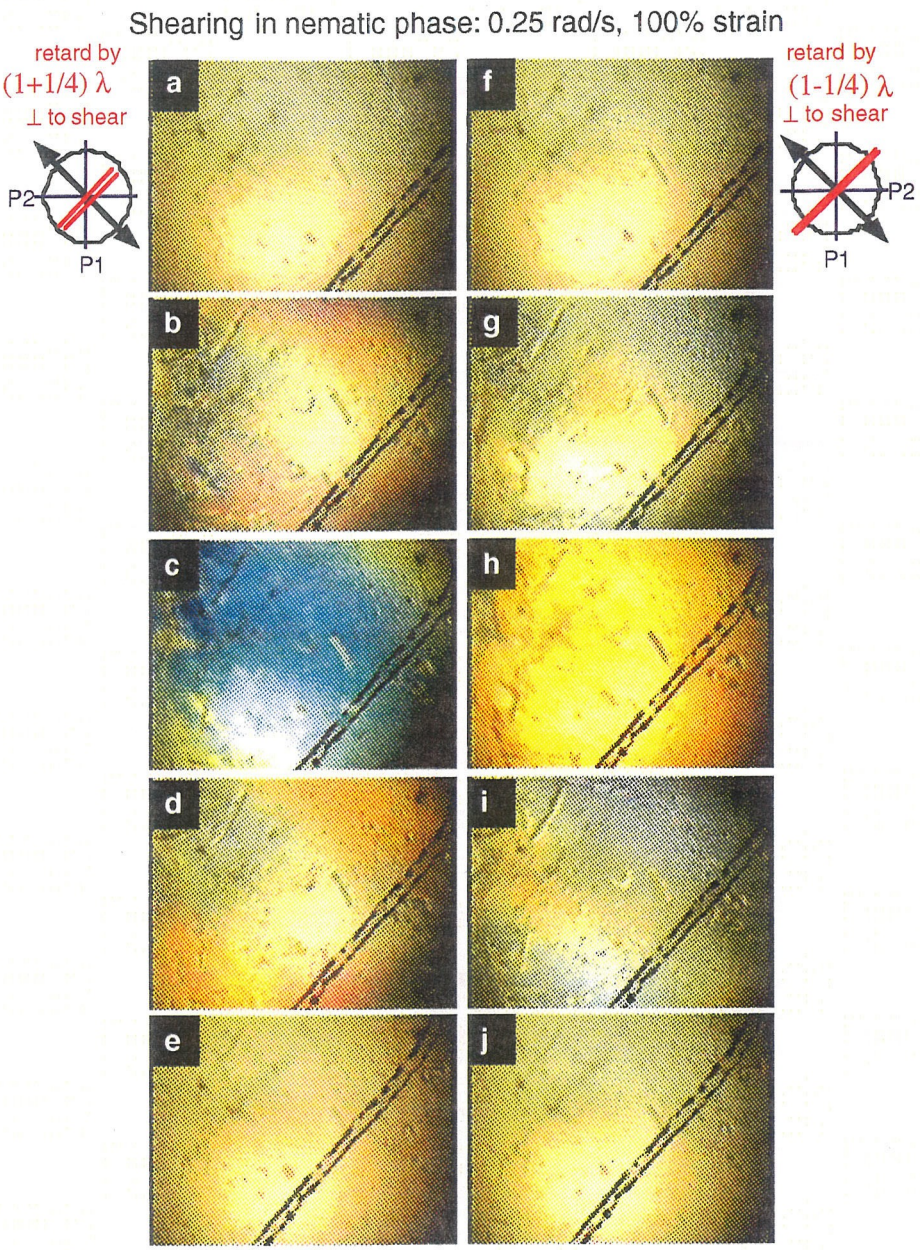

Figure 4.7: 2.5X magnification of PM6B-5 during shear and between crossed-polars. P1 and P2 (axes for the polars indicated by the blue lines) and shearing direction at 45° w.r.t. flow direction (indicated by the double arrow). **(a)-(e)** a combination full-wave retarder plate and a quarter-wave plate has been inserted such that both accessories have their slow-axes mutually parallel [producing an effective retardation of $(1 + 1/4)\lambda$] but perpendicular to the shearing direction. **(f)-(j)** the combination full-wave retarder plate and a quarter-wave plate inserted such that the slow axes of the two accessories are mutually orthogonal [producing an effective retardation of $(1 - 1/4)\lambda$]; the slow axis of the full-wave retarder plate is also perpendicular to the shearing direction.

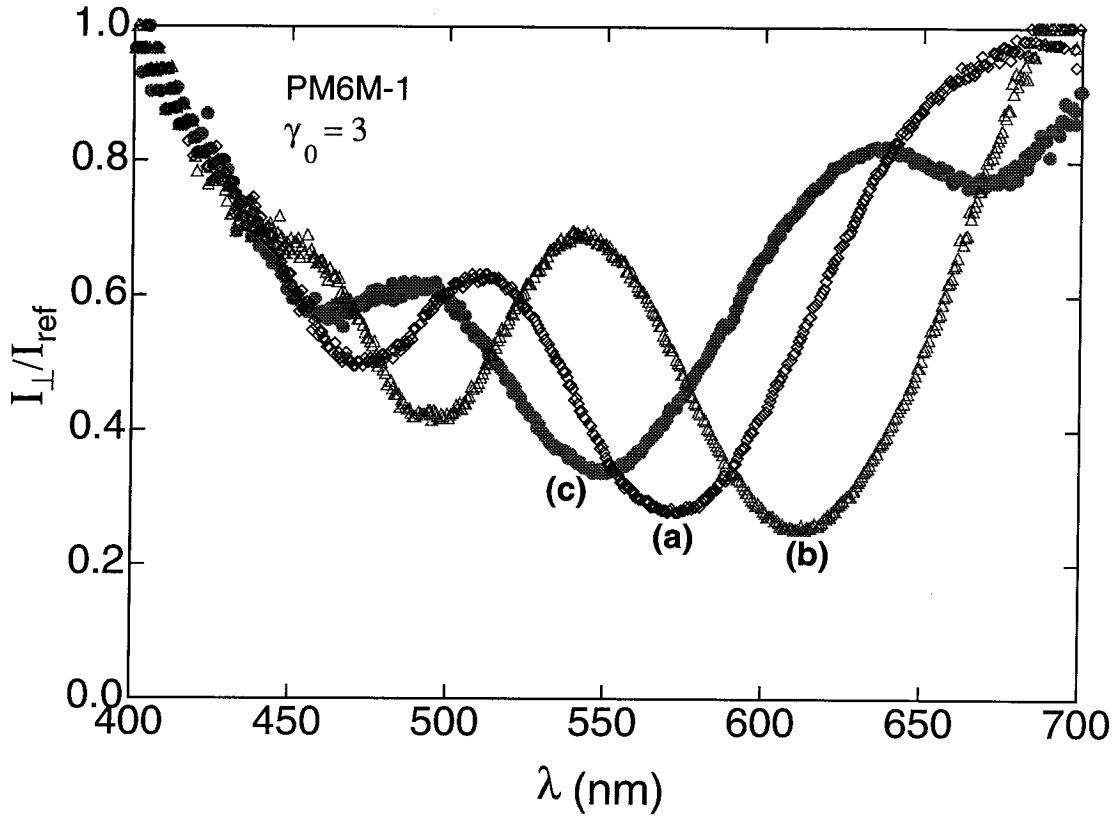

Figure 4.8: Normalized intensity obtained by transmission of light through cross-polars during shearing of a sample of PM6M-11. The sample was examined using a spectrographic birefringence technique (see section 2.3.2) and the data is shown for a point in shearing cycle corresponding to maximum displacement. **a** Sample between cross-polars, **b** Sample along with quarter-wave retarder plate that is oriented perpendicular to the shearing direction **c** Sample along with quarter-wave retarder plate that is oriented paralle to the shearing direction.

the retardation was over many orders. Therefore, to determine the orientation of the optical axis of the sample at points corresponding to the maximum displacement, the sample was observed using the spectrographic birefringence technique described in section 2.3.2. A step shear was applied with a strain amplitude of approximately 300% and the intensity transmitted between cross-polars was recorded as a function of wavelength of light (Figure 4.8a). A quarter-wave retarder plate was inserted into the optical path with its slow axis perpendicular to the shearing direction. The minima

in the intensity shifted towards higher wavelengths indicating that the net retardance increased (Figure 4.8b). Insertion of the retarder plate parallel to the shearing direction caused the minima in the intensity to shift to lower wavelengths indicating a decrease in the net retardance (Figure 4.8c).

4.3.2 Mechanical Properties During and After Shear

During shear, the effective dynamic moduli decrease by approximately 10% (Figure 4.3b). This decrease is more gradual than the increase of the transmittance. The true dynamic moduli (as opposed to the effective moduli) measured at the same frequency, $\omega = 0.1$ rad/s, but with small strains before and after the alignment process are indicated by arrows on the vertical axes. The moduli observed at 100% strain are significantly higher than those observed in the linear regime: at the inception of large amplitude shearing G'_{eff} is nearly 73% greater than G', while G''_{eff} is 16% greater than G''. Just after cessation of prolonged shearing, the strain hardening is even more dramatic, with G'_{eff} being twice as large as G'.

As discussed previously in Chapter 3, in the isotropic phase, the strain dependence of the dynamic moduli is like that of an amorphous homopolymer: the behavior is linear to strain amplitudes of 80%, with a hint of strain softening observed at 100% strain. However, the nematic phase shows a significant strain-dependence of G^*: for an unaligned nematic observed over the same range of strain amplitudes, at strains greater than 10% the modulus increases with increasing strain. At the frequency used for flow alignment experiments, the modulus observed at 90% strain

is approximately 75% greater than that observed in the linear regime ($\gamma_o \leq 3\%$), in agreement with the modulus observed at the beginning of prolonged large-amplitude shearing (Figure 4.3b). This strain hardening behavior is only observed at frequencies that correspond to reduced frequencies below ω_c' in the case of G' and ω_c'' for G'' (Figures 4.9a & 4.9b).

To characterize the impact of prolonged shearing on the mechanical properties of nematic SG-LCP melts, we perform frequency sweeps on the sample at small strains before and after shear alignment at high strains. Then, to monitor the subsequent recovery of the mechanical response to flow-induced alignment, we measure the viscoelastic spectrum's transient response over a 10-hour period following the shear-alignment process. In doing so, we find that the modulus is independent of strain amplitude in the range of 0.06% to 3% for all accessible frequencies at 110°C. Above a critical frequency, G' and G'' are insensitive to the state of alignment ($\omega_c' \approx 40$ rad/s, $\omega_c'' \approx 2$ rad/s). Below these critical frequencies, when measured within minutes after cessation of large-amplitude shearing, there is a significant drop in the dynamic moduli (Figures 4.9a & 4.9b). However, after several hours at 110°C, the low frequency moduli recover toward the values measured in the unaligned nematic state.

4.3.3 Mechanical Properties of Magnetically Aligned Samples

Using the protocol outlined in the previous section, we aligned the mesogens of the present SG-LCP in a magnet. Two directions of alignment have been investigated:

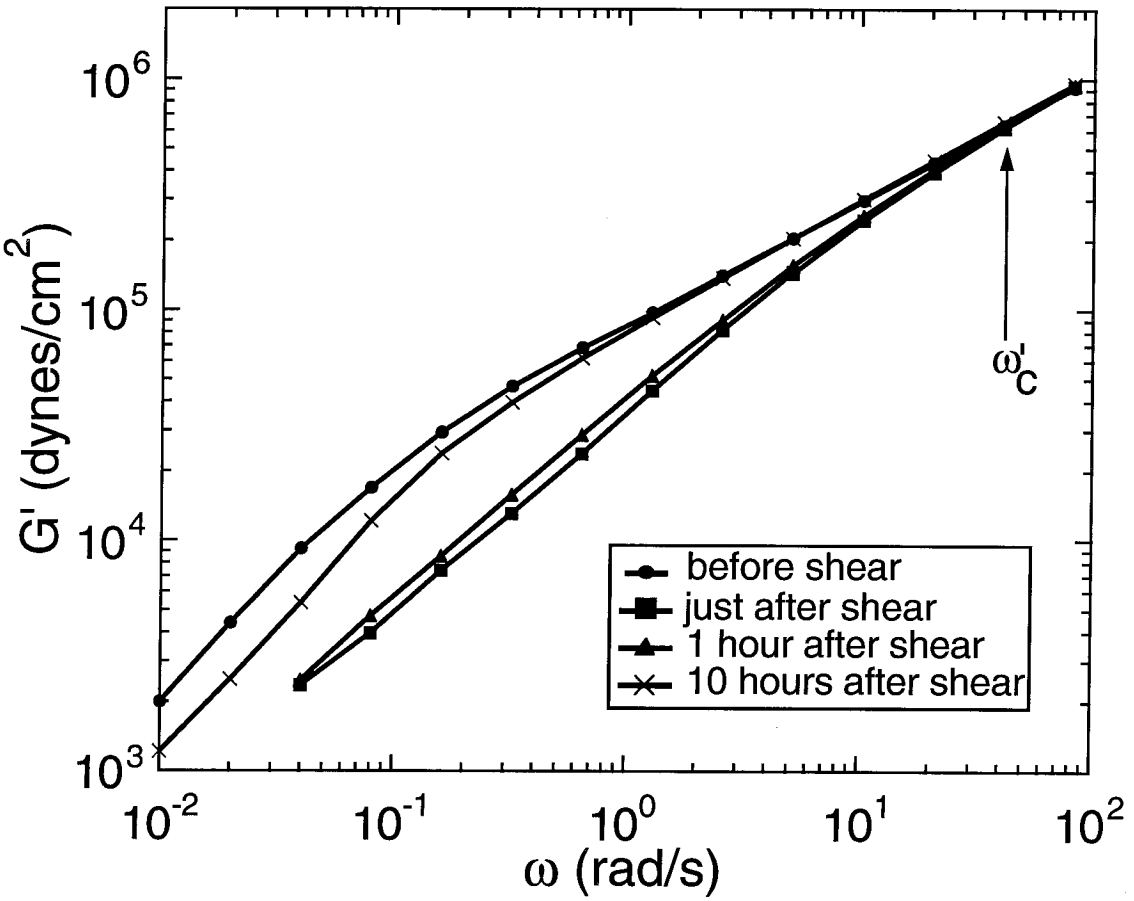

Figure 4.9a: Effect of shearing and subsequent recovery on the linear dynamic moduli G'. Shear-induced alignment at 0.1 r/s with 100% strain at 110°C for 4 hours. Lines drawn through the data points to guide the eye.

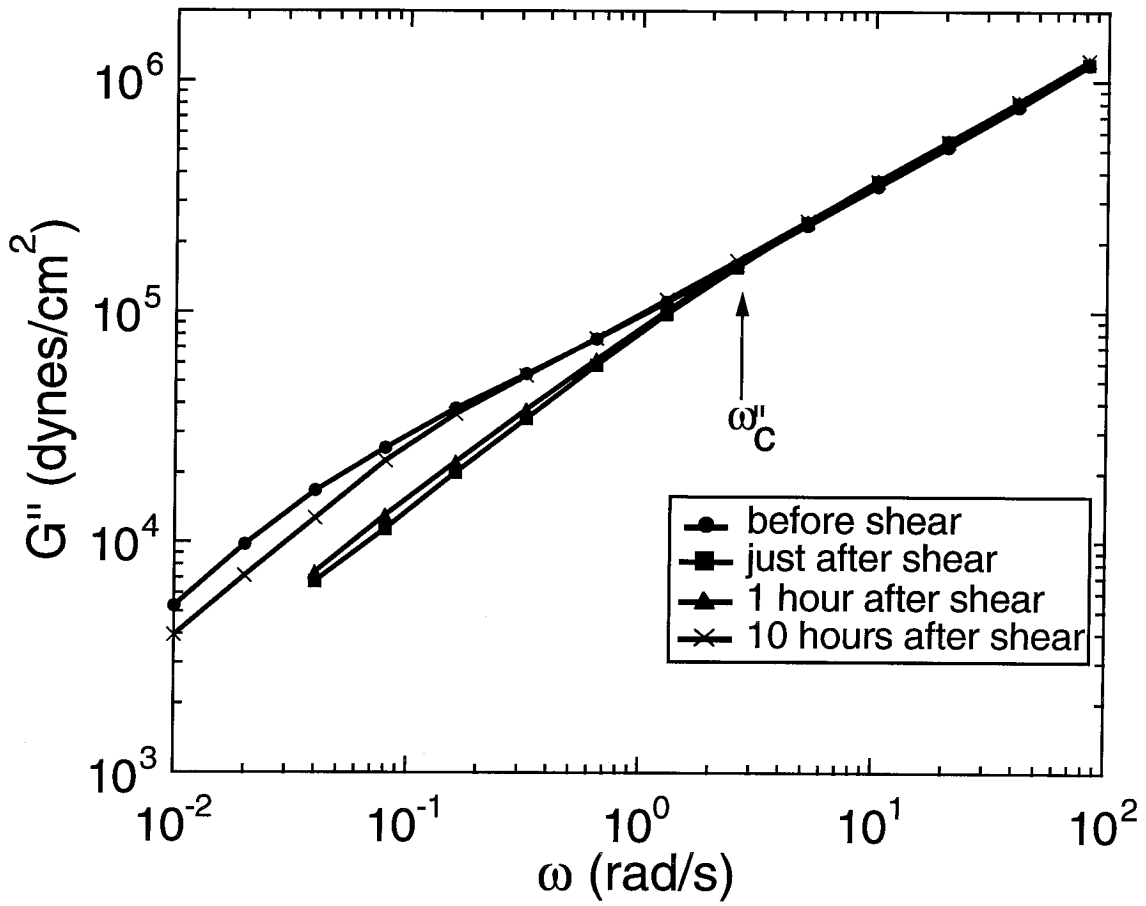

Figure 4.9b: Effect of shearing and subsequent recovery on the linear dynamic moduli G''. Shear-induced alignment at 0.1 r/s with 100% strain at 110°C for 4 hours. Lines drawn through the data points to guide the eye.

along the shear direction (direction 1 in Figure 4.1) and along the vorticity direction (direction 3 in Figure 4.1). Comparison of the small strain dynamic moduli of poly-domain, shear-aligned and magnetically-aligned samples (Figures 4.10a & 4.10b) at 110°C reveals the following features: (1) Above the critical frequencies (ω'_c and ω''_c) the moduli are insensitive to macroscopic (magnetic or shear-induced) alignment. (2) Throughout the experimental frequency range, the dynamic moduli of the unaligned sample and both of the magnetically aligned samples are nearly the same. Since

the moduli of the unaligned nematic can be thought of as a weighted average of the moduli with the director oriented in each of the principal directions, we infer that the dynamic moduli of a sample with the director aligned along the shear gradient direction would also be similar to that of the unaligned nematic.

4.4 Discussion

4.4.1 Magnetic Alignment

The dynamic moduli of the present SG-LCPs are insensitive to magnetic field induced alignment. This suggests the following: (1) Macroscopic alignment of the director does not reduce the modulus. This discounts an alignment mechanism based on anisotropy in the viscoelastic properties and suggests that the drop in the modulus upon shear-induced alignment is not due to macroscopic director alignment. (2) Elimination of defects alone cannot explain the drop in the low frequency modulus observed upon shear-induced alignment, as defects are minimized upon magnetic alignment as well. (3) At small strains, the distortion of the macroscopic director field must not contribute significantly to the moduli. On the other hand, the moduli may be dominated by the distortion of the polymer backbone. This is reasonable, because at the length scale of the backbone, the director orientation is uniform, irrespective of the state of macroscopic alignment. Thus, the dynamic moduli can be sensitive to the phase transition (evident below ω_c'), yet insensitive to the state of macroscopic alignment.

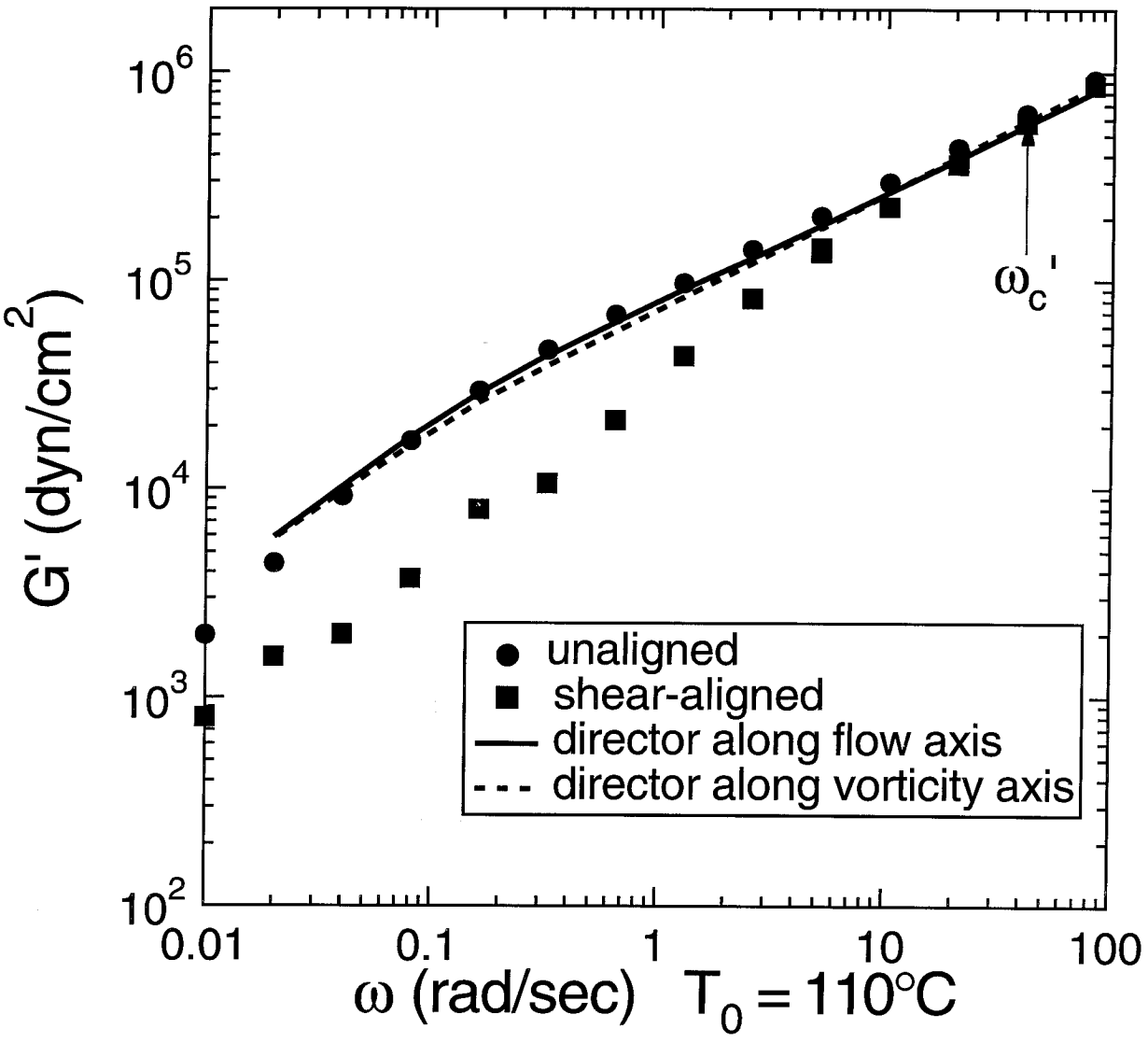

Figure 4.10a: Comparison of the effect of magnetic field-induced alignment and shear-induced alignment on the linear dynamic moduli G'. The data on the magnetically aligned sample are represented by lines through the data points, for clarity.

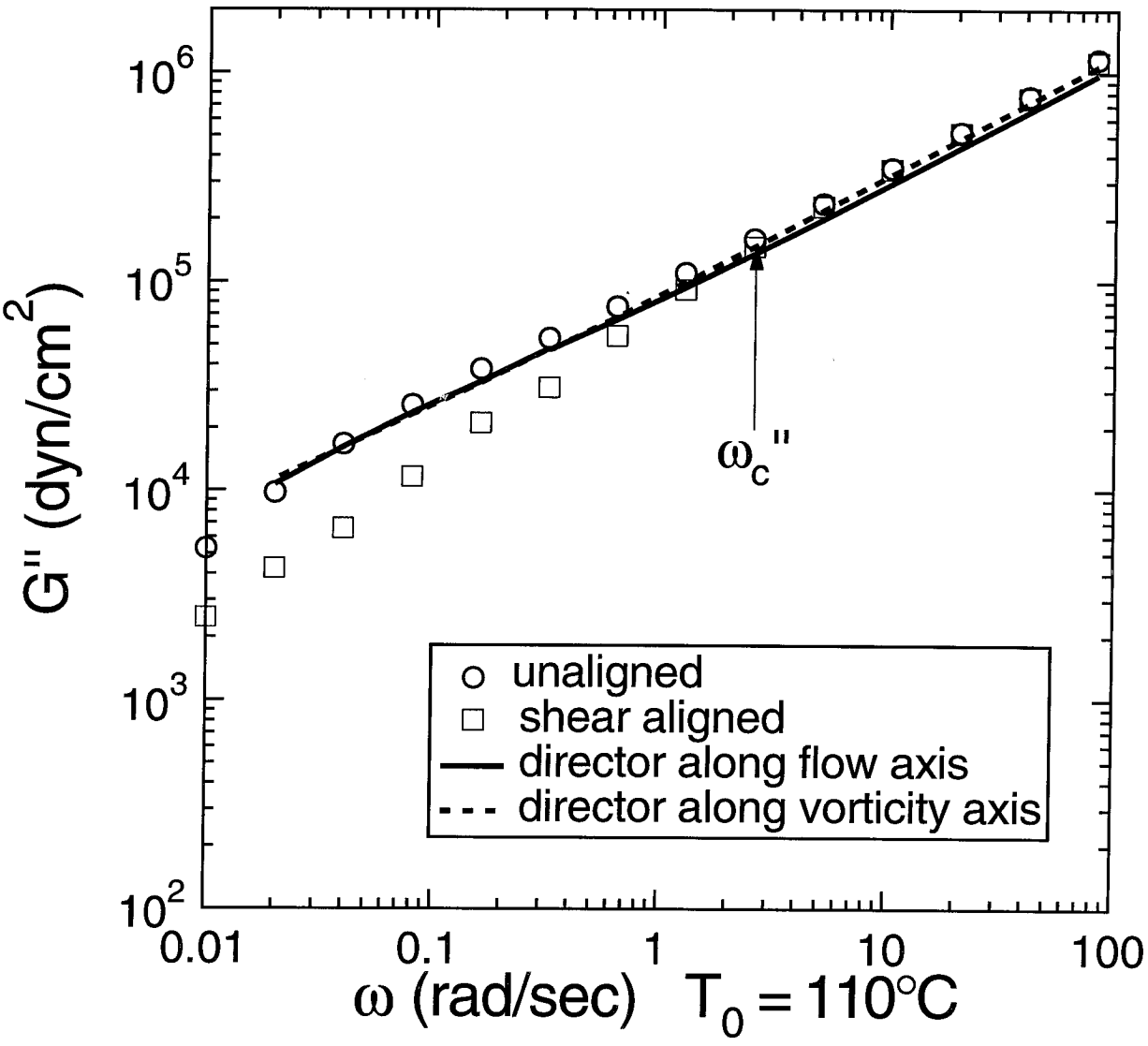

Figure 4.10b: Comparison of the effect of magnetic field-induced alignment and shear-induced alignment on the linear dynamic moduli G''. The data on the magnetically aligned sample are represented by lines through the data points, for clarity.

4.4.2 Strain Hardening

As shown in Figure 4.3b as well as in the previous chapter (Figures 3.11a and 3.11b), the present SG-LCP exhibits strain hardening behavior when strain is increased beyond the linear regime. Most flexible chain homopolymers are 'strain softening' in shear (the modulus decreases with increasing strain), with the non-linearity becoming significant when $\gamma_o \geq 100\%$. Strain hardening is usually observed only during extension and at high strains [71, 72], and is associated with chain branching, a high degree of entanglement or strain induced crystallization. It has also been observed recently in thermotropic LCP solutions in extensional flow ([73], for example), and attributed to the presence of residual crystallinity, polydispersity or contributions from the distortion of the director field. None of these applies to the present SG-LCP.

Since the flexible chain characteristics of SG-LCPs would suggest strain softening, and the distortion of the director field does not contribute significantly to the stress in the frequency range of interest, we focus on the role of the coupling between the backbone and the mesogens as a possible source of strain hardening.

As in the model suggested by Götz et al. [55] for the response of a nematic sample to an applied field, the average chain conformation of an SG-LCP within a domain having director $\hat{\mathbf{n}}$ can be described by an ellipsoid whose axis of rotation is oriented in a direction $\hat{\mathbf{n}}_B$. At equilibrium, $\hat{\mathbf{n}}_B$ is parallel to $\hat{\mathbf{n}}$. In the present sample, the backbone and the mesogens tend to be perpendicular to each other leading to an oblate ellipsoid of gyration (Figure 4.11a). In an unaligned sample, the domain size (*i.e.*, the length scale over which the director orientation is uniform) is typically of the

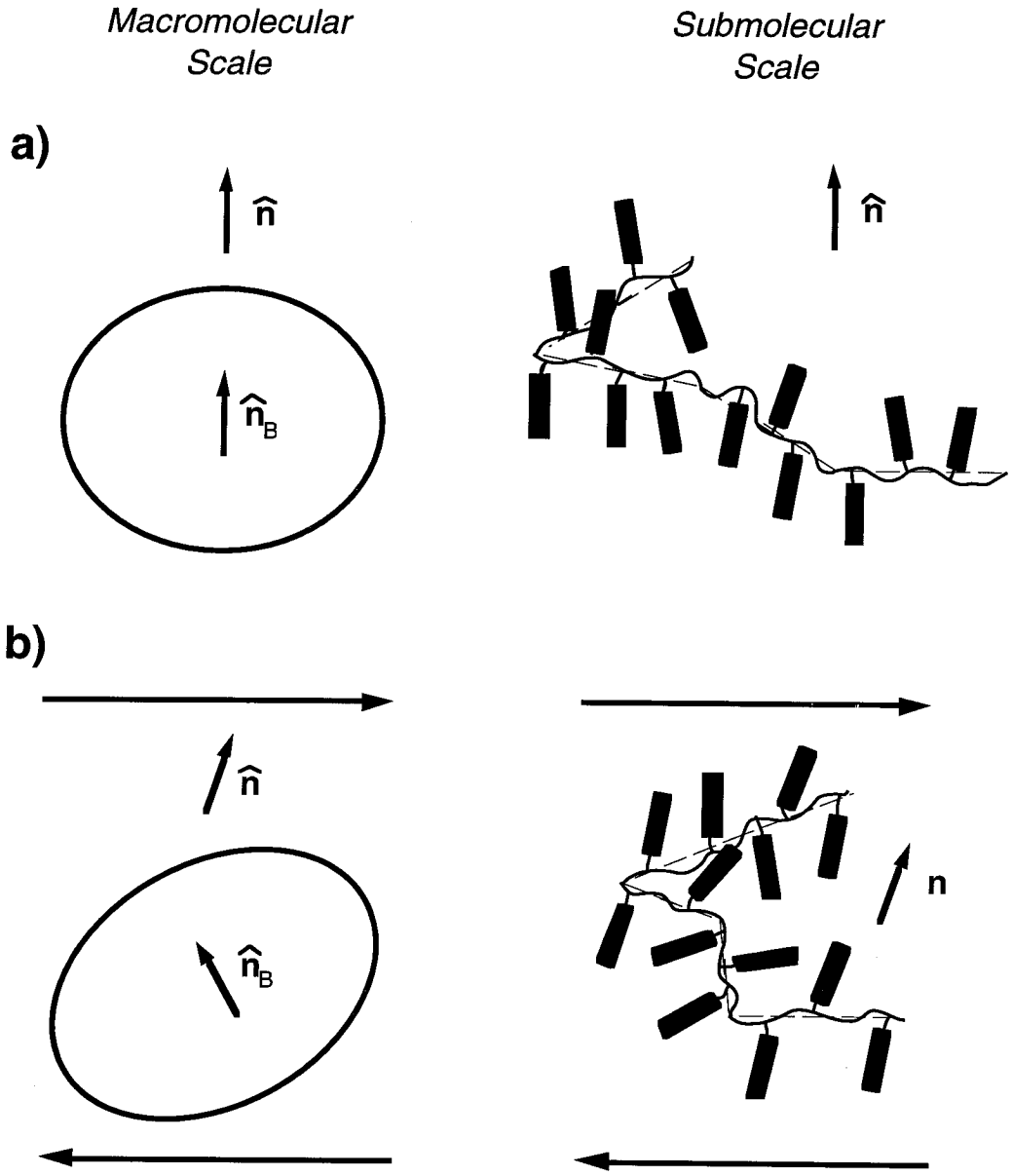

Figure 4.11: **(a)** At rest or at small strains, the backbone conformation is nearly random, with a small bias perpendicular to the local director ($\hat{\mathbf{n}}$). At equilibrium, the orientation of the axis of rotation of the "ellipsoid of gyration" ($\hat{\mathbf{n}}_B$) and of the director are the same. On a submolecular (segmental) scale, the mesogens are oriented on average along the director and perpendicular to the backbone. **(b)** At large shear strains, the backbone conformation is biased appreciably along the extensional axis and the director is reoriented. The distortion of the relative orientation of $\hat{\mathbf{n}}_B$ and $\hat{\mathbf{n}}$ forces the mesogens to adopt a new orientation dictated by the competition between the new, local segmental orientation and the local director.

order of microns and the radius of gyration of the present SG-LCP is roughly 200 Å [56]; thus, each chain sees an effectively uniform director orientation. The mesogen order parameter (S) within a domain at equilibrium is denoted S_o.

It is useful to consider how the director field and the configuration of the backbone are affected by shear, and how they are coupled through the spacer. Here we are concerned with modest strain amplitudes ($\gamma_o \leq 1$). Under these conditions, the polymer backbone conformation is dynamically biased essentially along the extensional axis of shear. This can be envisioned as a modulation in the aspect ratio and orientation of the ellipsoid of gyration. In addition, shear reorients the director. Together, these two effects change the relative orientation of $\hat{\mathbf{n}}_B$ and $\hat{\mathbf{n}}$ (Figure 4.11b). Thus, the mesogens are subjected to two competing influences: they tend to be perpendicular to the backbone, but also tend to orient along the director orientation within a domain. This competition could result in the mesogen choosing an intermediate orientation, perhaps causing a reduction in the order parameter ($S \leq S_o$) (Figure 4.11b). This can be thought to produce a stress (σ_C), arising from the energy penalty for changing the local mesogen orientation from that dictated by the director. Therefore, in a simplistic sense, the stress response can be described by $\sigma_T = \sigma_B + \sigma_C$, where σ_T is the observed shear stress, σ_B is the contribution from the distortion of the polymer backbone and σ_C is the contribution due to the coupling between the mesogen and the backbone.

We believe that at small strains, the distortion of the relative orientation of the backbone with respect to the director is so small ($\hat{\mathbf{n}}_B$ nearly parallel to $\hat{\mathbf{n}}$) that

the contribution arising from the coupling between them σ_C is negligible relative to σ_B. Since σ_B is expected to scale linearly with strain for $\gamma_o \leq 1$, we observe linear behavior. If this picture is correct, then the observed strain hardening would indicate that σ_C varies nonlinearly with strain. As the strain is increased beyond the linear regime, the magnitude of the reorientation of $\hat{\mathbf{n}}(\mathbf{r})$ by shear and the distortion of the backbone both increase, causing a significant change in the relative orientation between $\hat{\mathbf{n}}_B$ and $\hat{\mathbf{n}}$ (Figure 4.11b). When the backbone contribution to the stress is sufficiently small (i.e. at low enough frequencies), the contribution from σ_C can produce an observable increase in σ_T, manifested in the strain hardening behavior.

In summary, we suggest that, in the linear regime the dynamics arise due to the distortion of the polymer backbone. As strain increases, we believe strain hardening in the present SG-LCPs arises due to the contributions from the distortion of the relative orientation of the director with respect to the backbone.

4.4.3 Mechanism of Shear-induced Alignment

Measurements on the magnetically aligned samples discount an alignment mechanism based on the anisotropy in viscoelastic properties. The observed direction of alignment induced by shear is found to be along the vorticity axis, which rules out a mechanism analogous to the shear-induced alignment in other nematic liquid crystals. Instead, we believe that a mechanism analogous to the one we propose for strain hardening may be responsible for shear-induced alignment. During shearing at the frequencies and strain amplitudes described here, the backbone is biased essentially

along the extensional axis of the flow. Prolonged shearing continuously biases local director orientation to be perpendicular to the extension direction, perhaps forcing the mesogen orientation to propagate to macroscopic dimensions. In particular, shear appears to enhance mesogen alignment along the vorticity direction. Therefore, it appears that the perpendicular relative orientation between the backbone and the mesogen is maintained even after shear-induced alignment. This is consistent with the results on analogous, crosslinked SG-LCPs under uniaxial extension [17, 62], and that observed in analogous, uncrosslinked SG-LCPs [61] upon magnetic alignment.

4.4.4 Melt Fracture During Shear?

Shear-induced alignment is accompanied by a significant drop in the low frequency dynamic moduli measured at small strains which recovers slowly (Figures 4.9a & 4.9b). Such a drop in modulus is *not* observed in magnetically aligned samples. The decrease in the modulus of the flow-aligned sample may reflect a change in the SG-LCP conformation (*e.g.* a change in backbone conformation or change in the orientation of mesogens relative to the backbone), or it may simply reflect large scale changes in fluid structure that occur in some polymer melts under large amplitude oscillatory shear (*e.g.* "melt fracture").

To address the possibility that melt fracture may be occurring in our samples, we performed experiments at different strains, frequencies and temperature and observed the sample before, during and after shear alignment. Two critical features of our results virtually rule out melt fracture as an explanation of the drop in modulus: (1)

If melt fracture were occurring during large amplitude shearing, it would be evident in the moduli measured at all the frequencies. However, we observe a drop in the modulus, only below a critical frequency ($\omega_c' \approx 40$ rad/s, $\omega_c'' \approx 2$ rad/s), which coincides with the frequency where the effect of microstructure on the dynamic moduli are evident [1]. (2) Under otherwise identical conditions, flow-alignment at higher strain produces a higher modulus during shear. If melt fracture were indeed occurring, it should be increasingly evident at higher strains, resulting in a larger drop in the modulus during alignment at higher strain.

In addition, we present the following observations which further suggest that the changes in the present SG-LCP during flow-induced alignment are not consistent with a typical melt fracture process: (1) During alignment at high strains, the decrease in the magnitude of stress is only about 10%. Typically, melt fracture is associated with a large drop in the magnitude of stress [70]. (2) The stress is sinusoidal throughout the alignment process. This is in contrast to the results of Hatzikiriakos & Dealy [67] who observed asymmetric, non-sinusoidal waveforms during melt fracture. (3) During shear, we view the sample between crossed polarizers using a long working distance microscope (25×). We do not see any visible evidence of edge fracture, gross melt fracture, or wall slip of the sample during the alignment process. The sample appears nearly homogeneous. (4) In most polymeric materials, melt fracture is observed at large strains, at high stress and frequencies near the glassy regime. In our experiments, we observe a drop in the modulus upon alignment even at strains as low as 34%, at stresses as low as $\sim 10^4$ dyn/cm^2, and at conditions near the terminal

regime.

Based on these observations, it appears that 'melt fracture', at least as it is referred to in the literature, is not causing the drop in the modulus observed during prolonged, large amplitude oscillatory shear. Therefore, we believe that the drop in the modulus upon shear alignment reflects some change in SG-LCP conformation induced by the shear.

4.5 Conclusion

Our studies on magnetically aligned samples indicate that the dynamic moduli are insensitive to macroscopic director alignment, and discount a mechanism of flow-induced alignment due to anisotropic viscoelastic properties. Rather, a mechanism of alignment driven by the distortion of the backbone is consistent with our results. At small strains, the dynamic response of the present SG-LCP, in the frequency range used in this study, is dominated by the distortion of the backbone. With increasing shear amplitude, strain hardening is observed. We believe this is due to the coupling of the mesogens to the backbone, combined with the distortion of the relative orientation of the director and backbone. The same coupling may cause flow-induced alignment during prolonged large amplitude oscillatory strain. During flow-induced alignment, the mesogens appear to maintain the perpendicular sense of orientational coupling to the backbone that they possess at equilibrium (before shear).

Upon cessation of shear, the SG-LCP is left in a distorted state. This may involve a distorted backbone conformation, unfavorable relative orientation of the backbone

and the director field, and/or defects being forced near each other by shear. Afterward, the relaxation of the backbone conformation should take place within several minutes. This may account for the initial drop in the transmittance. The subsequent recovery is much slower and must be associated with larger-scale relaxation of the fluid microstructure. The fact that lower frequencies and longer durations of large-amplitude shearing produce more stable alignment suggests that the microstructural changes achieved at longer times, even though not manifested in the transmittance or G^*_{eff}, play a crucial role in the refinement of alignment. It is not yet clear why shear-induced alignment produces a drop in the low frequency dynamic moduli measured at small strains. However, our results suggest that it is due neither to melt fracture nor to macroscopic director alignment.

Chapter 5

Alignment of SG-LCPs Using High Magnetic Fields

5.1 Introduction

Many of the proposed applications for SG-LCPs, particularly those related to field-active optical data-storage devices, depend on external fields (*i.e.* magnetic or electrical fields) to induce uniform orientation in mesophasic SG-LCPs, or to alter mesogen orientation within a uniformly-aligned SG-LCP material. Although both electrical and magnetic fields are known to be effective in orienting low molecular-weight LCs [10], the large viscosities associated with LCPs necessitate use of high-voltage electrical fields to induce orientation [7, 8]. Operation of such high electrical fields is hazardous and these high fields can often ionize LCPs. Therefore, the use of magnetic fields to align LCPs possesses distinct advantages. Furthermore, a static magnetic field is believed to produce minimal hydrodynamic disturbances in the LCP material during alignment.

A major difference between low molecular mass (LMM) liquid crystals and LCPs is the high viscosity of LCPs, and it is well known that the alignment of a polydomain material occurs in times less than a second for LMM-LCs but the process of alignment is much slower for LCPs. Investigation of the kinetics of the magnetic alignment of a macroscopically unaligned material and the relaxation upon reorientation of an initially aligned material can, therefore, allow insight into the nature of the dynamic coupling interactions between the aligning mesogens and the polymeric backbone. Extensive studies of both alignment and realignment using magnetic fields have been performed for main-chain LCPs ([8, 74, 75] and references therein) and for a variety of SG-LCP materials with different backbone and mesogen combinations [7, 76–80]. The

evolution of alignment of a polydomain material has been characterized as a function of parameters such as magnetic field strength, temperature and molecular weight using measurement of NMR line shapes [2, 7, 76, 78, 81], diamagnetic susceptibility [82] or infra-red dichroism [79].

The driving force for director alignment of SG-LCPs in external magnetic fields is the anisotropy in the diamagnetic susceptibility ($\Delta\chi_a = \chi_{\parallel} - \chi_{\perp}$) of the mesogenic unit, and the consequent torque (L_m) due to an external magnetic field of strength H. Upon the application of a magnetic field, the mesogen in an SG-LCP orients parallel to the field (for $\Delta\chi_a > 0$); the polymeric backbone conformation is affected primarily through the flexible spacer and orientational coupling to the mesogen. Consequently, while the mesogen's anisotropic diamagnetic susceptibility is the primary parameter responsible for alignment, the processes by which global alignment occurs depends on not only the characteristics of the magnetic field and the mesogen's response to the magnetic field, but also the rotational viscosity of the material, which is a function of temperature and polymer molecular weight, the spacer tethering the LC unit to the main chain, and the ability of the polymer backbone to reorient to accommodate the changing orientation of its pendant mesogen groups [7–9, 83–86]. In contrast to magnetic alignment, shear-induced alignment (in mesophasic SG-LCPs such as the ones discussed in preceding chapters) appears to depend on the backbone response to the shear flow and its consequent effect on the mesogen through the flexible spacer. As we have demonstrated in the previous chapter, for the SG-LCP used in our study, the mesogen orients not along the flow direction but along the vorticity direction.

A central question in a number of past studies has been whether the standard continuum approach used to describe liquid crystalline behavior [10, 11] can be used for LCP systems. If one assumes the LCP behaves like an ordinary low molar-mass LC system, but with an enhanced viscosity, then for a single domain with a nematic director at an angle ϕ relative to the magnetic field, the magnetic torque can be written as [10]

$$L_m = -\frac{\Delta\chi_a H^2 \sin 2\phi}{2\mu_o} \tag{5.1}$$

where μ_o is the magnetic permeability. Upon reorientation of the domain, the equation of motion for the evolution of the director orientation (under the assumption that the domain reorients without distortion of the director field) can be described by the differential equation obtained by the balance of the magnetic torque with the viscous torque

$$\gamma_1(d\phi/dt) + \frac{\Delta\chi_a H^2 \sin 2\phi}{2\mu_o} = 0 \tag{5.2}$$

where γ_1 is the rotational viscosity. The solution of this equation is

$$\tan\phi(t) = \tan\phi|_{t=0} e^{-t/\tau_o} \tag{5.3}$$

where $\tau_o = \frac{\mu_o \gamma_1}{\Delta\chi_a H^2}$ is a characteristic time in the evolution of the director angle, ϕ. Thus, measurement of characteristic times (at different H) and the evolution of the alignment can allow investigation of the validity of the continuum description for LCPs [55, 78, 82].

Significant interest also exists in the understanding of the process of switching of

the direction of a pre-aligned SG-LCP material. Recent reorientation studies (using NMR) by Casquilho and coworkers [76] on a polysiloxane SG-LCP demonstrate that the relaxation behavior of a monodomain is homogeneous for all angles of rotation between the director and a static magnetic field. In contrast Roth [78] studied an SG-LCP with a polyacrylate backbone and a cyano-terminated mesogen and found that the reorientation process for an initial angle $\phi_0 < 45°$ is quite different than for an angle greater than for $\phi_0 > 45°$. The director field relaxes homogeneously, undisturbed for angles below 45° but inhomogeneously at angles larger than 45°. It is believed that this inhomogeneous relaxation is due to complex backflow effects [74]. Recently, Götz and coworkers [55] hypothesized that reorientation of a nematic monodomain SG-LCP melt is controlled by two rate processes: a rapid (relatively unhindered) reorientation of the mesogens permitted by the flexible spacer, and the subsequent, much slower completion of realignment at a rate controlled by the rearrangement of the backbone.

The goal of this part of our work is to focus on the reorientation process in our SG-LCP materials and to ascertain whether the hypothesized dual-rate process can be observed experimentally. The only past study of the kinetics of alignment and reorientation under a static magnetic field in SG-LCP samples with a polymethacrylate backbone and phenyl-benzoate mesogen (of comparable molecular weights to ours) is by Fuhrmann and coworkers [82]. The authors use a SQUID magnetometer to investigate the evolution of the anisotropy in the diamagnetic susceptibility ($\Delta\chi_a$) (which is related to the order parameter). Using the director orientation predicted

from the continuum theory (*i.e.* equation 5.3), the evolution of $\Delta\chi_a$ is calculated and compared to the experimental data. Fuhrmann and coworkers find good agreement for small reorientation angles ($< 60°$). From failure in agreement for larger angles they *infer* the presence of backflow effects. No dual processes were observed in their reorientation experiments. However, their experiments involved pre-aligning an SG-LCP melt in an electromagnet, quenching below the glass transition temperature, inserting into the magnetometer and reheating the sample. Significant artifacts can be introduced due to cooling and reheating. Furthermore, this technique of cooling and remounting does not permit tracking rapid changes in the initial few minutes of the orientation process; Fuhrmann and coworkers quote a measurement time of 3-5 minutes for the first data point. Even during the study of alignment of the polydomain material, their technique involved a time lag of 10-30 minutes before the first measurement could be performed. We investigated the dynamics of reorientation, *in-situ*, using the fast response of optical techniques. We aligned the SG-LCP in the magnetic field, characterized the effects of process parameters such as H, cell-gap, and molecular weight on the pre-alignment process from a unaligned material and then tracked the mean director orientation during a sudden reorientation experiment using polarized light. The following sections describe the material and methods we used, and a summary of our results, which is followed by a brief discussion.

5.2 Experimental Section

5.2.1 Materials and Apparatus

The side-group liquid-crystalline polymers used in this investigation consisted of a methacrylate backbone with hexa-methylene spacers and methoxy-terminated 4-hydroxy phenyl-benzoate mesogenic groups. The chemical structure of the repeat unit is as shown in Figure 3.1. Two molecular weights were studied: (a) PM6M-2 with $M_w \approx 222.7 \times 10^3$ g/mol and $M_w/M_n = 1.22$ (phase transitions: g 309K (32°C) n 390K (107°C) i, where g=glassy, n=nematic and i=isotropic), and (b) PM6M-1 with $M_w \approx 111.3 \times 10^3$ g/mol and $M_w/M_n = 1.26$ (phase transitions: g 317K (44°C) n 390K (107°C) i.

Approximately 50-250 mg of PM6M-2 or PM6M-1 was sandwiched between polished CaF_2 disks (Figure 5.1). A 50 - 250 μm sample thickness was maintained by an annular Teflon^{TM} or Kapton^{TM} spacer. The polymer sandwich was placed in an aluminum chamber which acted as a heat bath. This chamber was affixed to the tip of a phenolic tube (Figure 5.2) via a hollow snug-fit Teflon^{TM} spindle. The phenolic tube could be manually manipulated to either slide through a holding sleeve in a direction coaxial with its long axis (parallel to the propagation of light), or it could be rotated about the optic axis.

The sample was heated with Kapton^{TM}-insulated flexible resistance heaters and the temperature was monitored using a type T (copper-Constantin^{TM}) thermocouple. The sample temperature was controlled either (1) within ±2°C using an Omega^{TM}

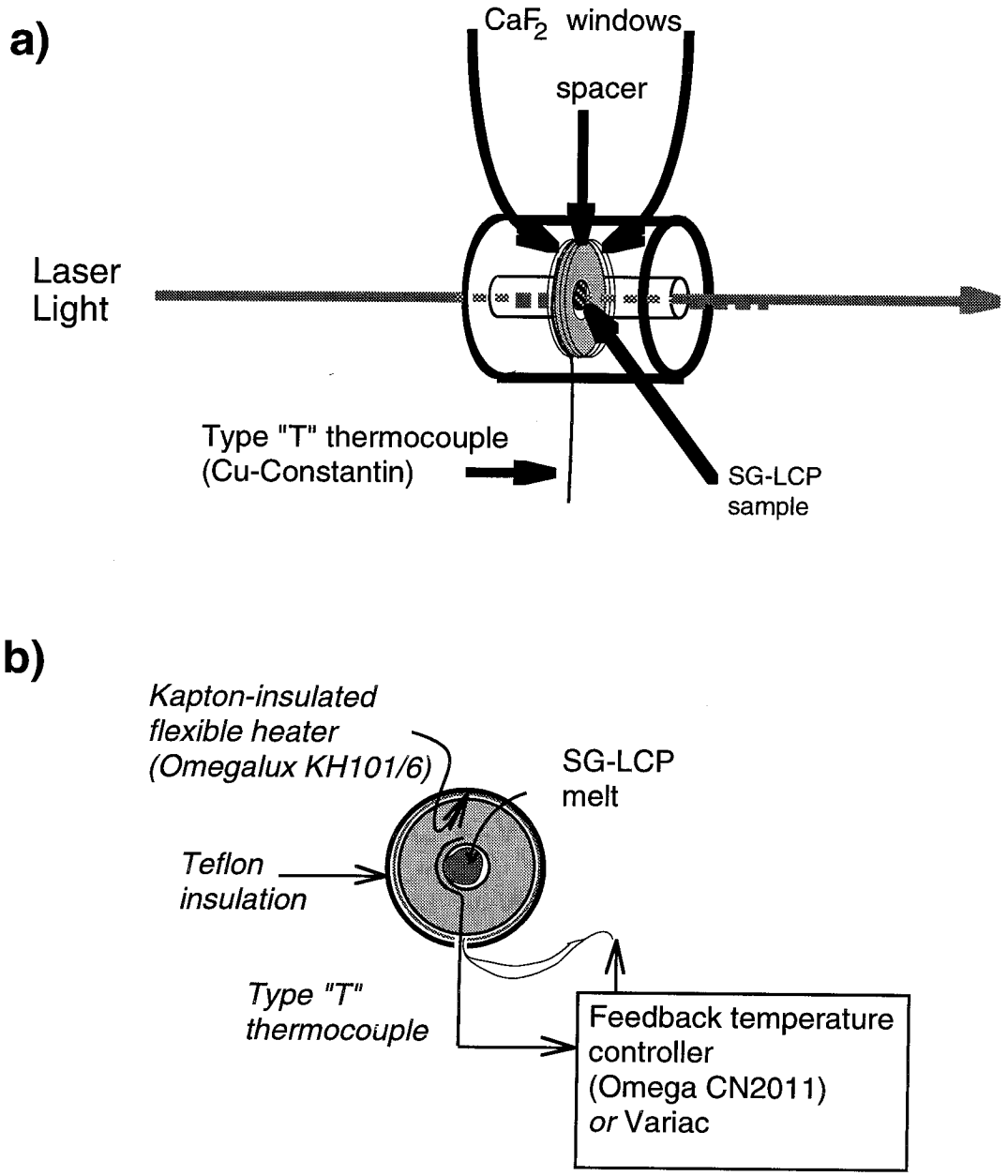

Figure 5.1: Schematic for the cell and holder for the SG-LCP samples for magnetic alignment. (a) Cell made with CaF_2 windows and loaded with sample is held inside an insulating tube that was used to insert and remove sample from the magnet. (b) View of the sample cell looking down the light propagation direction.

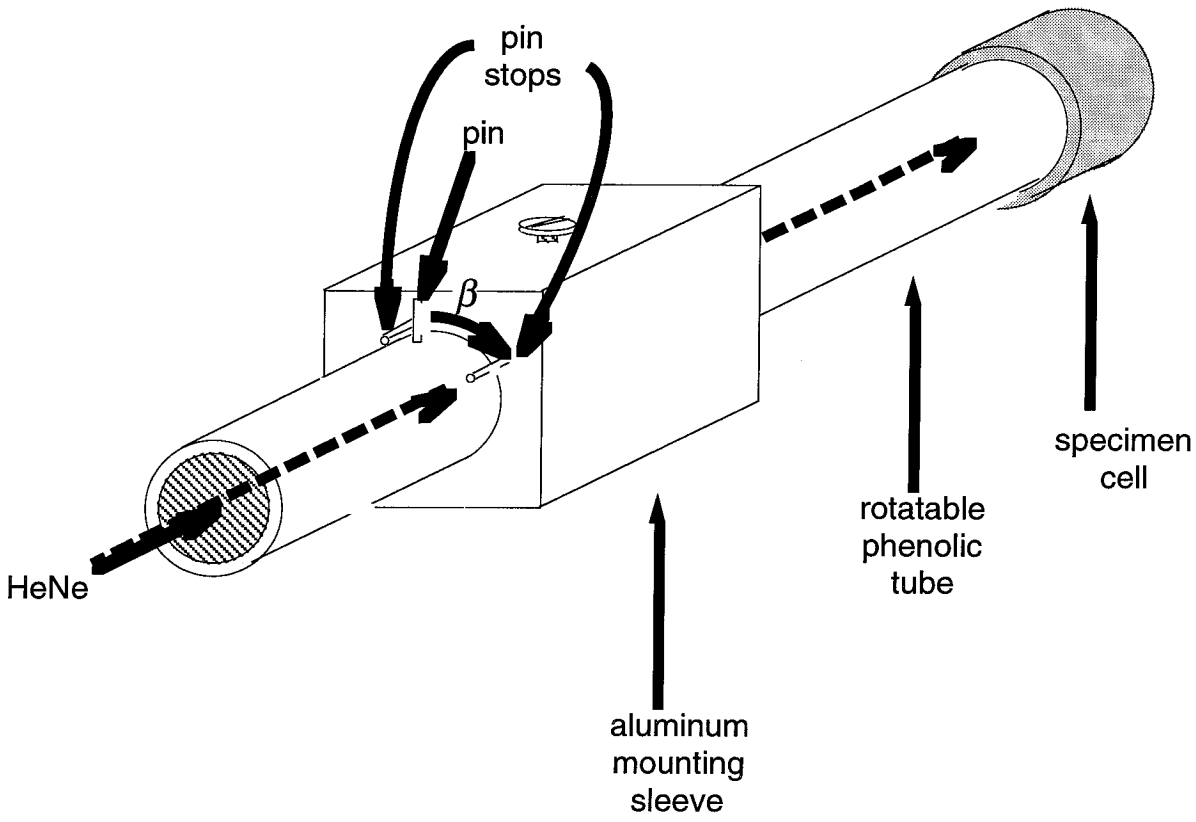

Figure 5.2: Illustration of apparatus used to hold and manipulate SG-LCP samples during magnetic alignment. The aluminum cell detailed in Figure 5.1 is affixed to the tip of a phenolic tube that can be rotated about the optic axis while holding the sample in a fixed position within the magnetic field. The sample can also be rotated by an angle $\beta = 15, 30, 45, 60$,or $90°$ about the optic axis. See Appendix for further design details.

controller CN 2011 or (2) within $\pm 0.2°$C using a Variac^{TM} variable-voltage source. Magnetic alignment was performed by sliding the sample into the center of a 2.4 Tesla field generated by a Varian 100-XL NMR electromagnet [1] (Figure 2.7). As discussed in Chapter 2 (Section 2.5.3) the sample was characterized *in-situ* by transmission of HeNe laser light ($\lambda = 633$ nm), polarized at an angle of $45°$ with respect to the orientation of the magnetic field. The intensity between crossed-polarizers ($I_{\perp}$) and

[1] Donated by AmerAsia, Inc.

parallel polarizers ($I_{\parallel}$) was measured by detectors 1 and 2 (Figure 2.7), respectively.

5.2.2 Alignment Method and Optical Characterization

Two types of magnetic alignment experiments were performed: (i) Alignment of an initially disordered ("polydomain") nematic to a more macroscopically oriented material (referred to as a "monodomain"), and (ii) reorientation of a monodomain after suddenly rotating the aligned nematic by an angle β about an axis parallel to the optic axis and orthogonal to the field.

Macroscopically aligning polydomain SG-LCP melts

Prior to magnetic alignment, the sample was heated into the isotropic phase ($T = 125°C \approx T_{ni} + 10°C$) for 20 minutes to erase any strain history acquired during loading and to provide a reproducible initial condition. The material was then slowly (1°C/min) cooled to a temperature within the nematic phase, where the sample forms a highly scattering, opaque, polydomain. After equilibrating for 20 minutes (outside the magnetic field) at this temperature, the sample was inserted into the center of the magnetic field by sliding the insulating tube (Figure 5.1 along its long axis. Since the alignment was performed for periods exceeding several hours and because the laser intensity may drift over these prolonged times, the recorded intensities $I_{\perp}$ and $I_{\parallel}$ were normalized using the intensity of light not transmitted through the sample using a third detector (D3 in Figure 2.7).

Since the material in the polydomain state is highly turbid and gets more transparent as alignment progresses, characterization of optical transmissivity provides a

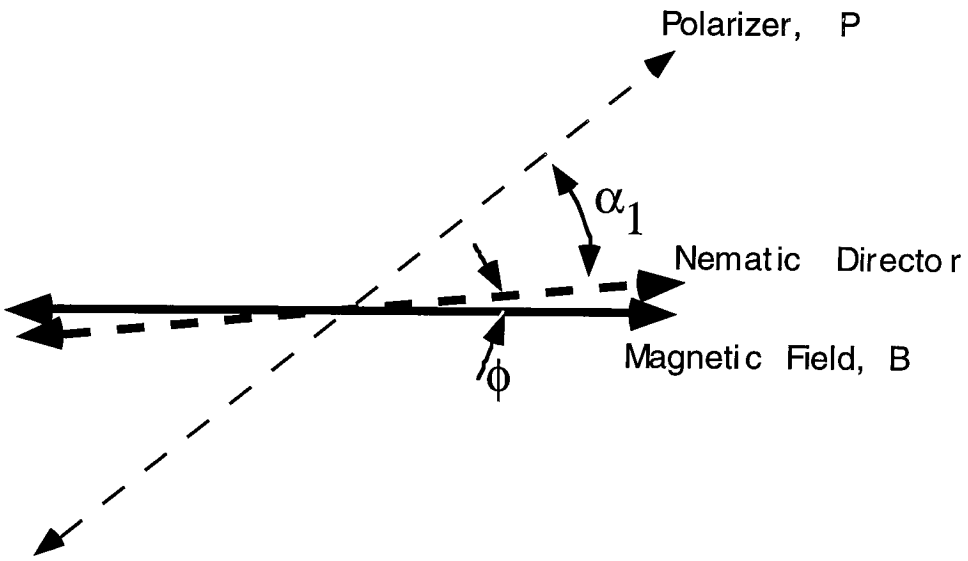

Figure 5.3: Relation between the orientation of the nematic director, the magnetic field and the polarizer. α_1 is the angle between the optical axis of an aligned sample and the polarizer. Ideally α_1 is 45° and $\phi \approx 0$.

measure of the rate of alignment. The ratio of $I_\perp + I_\parallel$ in the nematic phase to that in the isotropic phase (I_{iso}) was used to characterize the transmissivity of the sample and study the process of transformation from a polydomain SG-LCP sample to a monodomain SG-LCP sample. Ideally, at the end of an initial alignment process from a polydomain material to a monodomain the nematic director of the aligned SG-LCP melt should be along the magnetic field *i.e.* $\alpha_1 \approx 45°$ (Figure 5.3).

Reorientation of a Macroscopically Aligned "monodomain" SG-LCP melt

The sample which had been aligned along α_1 was rotated clockwise by a known angle to α_2 and allowed to realign. Sample rotation took approximately 0.2s. The reorientation of the sample was tracked using polarized light using the relations shown below.

As discussed in Chapter 2, for a uniformly birefringent sample with effective bire-

fringence (Δn) and a nematic director (*i.e.* the optical axis of symmetry) lying at an angle of α relative to the polarization direction of incident light (Figure 5.3)

$$I_{\perp} = A\, I_o \sin^2\left(\frac{\pi \Delta n d}{\lambda}\right) \sin^2 2\alpha \tag{5.4}$$

$$I_{\parallel} = A\, I_o[1 - \sin^2\left(\frac{\pi \Delta n d}{\lambda}\right) \sin^2 2\alpha] \tag{5.5}$$

where A is a factor which takes into account effects such as attenuation of light due to scattering and dichroism. The path-length the polarized light has to traverse is d.

This gives

$$(\sin^2 \mu \sin^2 2\alpha) = \frac{r}{1+r} \tag{5.6}$$

where $r = \frac{I_{\perp}}{I_{\parallel}}$ and $\mu = \frac{\pi \Delta n d}{\lambda}$. After performing a coordinate transformation and expressing α in terms of ϕ (*i.e.* $\alpha = \phi + 45$) we obtain

$$(\sin^2 \mu \cos^2 2\phi) = \frac{r}{1+r} \tag{5.7}$$

The known experimental values of r and $\alpha_2 - \alpha_1$ for an initial aligned state along α_1 and the rotated state to α_2 allow us to solve for α_1 and $\sin^2 \mu$. Under the assumption that the material reorients uniformly, we can use

$$\cos(2\phi) = \left(\frac{r}{\sin^2 \mu (1+r)}\right)^{0.5} \tag{5.8}$$

and

$$\tan(\phi) = \frac{(1 - \cos^2 2\phi)^{0.5}}{1 + \cos 2\phi} \tag{5.9}$$

to track the change in the angle of the nematic director with respect to the magnetic field (ϕ).

5.3 Results

5.3.1 Alignment From a Polydomain to a Monodomain

The dynamics of liquid crystalline polymers depend on the macromolecular properties as well as the processing conditions. In our study of the magnetic alignment of SG-LCP materials, we investigated the interplay between molecular weight of the SG-LCP, the magnetic field strength, the cell gap and the temperature in determining the kinetics of alignment of SG-LCP melts.

PM6M-1 ($M_w \approx 111.3 \times 10^3$g/mol) and PM6M-2 ($M_w \approx 222.7 \times 10^3$g/mol) melts were aligned in the nematic phase at identical conditions of magnetic field strength, gap and temperature (Figure 5.4). The initial induction time required before any transmission is observed through the sample appeared to be unaffected by this two-fold increase in molecular weight. Beyond this initial induction point, increase in molecular weight led to a decrease in both the rate and magnitude of the sample's rise in transmissivity. The samples turned near transparent (transmissivity $\sim 60-80\%$ of transmissivity in isotropic phase) in about 10^4 seconds, which was much slower than the typical time taken during large-amplitude shear alignment ($\sim$ 100s; Figure 4.3a).

To probe the effect of temperature on the rate of alignment of SG-LCP in a high magnetic field, PM6M-2 was aligned within the nematic phase at three different tem-

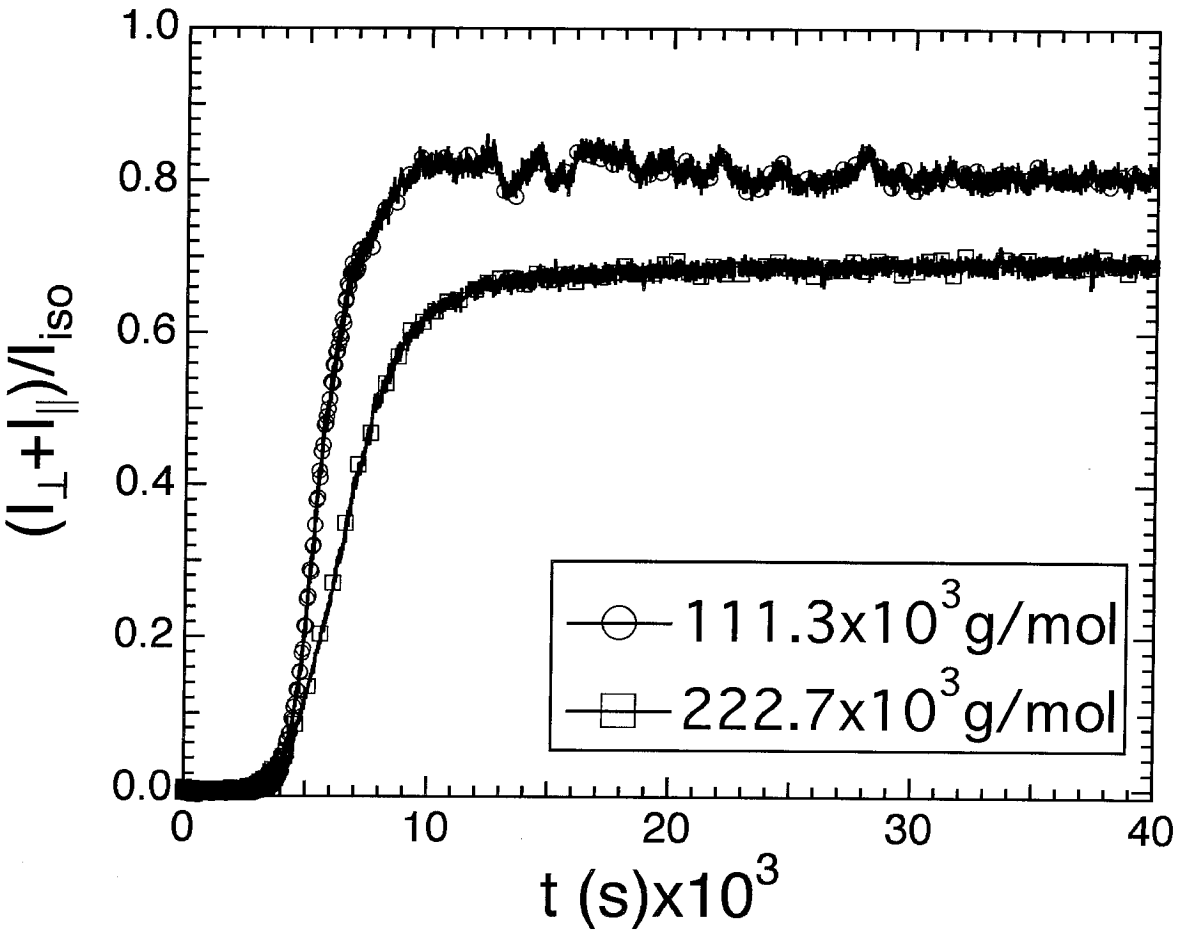

Figure 5.4: Effect of molecular weight of the SG-LCP on the rate of alignment as manifested in the transmission of light through the SG-LCP melt (shown relative to the transmission in the isotropic phase). Alignment was performed in a 2.4T magnetic field and at a temperature of 100°C using a 250μm gap. Sparse markers have been used.

peratures (Figure 5.5). Temperature affected the initial induction period significantly, and during alignment at temperatures deeper into the nematic phase (*i.e.* increasing $T_{ni} - T$) the samples remained turbid for a greater duration of time. The rate of increase in the transmission of light and the magnitude of the transmission decreased with decreasing of temperature.

The torque on the mesogens during magnetic field-induced orientation depends

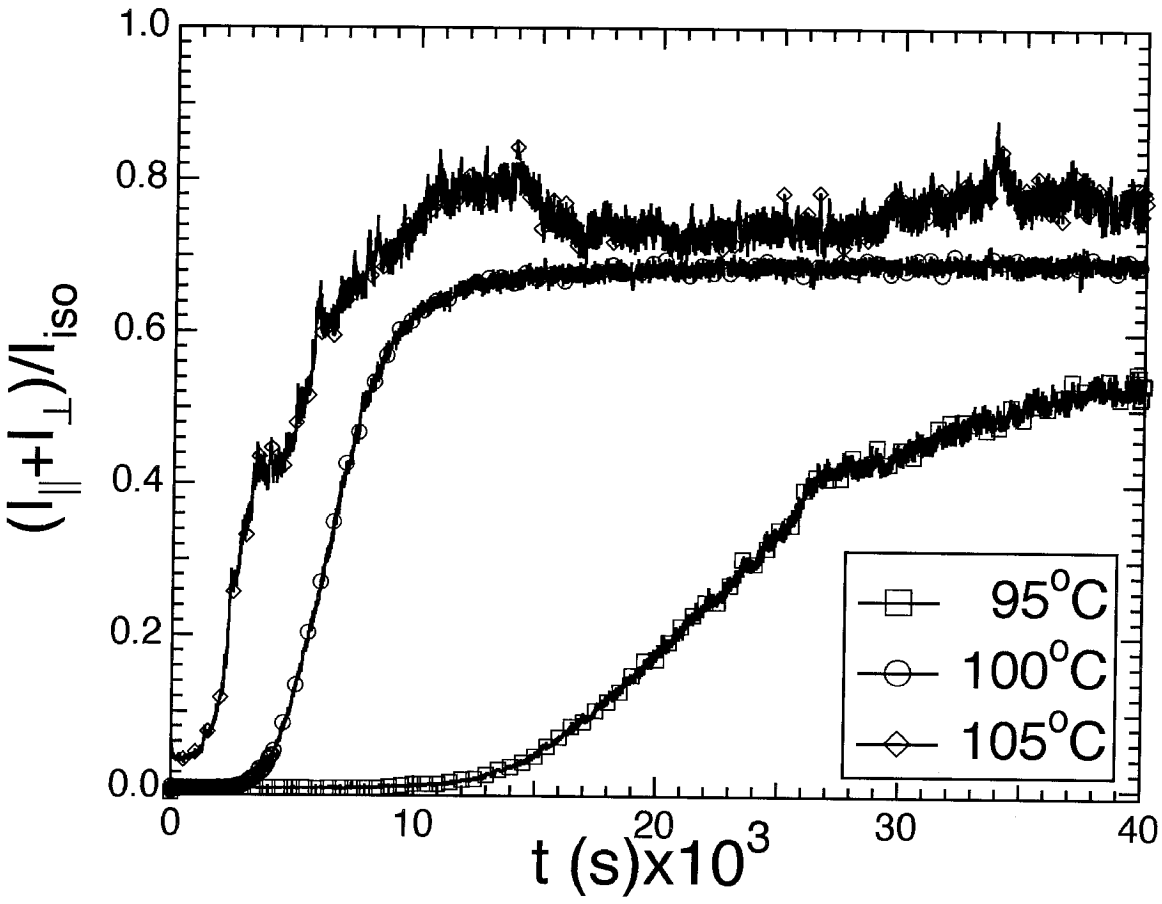

Figure 5.5: Effect of temperature at which magnetic alignment of PM6M-2 ($M_w \approx 222.7 \times 10^3$g/mol) melt on the transmissivity of the SG-LCP melt (normalized by the transmission in the isotropic phase). Alignment was performed in a 2.4T magnetic field using a 250μm gap. The drifts in the transmission for alignment at 105°C are, plausibly, due to nearness to T_{ni} and a temperature control of ± 2°C. Sparse markers have been used.

on the strength of the field (H). Consequently, the magnetic field strength affects the rate of alignment. An approximately 1.5-fold reduction in the magnetic field strength had significant effect on the induction time during alignment as well as the rate of alignment for PM6M-1 (Figure 5.6a). For alignment at $H = 2.4T$, the SG-LCP melt reached a value of ≈ 0.8 transmissivity in about three hours. Upon reduction of the field to $H = 1.6T$, alignment for even ten hours led to only 60% of the transparency

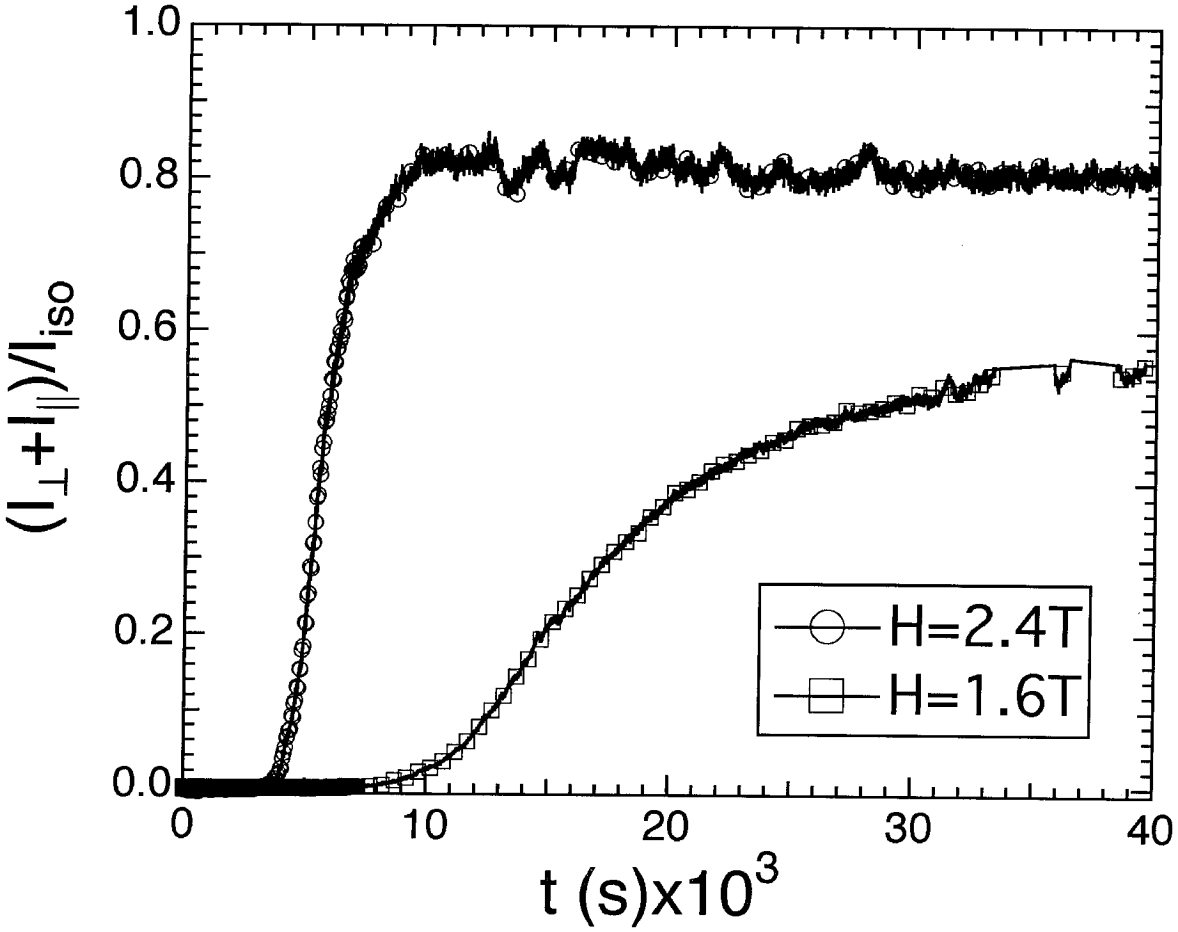

Figure 5.6a: Effect of magnetic field strength used for alignment of PM6M-1 ($M_w \approx 111.3 \times 10^3$g/mol) melt. Alignment was performed at 100°C using a 250μm gap. Sparse markers have been used.

seen in the isotropic phase. A plot of the optical signal versus time scaled by H^2 does not superpose the curves (Figure 5.6b).

The effect of cell gap on the alignment process was studied for PM6M-2 by using two gaps of 100μm and 250μ (Figure 5.7). The reduction in the induction time (4000s to 1500s) and the reduction in the time taken to reach near-maximum transmission (12000s to 4000s) appeared to be proportional to the reduction in the cell gap (reduced by a factor of 2.5). We believe that the effect of increase in cell-gap is manifested

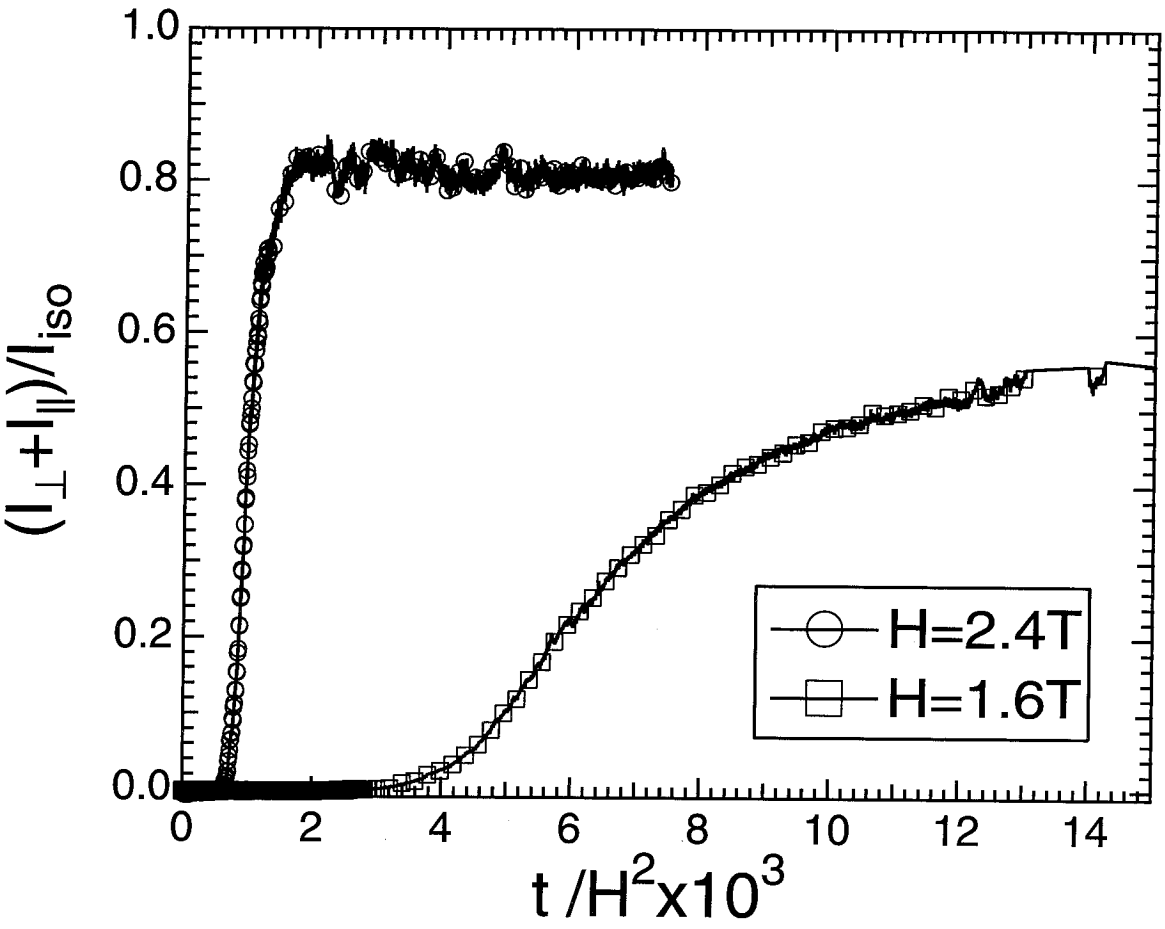

Figure 5.6b: Effect of magnetic field strength used for alignment of PM6M-1 ($M_w \approx 111.3 \times 10^3$g/mol) melt. The time axis has been scaled using the square of the magnetic field. Alignment was performed at 100°C using a 250μm gap. Sparse markers have been used.

primarily from the an increase in the volume of scattering domains encountered by the light as it propagates through the cell.

5.3.2 Reorientation of a Uniformly Aligned SG-LCP Melt

Past studies of reorientation in liquid crystalline polymers have distinguished between reorientations of less than 45° versus and those greater angles [10]. We investigated both types of reorientation in our SG-LCP materials.

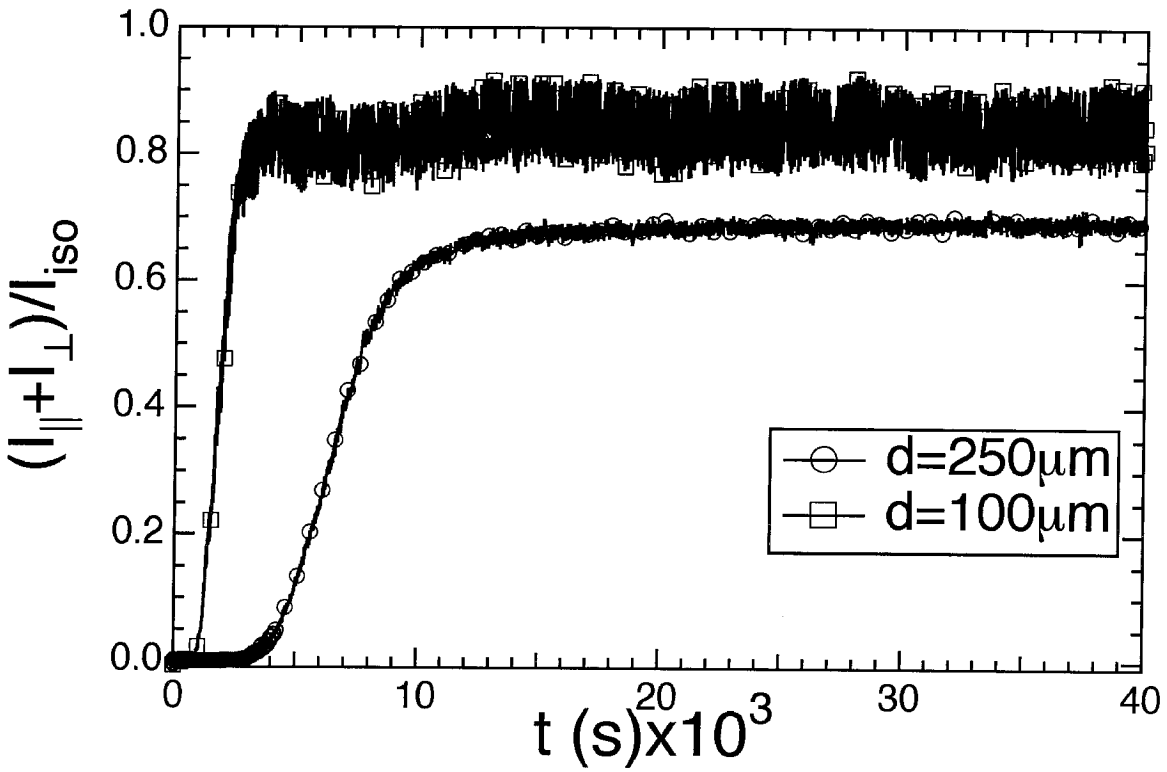

Figure 5.7: Effect of cell gap used for alignment of PM6M-2 ($M_w \approx 222.7 \times 10^3$g/mol) melt. Alignment was performed at 100°C using a 2.4T magnetic field. Sparse markers have been used.

The lower molecular weight sample PM6M-1 was aligned in the nematic phase for a period of 12 hours and then suddenly rotated by 90°. Upon rotation, the transmission (sum of $I_\perp$ and $I_\parallel$) of light showed an initial decrease of more than 50% within 1500s (Figure 5.8a). This initial decrease suggested an increase in the polydomain character. The fraction of light transmitted between crossed-polarizers ($\frac{I_\perp}{I_\perp+I_\parallel}$) also decreased within this initial period (Figure 5.8b). Large oscillations were observed in the ratio $\frac{I_\perp}{I_\perp+I_\parallel}$. These oscillations were later correlated with the temperature fluctuations of ± 2°C (due to the on-off control of the Omega^{TM} temperature controller). We believe that this variation in temperature causes small changes in the birefringence Δn. For

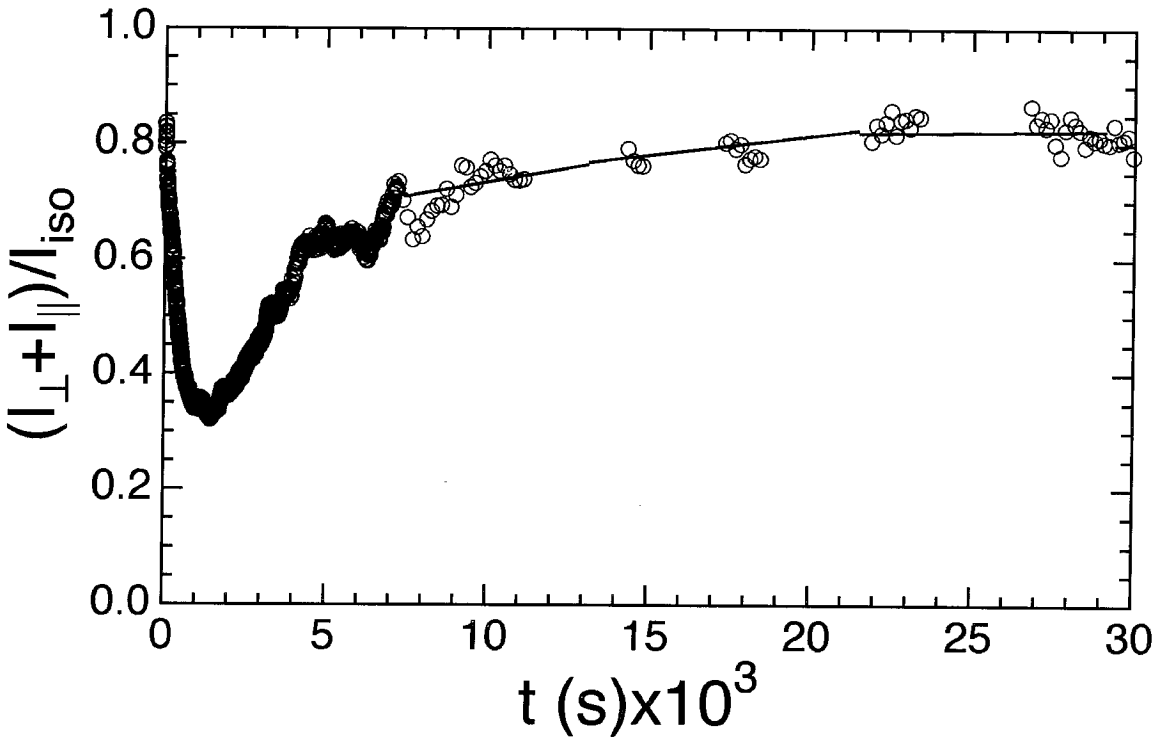

Figure 5.8a: Total transmittance measured during reorientation of an initially aligned PM6M-1 sample by 90°. Alignment and realignment was performed at 100°C using a 2.4T magnetic field and 250μm gap. Sparse markers have been used.

optical pathlength as large as 250μm, small variations in Δn can cause the retardation $(\frac{\pi \Delta n d}{\lambda})$ to wander, plausibly over an order. Since $I_\perp$ is proportional to $\sin^2\left(\frac{\pi \Delta n d}{\lambda}\right)$, such over-orders excursions can have significant effects on the optical signal.

For the conditions of alignment used in Figure 5.8a, after the initial 1500s the total transmission increased indicating progressive alignment of the sample. After approximately 12 hours of alignment, the material became nearly 80% transparent and showed a unique optical axis.

The oscillations in $I_\perp$ (and $I_\parallel$) signal do not permit tracking of changes in the nematic director orientation (ϕ) during a reorientation experiment. To address this issue, we used a Variac^{TM} for further experiments and equilibrated the sample for

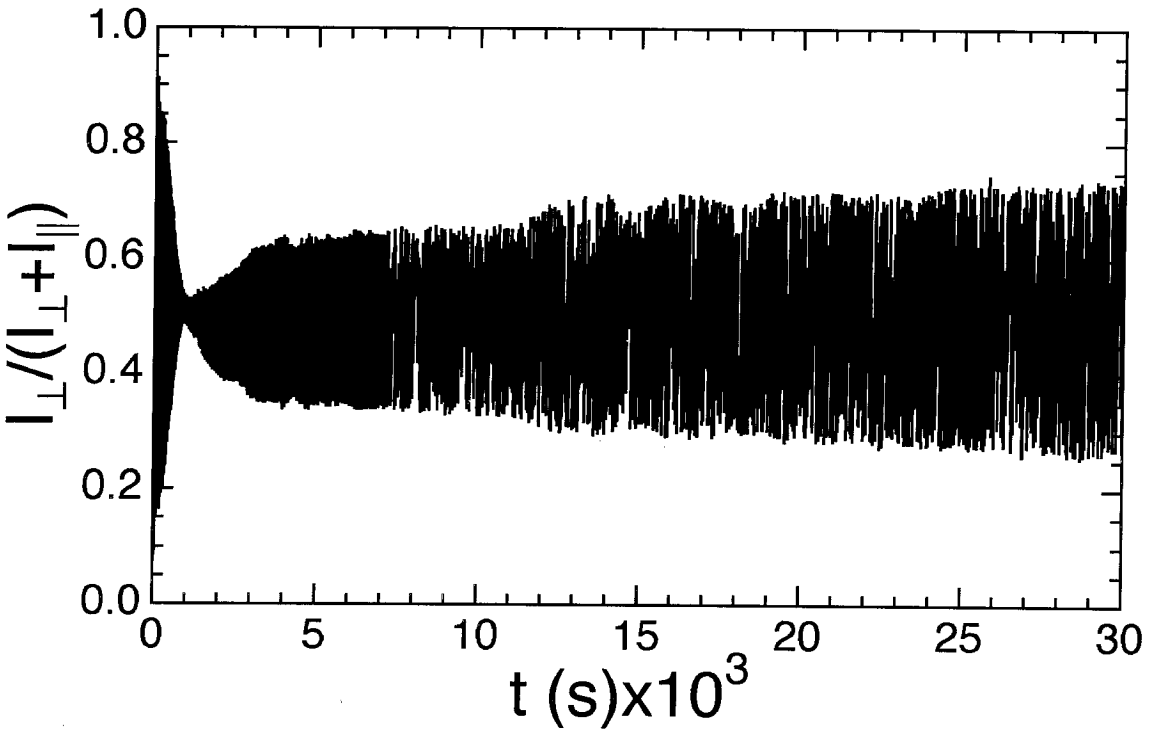

Figure 5.8b: Transmittance measured through crossed-polarizers during reorientation of an initially aligned PM6M-1 sample by 90°. The thin necking region corresponds to the minima in the transmission in Figure 5.8a. The large oscillations in the signal are due to changes of ±2°C in the temperature and the resulting changes in the optical retardation (see text).

periods exceeding several hours. The resulting temperature stability (±0.2°C) along with a thinner gap ($\sim 50\mu$m) allowed us to eliminate the oscillations in the optical signal for periods of an hour. Since the primary motivation for the magnetic alignment experiments was to investigate the existence of dual-rate processes in the early periods of alignment, this stability was sufficient. However, since the temperature of alignment depends on the exact Variac^{TM} setting and the ambient temperature conditions, we could not accurately preset the temperature to a particular value.

A reorientation experiment was performed using PM6M-2 where an aligned sample was rotated by 30° (*i.e.* $\alpha_2 - \alpha_1 = 30$) and realigned in the magnetic field. The

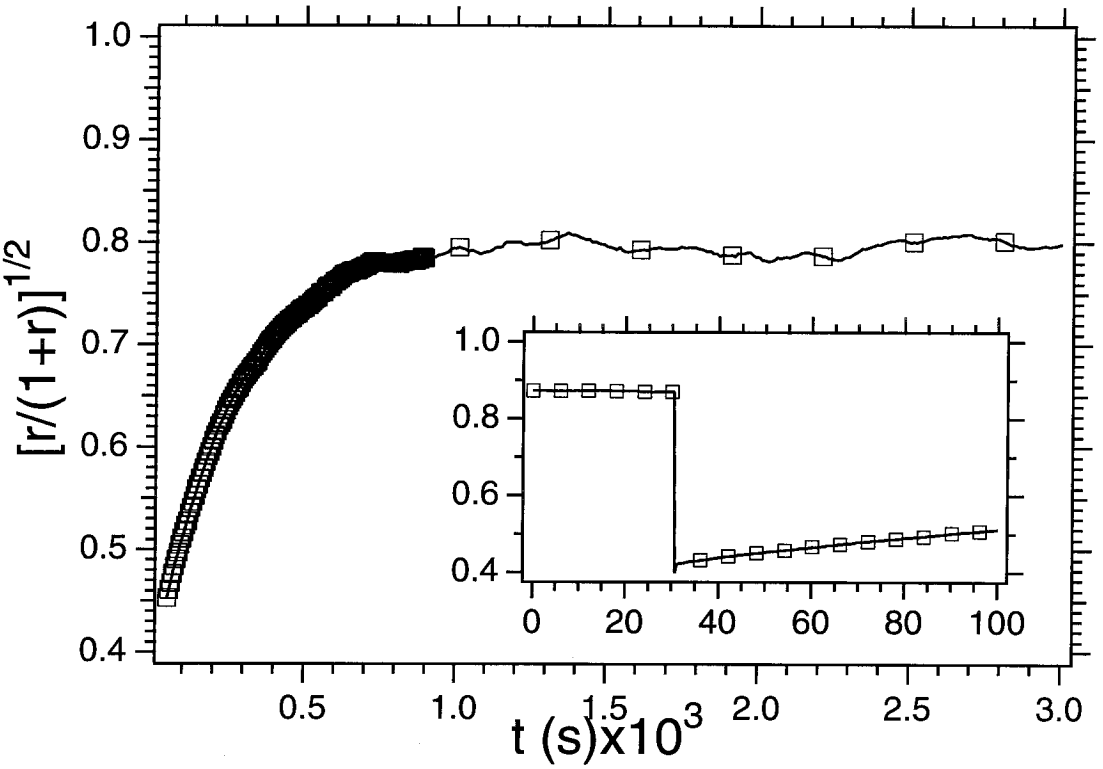

Figure 5.9: Change in $\left(\frac{r}{1+r}\right)^{1/2}$ ($r = \frac{I_\perp}{I_\parallel}$) upon rotating an aligned sample (*i.e.* initial state $\phi \approx 0°$) clockwise by 30°. The ratio $\left(\frac{r}{1+r}\right)^{1/2}$ shows the variation of $\sin\mu\cos 2\phi$ (see Equation 5.7). Inset shows the initial 100s of the process; the sample was rotated at $\approx$ 30s. Alignment was performed at 95.4°C using a 2.4T magnetic field and 50μm gap. Sparse markers have been used and the solid line is drawn as a guide.

ratio (r) of $I_\perp$ to $I_\parallel$ was used to plot (in accordance with equation 5.7) the variation in $\sin\mu\cos 2\phi$ (Figure 5.9). Under the assumption that the initial monodomain structure is preserved during reorientation, the plot of $\sin\mu\cos 2\phi$ demonstrates that the director orientation (ϕ) evolves in a smooth fashion. Reorientation of an aligned sample by 60° also produced a continuous variation in $\sin\mu\cos 2\phi$ (Figure 5.10) in the initial 3000s.

For PM6M-2, a 90° reorientation in a 250μm gap produced results very different from the 90° reorientation of the lower molecular weight PM6M-1. The total trans-

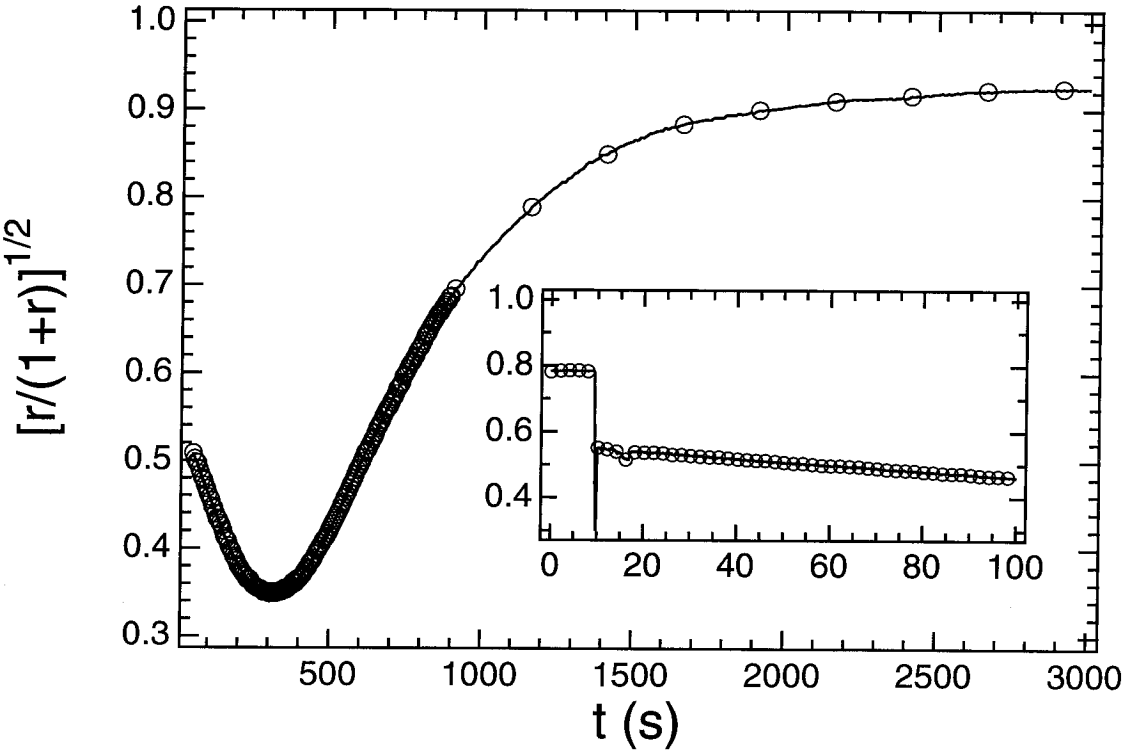

Figure 5.10: Change in $\left(\frac{r}{1+r}\right)^{1/2}$ ($r = \frac{I_\perp}{I_\parallel}$) upon rotating an aligned sample (*i.e.* initial state $\phi \approx 0°$) clockwise by 60° (Figure 5.3). Inset shows the initial 100s of the process; the sample was rotated at $\approx$ 10s. Alignment was performed at 102.6°C using a 2.4T magnetic field and 50μm gap. Sparse markers have been used and the solid line is drawn as a guide.

mission fell rapidly to zero (Figure 5.11a) and stayed at zero for the remainder of the 12 hour run. The sample did not go completely turbid, as light still was able to pass through the sample. However, the laser spot exiting the sample 1 hour after the sudden 90° rotation appeared to be a diffuse streak oriented parallel to the aligning field, rather than the circular laser spot entering the sample. Upon cooling the sample and studying it under a polarizing microscope, we observed a banded texture, with striations running parallel to the original alignment direction and perpendicular to the direction of realignment (Figure 5.11b). The banded morphology did not change

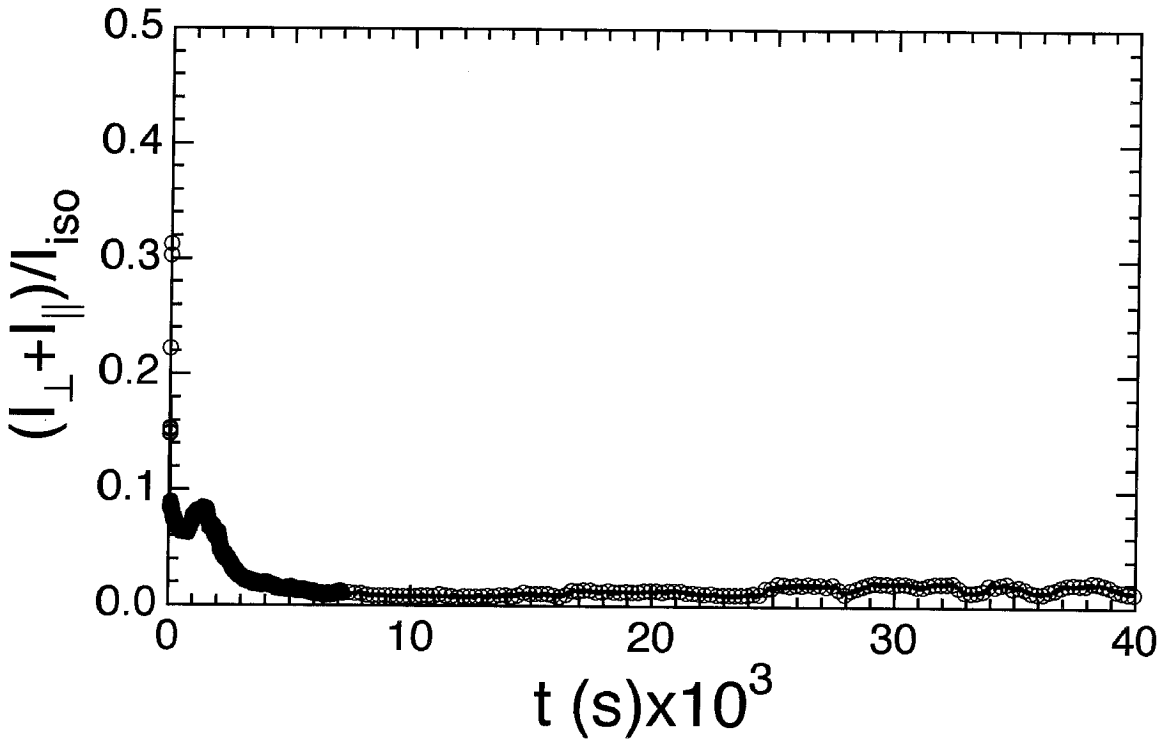

Figure 5.11a: Total transmittance measured during reorientation of an initially aligned PM6M-2 sample by 90°. Alignment and realignment was performed at 100°C using a 2.4T magnetic field and 250μm gap.

appearance either during rotation of the crossed polars through which it was viewed, or after removal of the analyzer. The sample appeared brightest when the polarizers were oriented at ±45° to the original field direction, and appeared somewhat darker when the polarizers were aligned parallel and perpendicular to the field direction, indicating that despite the formation of the striated morphology, a significant degree of alignment was achieved by the magnetic field. However, the extinction was not nearly as dramatic as it was for experiments that did not lead to striated morphologies (*e.g.*, for $\beta = 30°$).

Reorientation at higher temperatures, closer to T_{ni} ($T = T_{ni} - 2°C$), produced striations with slightly larger periodicity and a more "thread-like" texture.

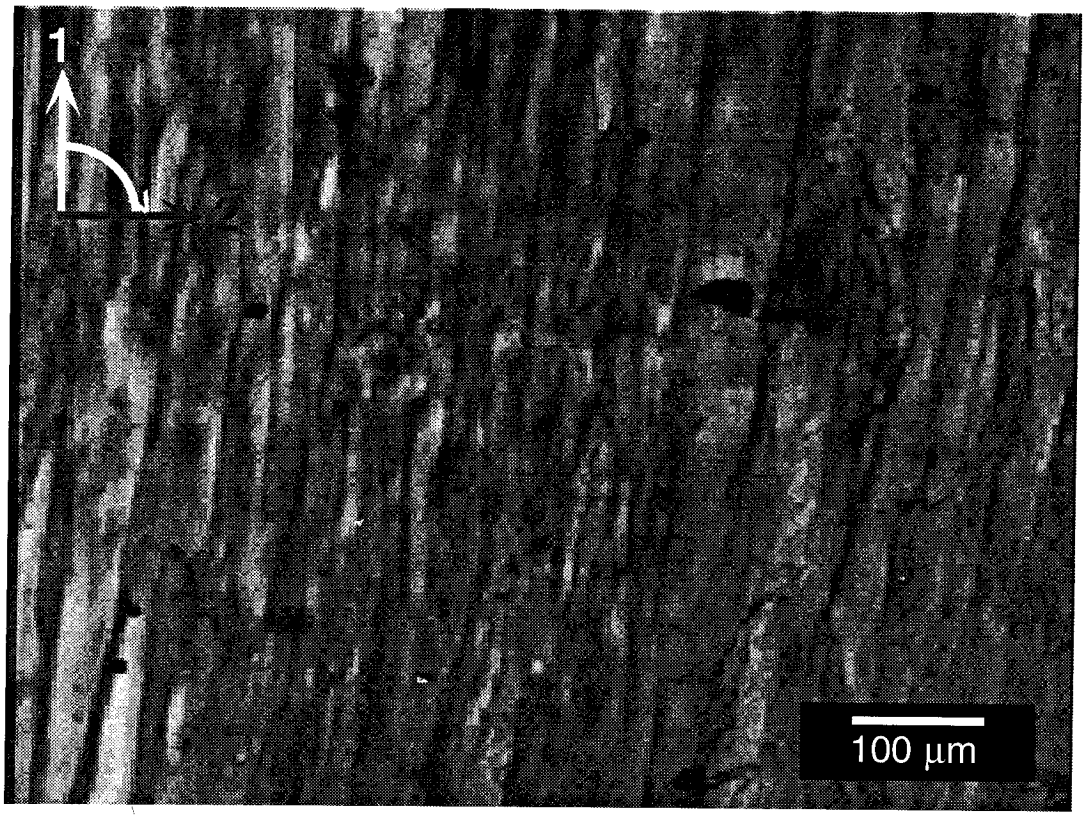

Figure 5.11b: Image of the PM6M-2 sample (between crossed-polarizers) that was subjected to a reorientation of 90° and aligned for 12 hours (Figure 5.11a).

The 90° reorientation experiment was repeated using PM6M-2 at an identical temperature and field strength, but in a thinner ($d = 150\mu$m) gap, to see whether the gap thickness influences the periodicity of the striated morphology that develops upon reorientation. However, for these thinner gap widths, alignment proceeds to completion, without a striated morphology ever forming.

5.4 Discussion

5.4.1 Alignment of a Polydomain Towards a Monodomain

Practically all imaginable applications of the side-group liquid crystalline polymers involve the creation of well-oriented structures. Even investigations of the structural properties of a SG-LCP require that a monodomain structure be preliminarily established. Therefore, it is a matter of importance to understand the conditions and parameters that lead to such alignment.

It is well known that increasing the number of repeat units in the main-chain (*i.e.* increase in the molecular weight) leads to increase in the viscosity of the melt [7–9] and that this increase in viscosity slows down the alignment process. Indeed we observe that a two-fold increase in the molecular weight from $\approx$ 111.3kg/mol to $\approx$ 222.7kg/mol causes a slower change in the transparency of the sample, and hence a slower increase in the size of the domains (Figure 5.4). For example, 60% transparency is reached in approximately 6000s for the lower molecular weight and in approximately 9000s for the higher molecular weight. This indicates a nearly linear effect of the molecular weight, which is consistent with past reports [8, 55]. Götz and coworkers [55] have used copolymeric nematic SG-LCPs having a polymethacrylate backbone with a random combination of cyano-terminated and methoxy-terminated mesogens. Using dielectric spectroscopy they find that the molecular weight dependence of the contribution of the backbone to the rotational viscosity is $\sim N^{0.8\pm0.1}$ (N is the degree of polymerization).

The final value of transmissivity is different for the two different molecular weights of PM6M studied here, with a lower transmissivity for the melt comprised of longer chains. One reason that could explain this effect is that the final transmissivity may depend on the stationary state reached where the total number of defects remains constant. Relatively lower defect mobility in the higher molecular weight sample could lead to significantly more defects and consequently, lower transmission. Past studies employing NMR, dielectric spectroscopy, or diamagnetic susceptibility measurements of alignment of relatively high molecular weight SG-LCPs have not, simply due to the techniques employed, discussed the changes in turbidity (or transmission) during the initial few minutes of the alignment process.[2] We find that the induction period before the sample permits transmission of light is on the order of 4000s and surprisingly, does not show a dependence on the molecular weight (at least over the range investigated here). This suggests that the initial coarsening of domains by annihilation of orientational defects (or disclinations) occurs unaffected by the presence of the polymeric backbone. However, at later times a larger degree of cooperativity is required between the mesogens; we presume that these cooperative motions cannot be achieved without the participation of the polymeric backbone, and are therefore dependent on chain length.

The above hypothesis is supported by the effect of temperature at which alignment

[2]Schwenk and coworkers [2] have studied alignment (using rotating magnetic field) in polysiloxane SG-LCPs with $M_w = 2.7 \times 10^4$ g/mol, as well as PM6M with a $M_w = 143 \times 10^3$ g/mol (comparable to PM6M-1 and PM6M-2) in a 250 μm gap. The authors report that although NMR spectra indicated increase in order parameter after a few minutes, optical microscopy of samples quenched intermittently in the course of the aligning process revealed that significant number of defects were annihilated only after $\approx$ 5 hours of alignment. Because defects constitute only a small volume of the sample, they are not detected by NMR [2].

is performed (Figure 5.5). Since increase in the temperature leads to increasing rate of defect annihilation [10, 11], the initial coarsening should be faster. Indeed a decrease in the initial induction time is observed with increase in temperature. For example, it takes approximately 4000s for transmission of light through the nematic SG-LCP at 100°C ($\approx$ 7°C below T_{ni}) and approximately 11000s at 95°C ($\approx$ 12°C below T_{ni}). This suggests an approximate quadratic[3] dependence of the initial induction time on $T_{ni} - T$. Since the increase in temperature reduces the rotational viscosity of the melt [7, 87], the rise in transmission beyond the initial induction time is also faster at elevated temperatures. Higher temperatures can lead to higher mobility of defects and therefore, a final stationary state with fewer defects, which should correspond to a higher final value of transmission.

As discussed in the introduction, the characteristic time for monodomain formation scales as H^2. Fuhrmann and coworkers have investigated alignment of polydomain SG-LCP melts at different magnetic field strengths, and report that the time evolution of the anisotropy in the diamagnetic susceptibility $\Delta\chi_a(t)$, which is proportional to the average order parameter within each domain of the polydomain sample, does indeed follow this scaling [82]. In contrast, the total transmission that we measure is related to the size of the domains, which does not appear to follow this scaling (Figures 5.6a and 5.6b). In general we observe a smaller initial induction period ($\sim$ 4000s compared to $\sim$ 8000s), a faster rise in transmission, and a higher final value of transparency (in 12 hours of alignment) in the sample aligned at the higher magnetic

[3]We would like to caution that we have used only two points in stating this relationship.

field (2.4T compared to 1.6T).

5.4.2 Reorientation of an Aligned SG-LCP Melt

If a sudden rotation of 90° is applied to a nematic SG-LCP melt of sufficiently low molecular weight [such as PM6M-1 in a 250μm gap (Figure 5.8a)], or one residing in a sufficiently thin gap [such as PM6M-2 in a 150 μm gap (not shown)], the nematic director can eventually reorient so as to realign along the magnetic field. This observed reorientation is consistent with what was found in Casquilho and coworkers' study of SG-LCPs with siloxane backbones [76], as well as Roth's NMR studies of relatively low molecular-weight ($M_w \approx 12,000$g/mol) SG-LCPs with a polyacrylate backbone [78]. The intermittent turbid period that we find after 15 minutes into the realignment process, as evidenced by the dip in the total transmittance (Figure 5.8a), suggests that sudden orthogonal mis-alignment with the magnetic field breaks up the nematic monodomain. The SG-LCP sample then slowly reforms with its director parallel to the static magnetic field. This break-up and reforming of the monodomain after a sudden rotation of 90° is consistent with NMR studies of polyacrylates reported by Roth [78].

Polarization microscopy on PM6M-1 quenched to room temperature at the point at which turbidity reaches a maximum (or the transmission reaches a minimum in Figure 5.8a) reveals that the material does not possess a unique optical axis; rotation between crossed polarizers reveals small ($\approx 25\mu$m) "patches" of material that become extinct at different rotation angles, from which we infer that nematic domains within

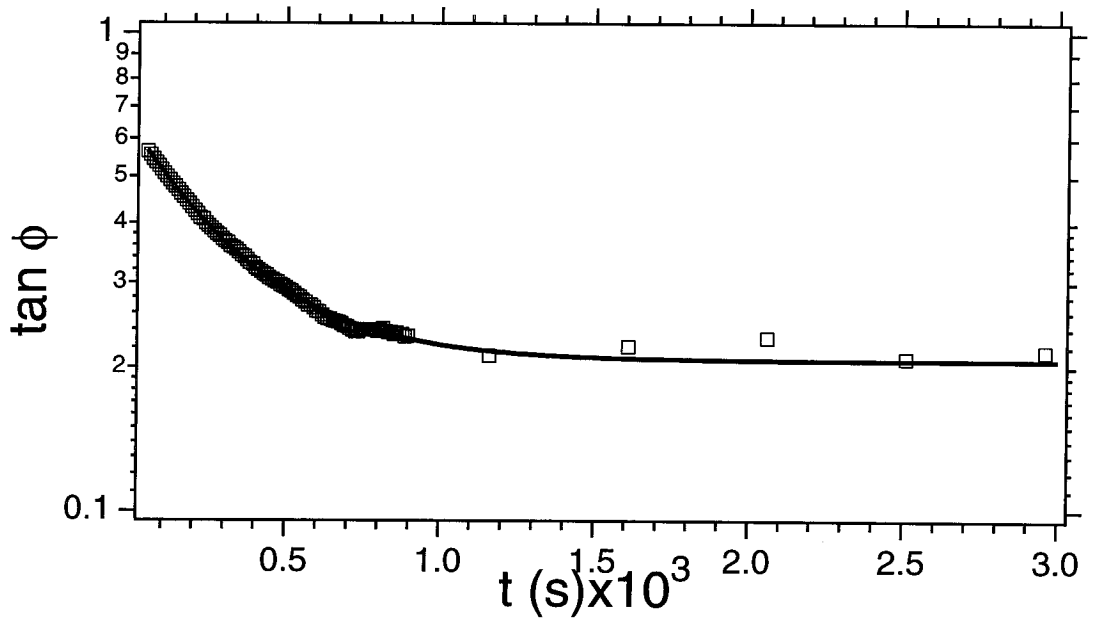

Figure 5.12: Evolution of the orientation of the nematic director during realignment after rotation of an aligned SG-LCP sample by 30°. The value of $\tan\phi$ is calculated from the experimental values of $\left(\frac{r}{1+r}\right)^{1/2}$ shown in Figure 5.9 using equation 5.8. The solid line corresponds to a fit – $\tan\phi = 0.20663 + 0.42281 * e^{(-t/305.91)}$. Sparse markers have been used for the experimental data.

the material are not globally aligned with each other. It is important to note that even at the point of lowest transmittance in the realignment process PM6M-1 never became as turbid as the material in the polydomain state formed upon cooling from the isotropic phase in the absence of an applied field. This suggests that the mean of the distribution of domain sizes at this stage in time is significantly larger than that in the polydomain material. We believe that it would be interesting to observe the reorientation process using microscopy to distinguish if the domain break up occurs at the few defect sites that exist in the final stationary state of the pre-aligned material.

For the sudden 30° rotation from the static magnetic field, the SG-LCP sample responds by gradually aligning along the field, as manifested in the variation of

$\sin\mu\cos 2\phi$ (Figure 5.9). This is consistent with past observations of evolution of the order parameter by Fuhrmann and coworkers [82]. Using the experimentally measured values of $I_\perp$ and $I_\parallel$, and equations 5.7 and 5.8 we calculated $\tan\phi(t)$ during the reorientation by 30° (Figure 5.12). We then used equation 5.3 to fit the evolution of ϕ as a function of time with good agreement. The calculated characteristic time of $\approx$ 306s in combination with the earlier reported estimate of $\Delta\chi_a \approx 10^{-6}$ [81] gave $\gamma_1 \approx 1.4 \times 10^3$Pa-s (at 368.5K or $\frac{T}{T_{ni}} \sim 0.97$).[4] Fuhrmann and coworkers report a rotational viscosity of 93×10^3Pa-s (at a temperature about 20°C below T_{ni} for an SG-LCP with $M_w \approx 334 \times 10^3$g/mol).

The good agreement between the crossed-polar intensities and the single-exponential rate expression suggests that the reorientation of the director in nematic SG-LCP melts, at least at the conditions detailed above, can be described in a manner similar to that used in low molar-mass LCs; namely, magnetic alignment is dominated by the mesogen's anisotropic magnetic susceptibility, and the presence of the main chain and spacer is to effectively increase the viscous resistance to the aligning forces. This suggests that the bi-exponential realignment model proposed by Götz *et al.* [55], may not be present during this reorientation (unless the initial fast process Götz and coworkers hypothesize occurs at times faster than a few seconds). Indeed, Götz *et al.* speculate that the rapid process associated with mesogens rotating about the spacer is likely to significantly affect the kinetics of alignment only when using extremely high orienting fields together with materials with high diamagnetic anisotropies in

[4] In accordance with Fuhrmann and coworkers we used a density of 1000kg/m^3.

the mesogenic group.[5]

Intriguingly, the realignnment in ϕ during the 30° reorientation experiment becomes extremely slow after about 1100s when the nematic director is approximately 10° away from the magnetic field. Fuhrmann and coworkers have observed a complex pattern in the kinetics of realignment depending on the thermal aging of the sample and speculate on the possible role of defects. We believe a similar phenomena is occuring in our samples and is exacerbated by the prolonged equilibration of the sample for temperature stability when using a Variac^{TM}.[6]

At less modest reorienting angles, such as the 60° realignment (Figure 5.10), the evolution of $\tan\phi$ could not be fit by equation 5.3 over the complete time range, indicating that at this large angle of reorientation, a simple exponential time dependence can no longer describe the mean director orientation in the sample as it realigns from a starting angle of 60° relative to the magnetic field. Since the angle α with respect to the polarizer is 105°, if uniform rotation of the nematic director occurs towards the magnetic field, then the nematic director would have to rotate across the analyzer (orthogonal to the polarizer) upon counter-clockwise rotation, or it would have to cross the polarizer upon clockwise rotation. In either case case $I_\perp$ should go to zero,

[5]Götz and coworkers used the technique of dielectric spectroscopy to monitor the local motions of the mesogenic unit about the main chain, the so-called "δ" process. This δ process, while often presumed to be a function of temperature, mesophasic order, and the chemical structure of the repeat unit only, has been recently shown to be influenced by the sample molecular weight and has been presumed to be influenced by cooperative motions of the backbone [88–90]. Past studies (cited in [91]) have revealed that the rotational viscosity and Leslie viscosity coefficients (α_3, α_2) [10] in nematic SG-LCPs are strongly influenced by the participation of the main chain, and that the "polymeric" viscosity of SG-LCP melts contributes strongly to all the basic features of the orientational processes in external fields.

[6]We do observe a final realignment after 30° reorientation for the thicker cell-gap of 250μm which shows oscillatory optical signals.

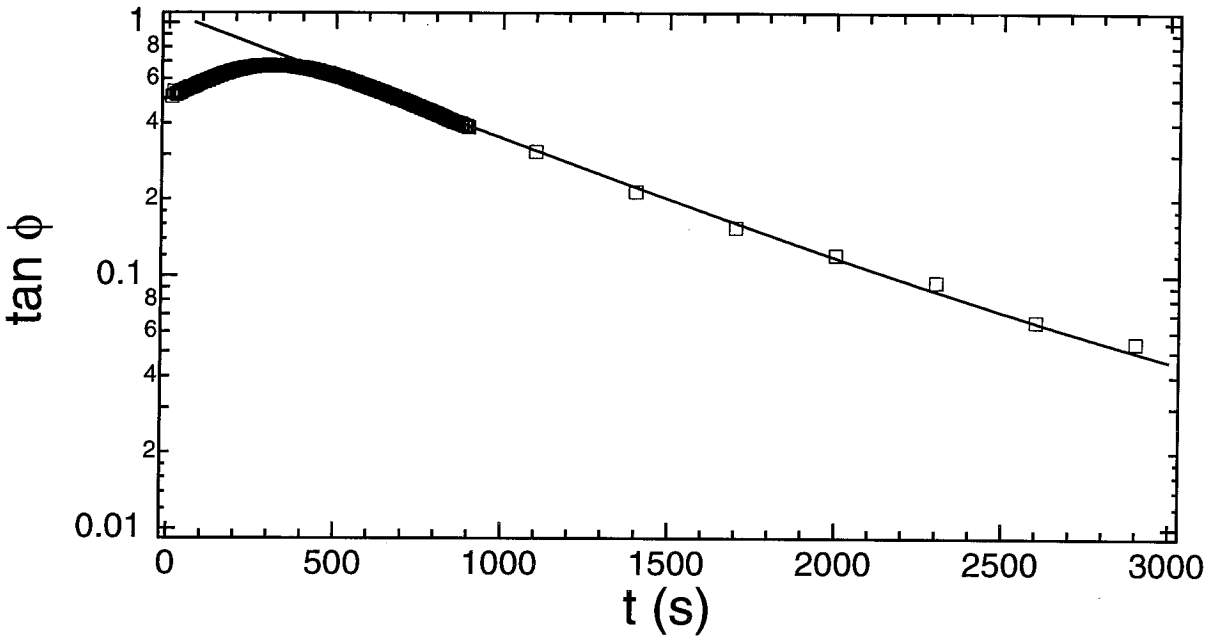

Figure 5.13: Evolution of the orientation of the nematic director during realignment after rotation of an aligned SG-LCP sample by 60°. The value of $\tan\phi$ is calculated from the experimental values of $\left(\frac{r}{1+r}\right)^{1/2}$ shown in Figure 5.10 using equation 5.8. The solid line corresponds to a fit – $\tan\phi = 0.013712 + 1.0783 * e^{(-t/854.7)}$. Sparse markers have been used for the experimental data.

which is not observed. Beyond 400s into the realignment process, equation 5.3 does fit the evolution of $\tan\phi$. The characteristic time (τ_o) is, however, 854.7s. The inability to fit data gathered after a 60° rotation to equation 5.3 is not unexpected, since for large reorientation angles > 45°, the geometry of the process of realignment is likely to produce backflow. This has been inferred experimentally in investigations of SG-LCP alignment using NMR [78, 74] and measurements of magnetic susceptibility [82]. Fuhrmann and coworkers [82] report that realignment of nematic monodomains of PM6M in a similar molecular-weight range to the SG-LCP studied here can be adequately described by equation 5.3 for angles up to 60° without any significant evidence of backflow effects. However, their experimental technique limits the ini-

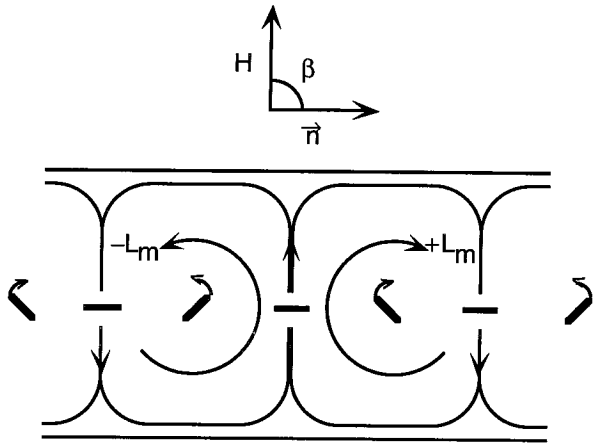

Figure 5.14: Convection rolls evolving due to non-linear coupling between director rotation and and viscous flow. At a reorientation angle 90° and 270°, the magnetic torque Γ has the opposite sign in areas which are half of a periodic length apart. Adapted from [2].

tial time for data acquisition to $\approx$ 3 minutes (180 s) into the realignment process, which is approximately the amount of time which elapses before we observe the dip in the optical signal to occur (Figure 5.10). Also, we have observed that gap width plays an important role in the reorientation process; Fuhrmann and coworkers [82] do not report gap width, but cite that their samples were "enclosed in a small glass bulb containing approximately 50 mg of the sample." Assuming a spherical bulb, this means that their sample was confined in a $\approx 4800\mu$m gap; we have used a gap which is approximately 20-100 times thinner.

When the director of the pre-aligned high molecular-weight sample (PM6M-2) in a relatively thick (d=250μm) gap is suddenly oriented orthogonal to the applied field, striations form parallel to the original director orientation (Figure 5.11b). Shear- and field-induced periodic structures in LC fluids have been previously reported (see, for

example, an extensive review by Blinov *et al.* [92]). Many shear-induced instabilities, such as spatially periodic patterns (bands), have been observed during flow or after cessation of shear in low molar-mass LCs [10] and main-chain LCPs [93]. These instabilities have been attributed to the relaxation of a structure with an alignment which is flawed, with the director periodically deviating from the flow direction by alternating angles $\pm\theta$. However, these structures are visible only when the sample is viewed between crossed polarizers, whereas the striations we observe remain unchanged irrespective of polarizer orientation, and regardless of whether the polarizers are present at all.The formation of the "chevron" director pattern should not depend strongly on the dimensions of the gap to which the sample is confined. In contrast, PM6M-2 reoriented at 90° in a 250 μm gap forms striations (Figure 5.11b), whereas the texture of the same material oriented at an identical temperature and field strength in a 150 μm gap appears virtually featureless under crossed polars. In light of this information, we attribute the striated texture to a director deformation field distinct from the aforementioned shear-induced "chevron" structure. We suspect that the striated structures may be convective roll cells similar to those observed earlier for polysiloxane SG-LCPs (in a 250 μm-thick gap) that were quenched after continuous rotation in a 7 T NMR magnet [2]. As in our case, the periodic structures were reported to be visible without the aid of crossed polarizers [2]. Such deformations of the director field are believed to occur at reorientation angles near 90° because at these angles the magnetic torque acts in opposite directions in regions separated by half-wave period of the long-wavelength director fluctuation [94] and is balanced by the elastic torques

acting on the sample (Figure 5.14). Schwenk *et al.* [2] report that the evolution of roll cell formation reaches a steady state after approximately 2 hours, and does not relax into a monodomain structure. We also observed that the striated structure persists 10-11 hours after its initial formation (Figure 5.11a).

Based on the rationale that the gap width should play a large role in controlling the periodicity of convective rolls, we repeated the 90° reorientation experiment with PM6M-2 in a 150μm gap. However, as mentioned earlier, reorientation in this thinner gap appeared to result in uniform director alignment parallel to the magnetic field (the quality of the alignment appeared to be poorer relative to the final state after reorientation by 30° or 60°). The suppression of convective rolls can occur since the critical magnetic field required to induce bend, splay, or twist director deformations is inversely related to the cell thickness [2, 95].

5.5 Conclusions

We have performed an *in-situ* study, using optical techniques, of magnetic alignment of a high-molecular weight SG-LCP melt with a polymethacrylate backbone and a phenyl-benzoate mesogen. We find that for alignment of a polydomain nematic material in a static magnetic field one can discern three stages: an initial period where no light is transmitted through the sample, followed by a rapid rise in the total transmission and a final saturation to a constant value. The initial period of turbidity is approximately a few thousand seconds ($\sim 1-2$ hours) and depends on the interplay of magnetic field strength, temperature and cell-gap but is unaffected by molecular

weight (at least over the range studied here). The rate of rise of transmission in the later stage is, however, dependent on all four parameters.

We have investigated the reorientation of an aligned SG-LCP melt for two different molecular weights in combination with different angles. When the aligned sample is suddenly rotated in the magnetic field, such that after rotation the direction of uniform alignment makes a small angle (e.g., 30°) with the magnetic field, the alignment process appears to occur homogeneously and the director rotation towards the magnetic field direction can be adequately described using single exponential function, *i.e.,* is characterized by a single time constant. We believe that this suggests that director reorientation in this case is controlled largely by the viscous properties of the fluid and the elastic torques acting on the mesogens as they try to respond to the orienting magnetic field. These findings are consistent with previous literature reports of dielectric spectroscopy measurements, which indicate that mesogen reorientation in SG-LCPs is a cooperative effort between the mesogen and backbone, and hence is unlikely to be easily separated into independent, distinctly-occurring processes. At higher reorientation angles (e.g., 60°), the material appears to realign inhomogeneously and the evolution of the director orientation can no longer be fit to a simple exponential time-dependence, presumably due to backflow effects in the initial stages of the realignment process. At even higher reorientation angles (e.g., 90°) when the molecular weight is sufficiently high instabilities lead to striated morphologies that permit no light to pass through the sample. We believe these striated formations are convective roll cells that result from periodic distortions in the director field and are

similar to those observed in past studies that have used rotating magnetic fields.

Appendix A

A.1 Design Drawings for the Compact Shear Cell

The shearing-device referred to in Section 2.4 (Figures 2.6) is shown in Figure A.1 and the design drawings for the different components are shown in Figures A.2a- A.3c. This shear cell allowed for a relatively precise control of the gap-width across the plane of the shearing motion. The cell was designed to be compact (approx. 3/4" thick and about the size of a credit card). The SG-LCP melt ('a' in Figure 2.6) resides in a gap bounded by glass plates ('b' in Figure 2.6) attached to thin copper sheets ('c' in Figure 2.6). The copper sheets are bolted to a central aluminum piece into which a shallow circular depression has been milled. A thin, annular-shaped Kapton-insulated heater ('d' in Figure 2.6) resides in this depression. Thermal contact between the heaters and copper plates is maintained by filling in any space between these two elements with thermally conductive argentous epoxy (Aremco) ('e' in Figure 2.6). Co-axial holes in the heaters and aluminum heat sink allow for optical measurements in conjunction with shearing experiments. The central portion of the device is attached to an outer frame via beryllium-copper or stainless steel leaf springs ('f' in Figure 2.6), which serve dual purposes; they constrain the motion of the plate to achieve uniaxial shearing motion, and they thermally isolate sample-bearing portion of apparatus from the instrument in which the shear cell is mounted. Further insulation is provided by mounting the cell on a Bakelite (phenolic) platform which can be free-standing or can double as a non-rotating polarizing microscope stage. Different spacer bars ('g' in Figure 2.6) were used to maintain the desired gap width, which was typically 0.3 - 0.1mm. A motorizer (Newport Model 860-C2) fitted with a narrow spindle pushes

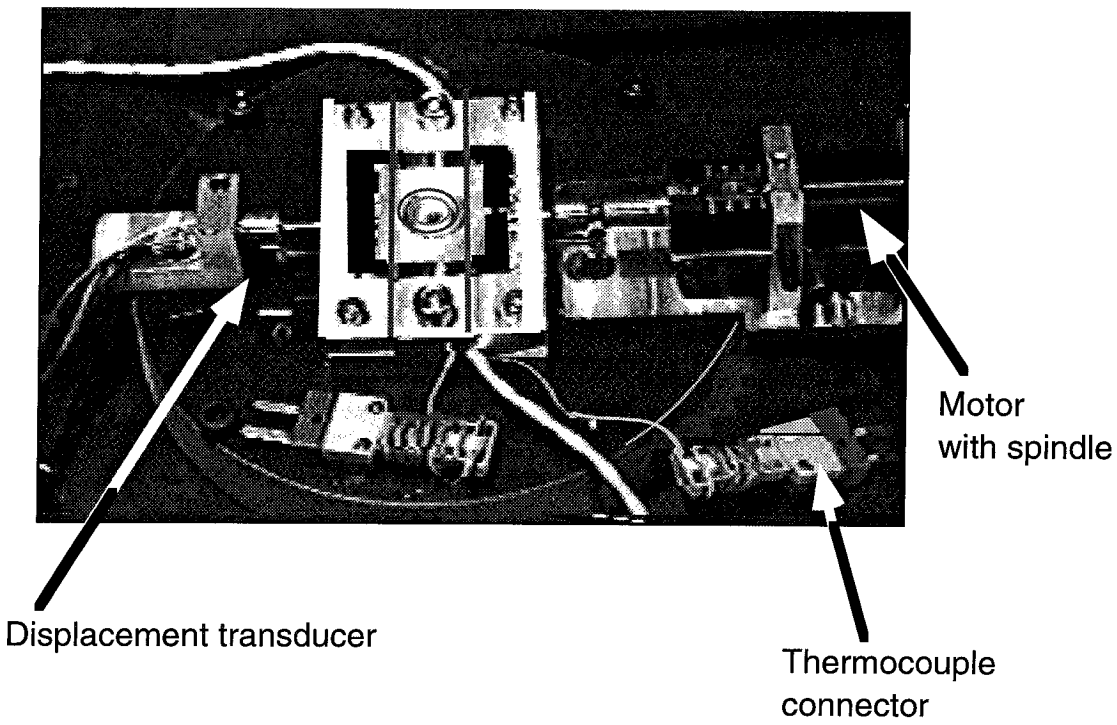

Figure A.1: Photograph of the shear cell assembly.

against the upper half of the sample-bearing portion of the device. The motorizer is controlled by a controller (Newport 860-C2) interfaced with a MacIntosh computer via a LabView control program and a National Instruments board.

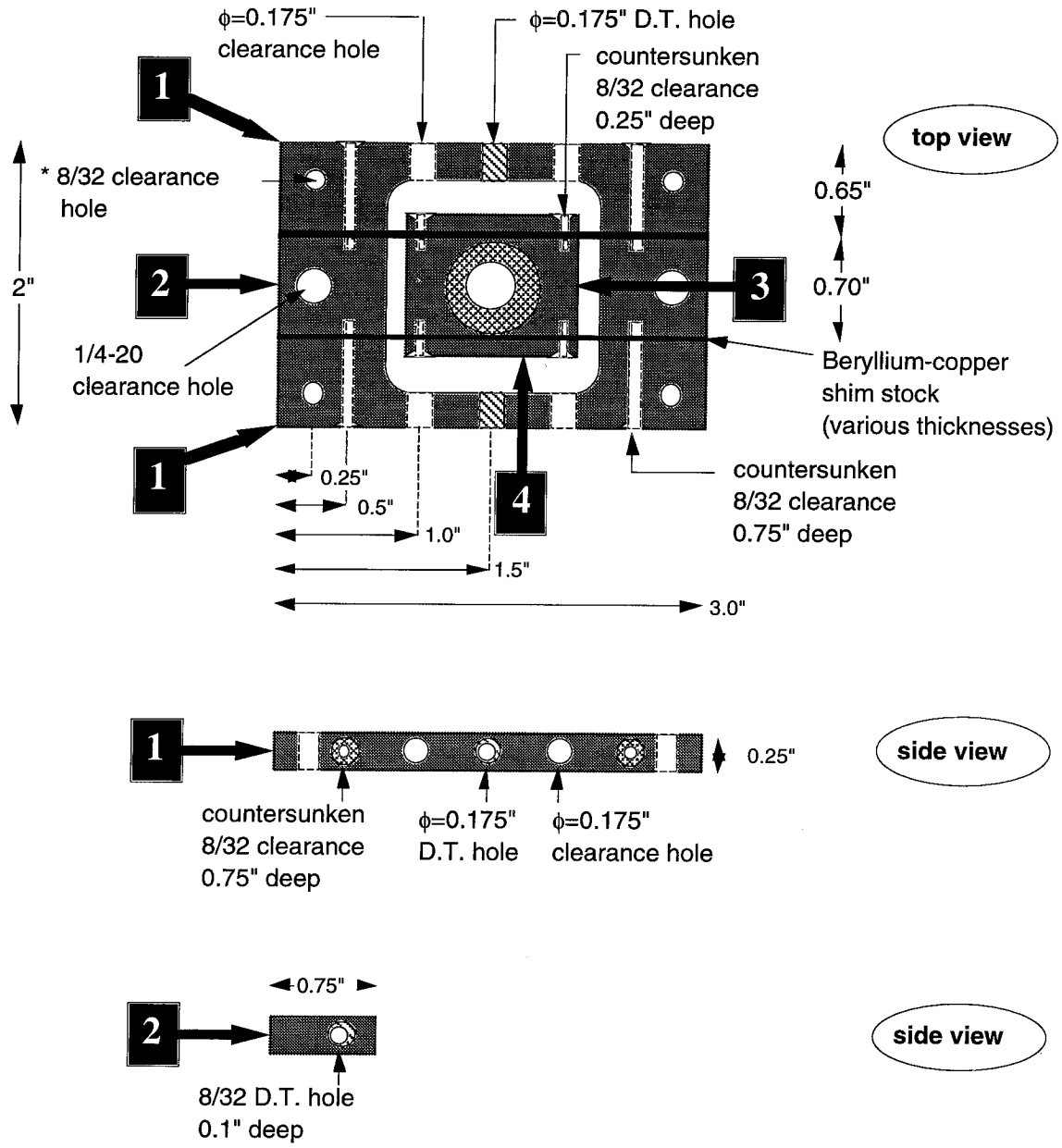

Figure A.2a: Schematic of the assembled shear cell showing the different component parts.

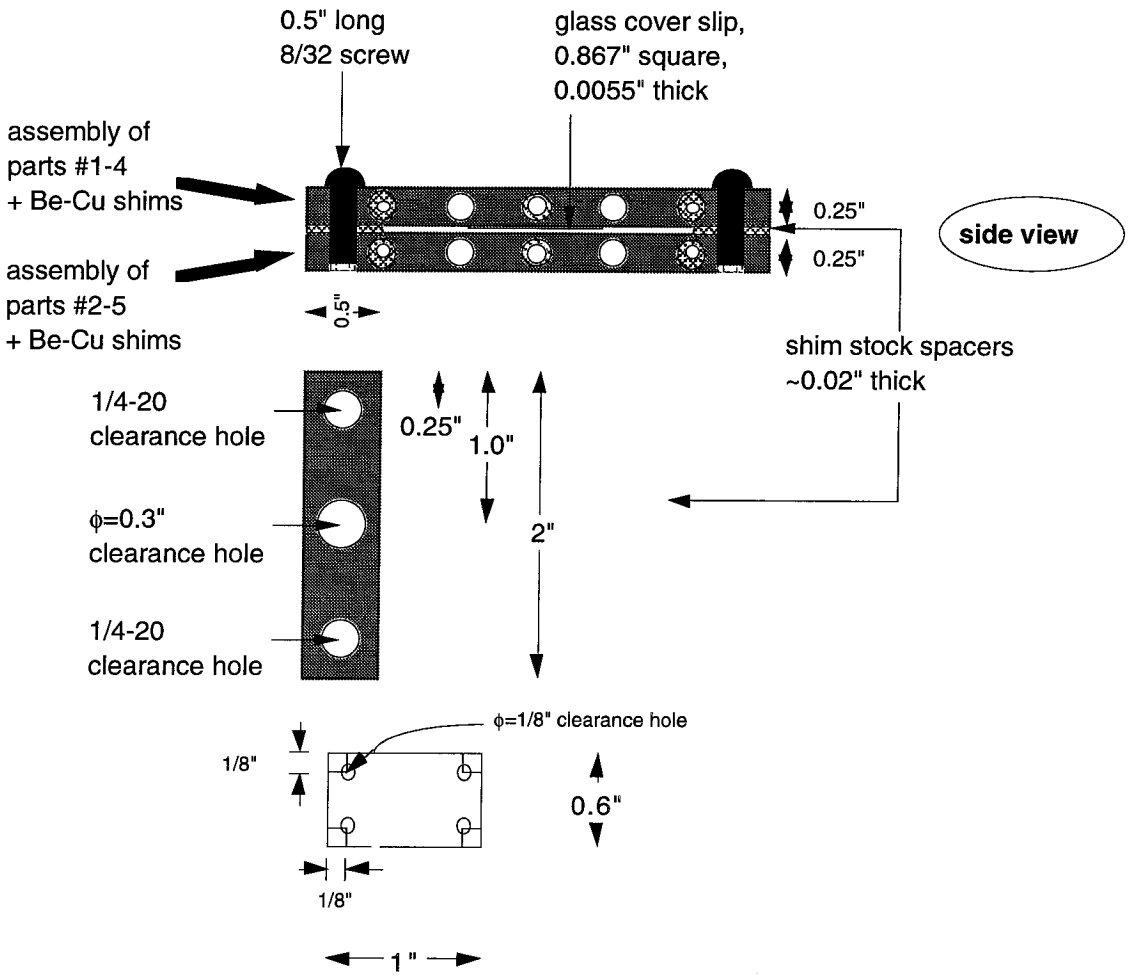

Material: aluminum shim stock, 0.03" thick.

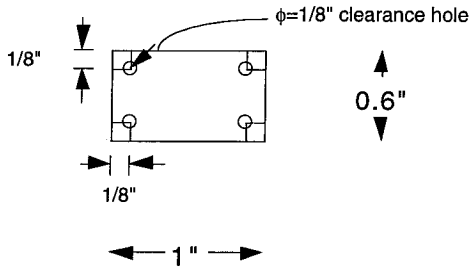

Material: glass microscope slides, 0.035" thick.

Figure A.2b: Design drawings for component parts 1 for the shear cell.

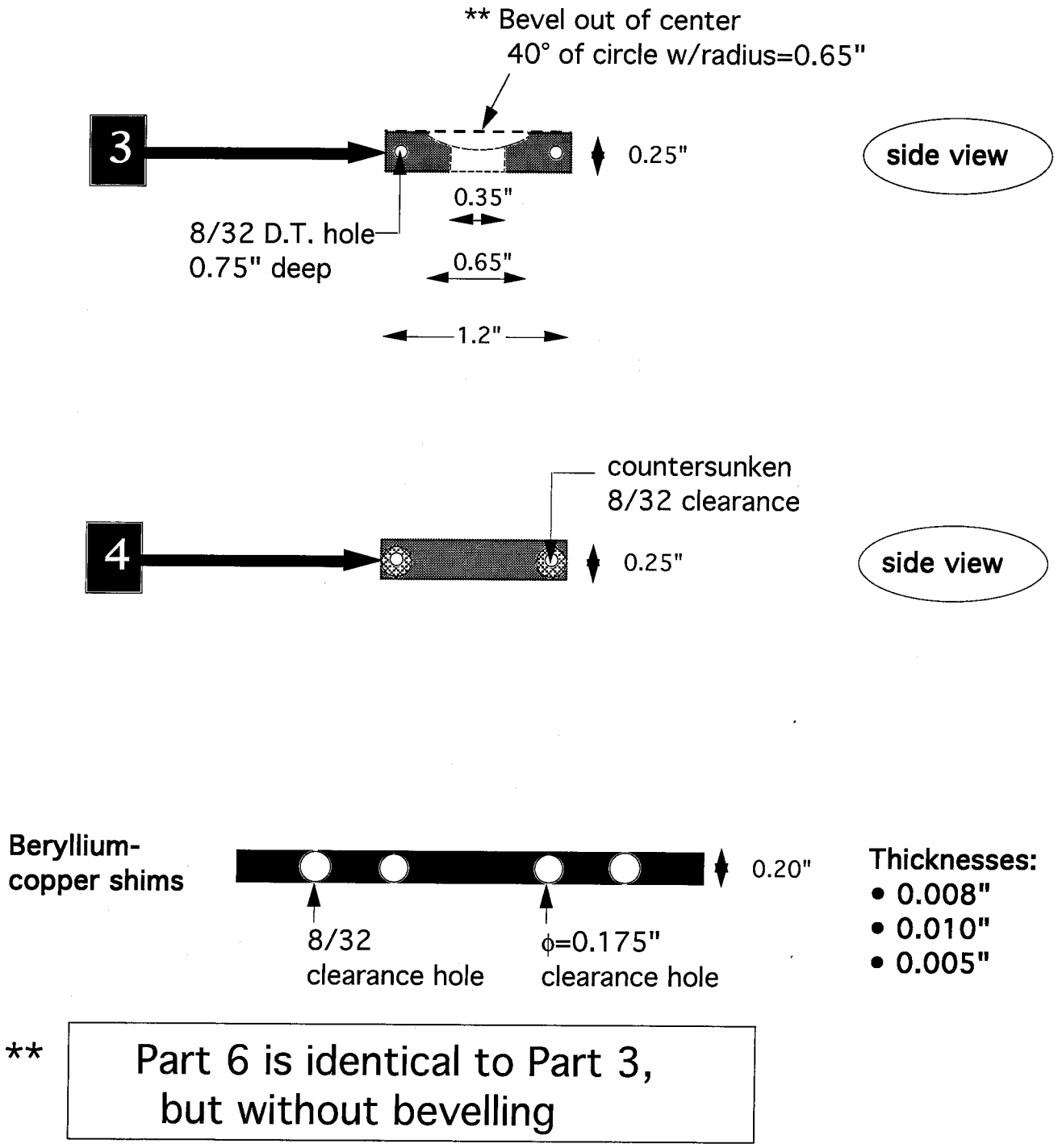

Figure A.2c: Drawings for the component parts 3-4 in the shear cell assembly.

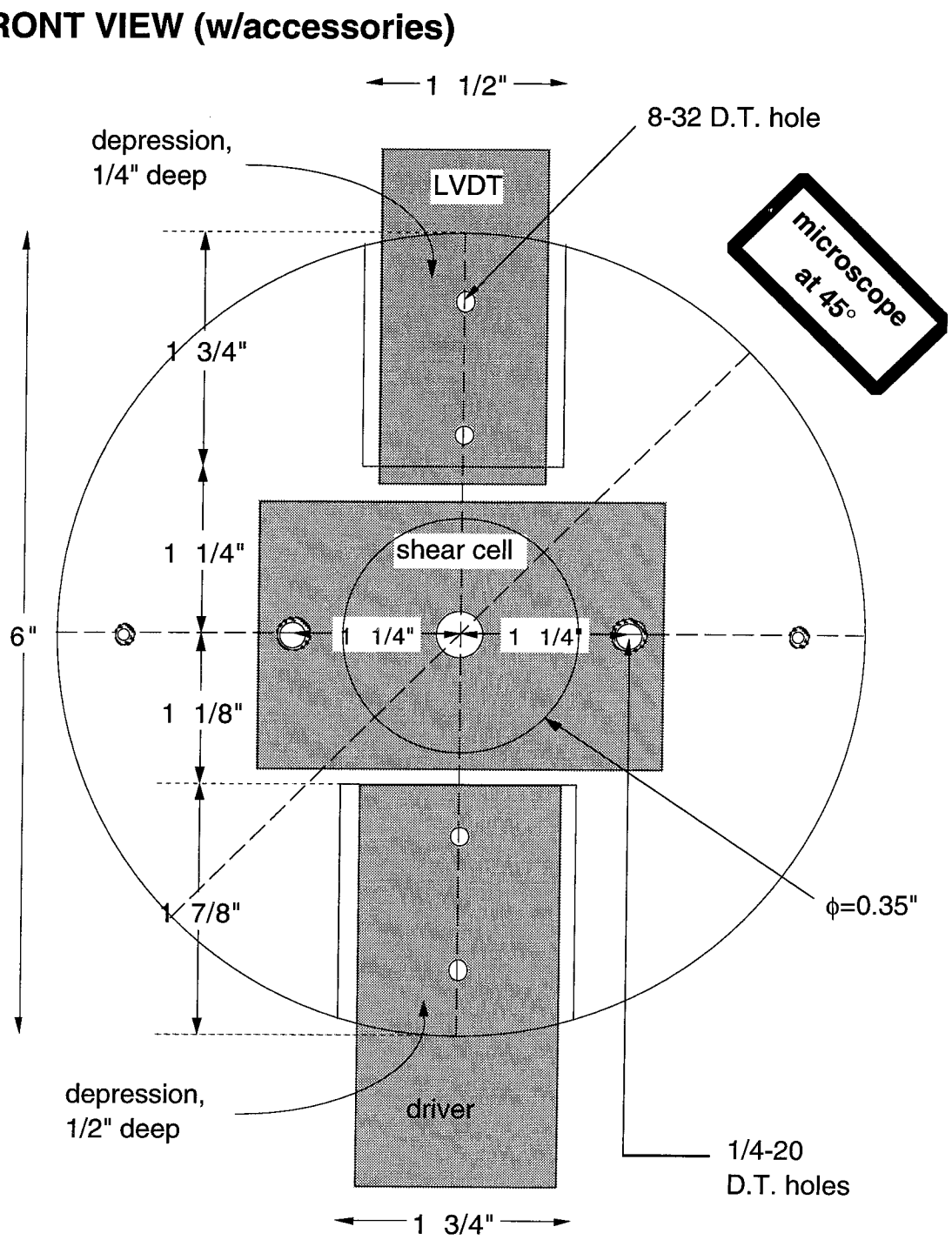

Figure A.3a: Schematic arrangement for mounting the shear cell on a platform.

BACK VIEW

Note: 8-32 holes shown here may go through to front, but do not appear on the front-view drawing.

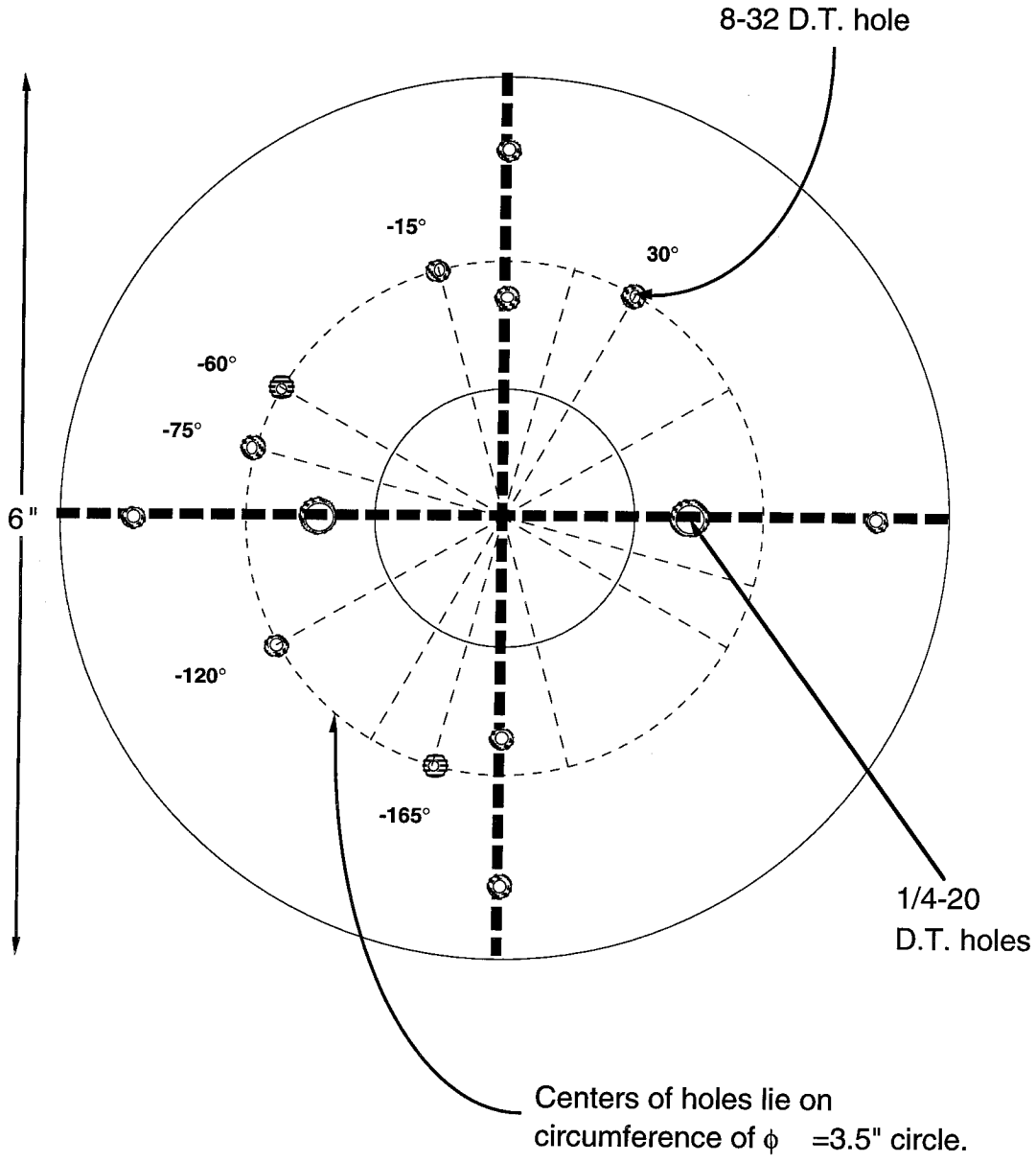

Holder puts center of LVDT 3/4" above mounting surface.

Figure A.3b: Design drawings for the mounting platform – back view.

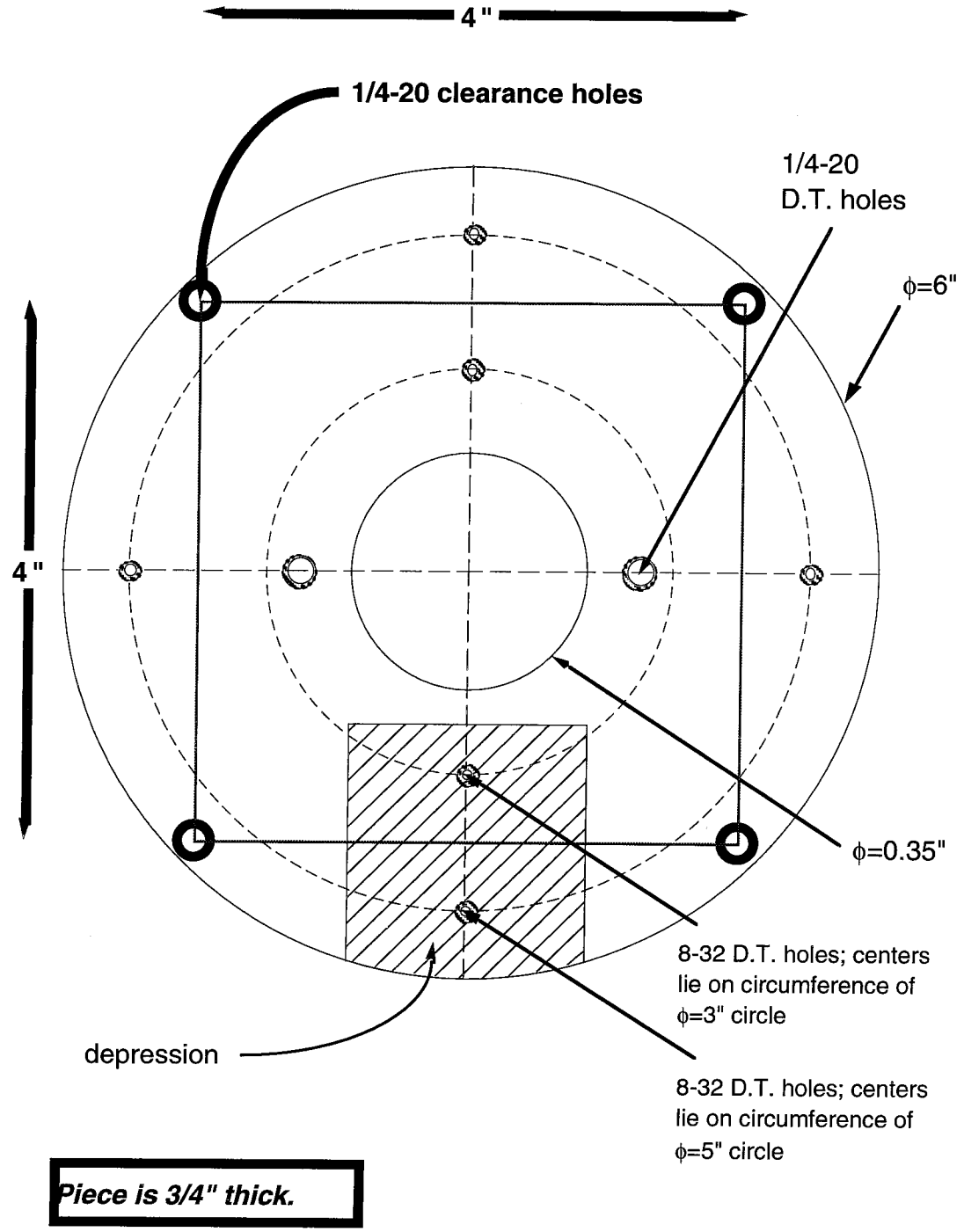

Figure A.3c: Design drawings for the mounting platform – front view.

A.2 Design Drawings for Components Used for Magnetic Alignment Set-Up

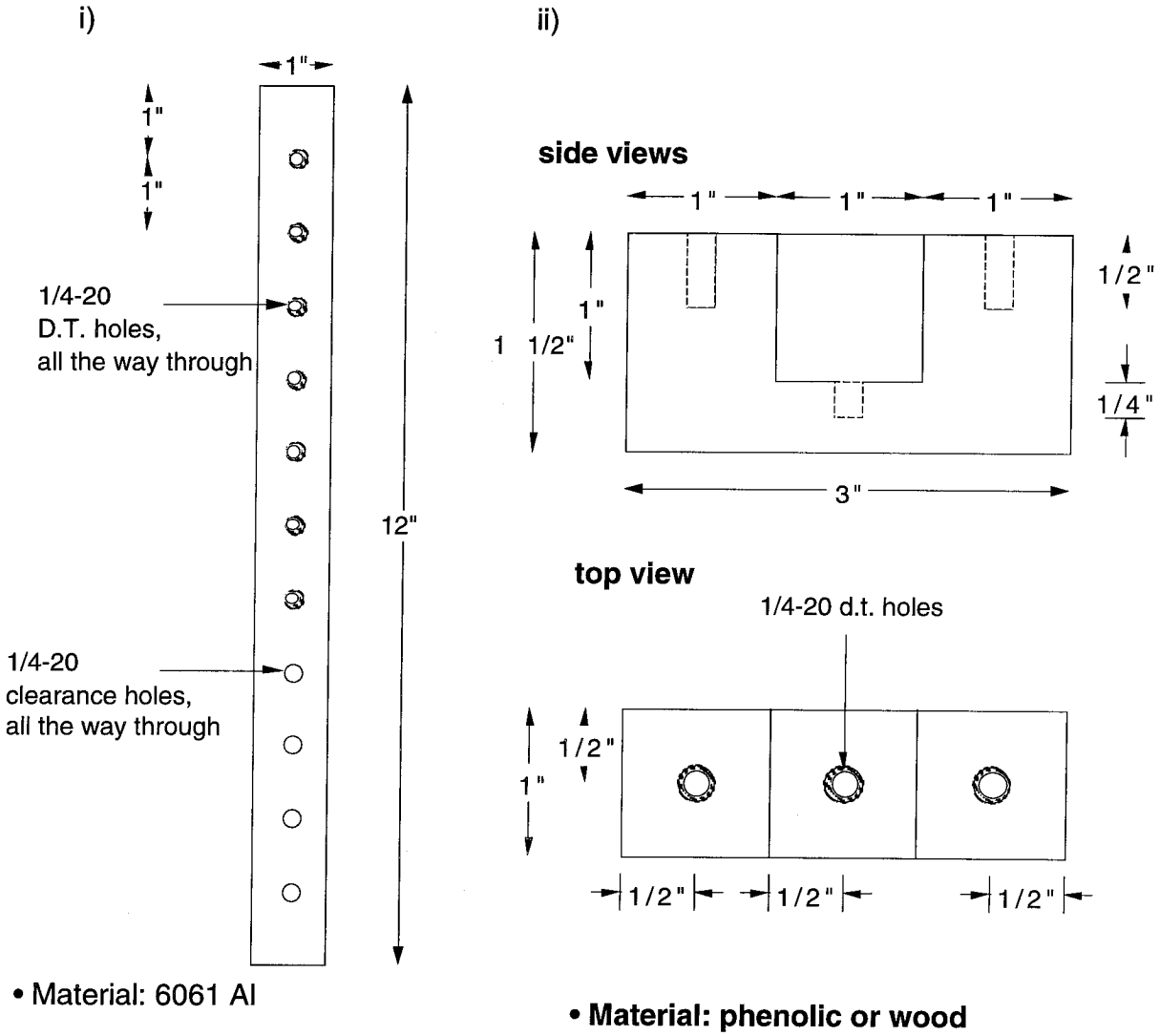

Figure A.4: Cross bar (i) used for mounting detectors 2 and 3 in the optical set-up (see Figure 2.7). Parts (ii) are used to attach the cross-bar to the center bar running between teh poles of the magnet and supporting the sample cell.

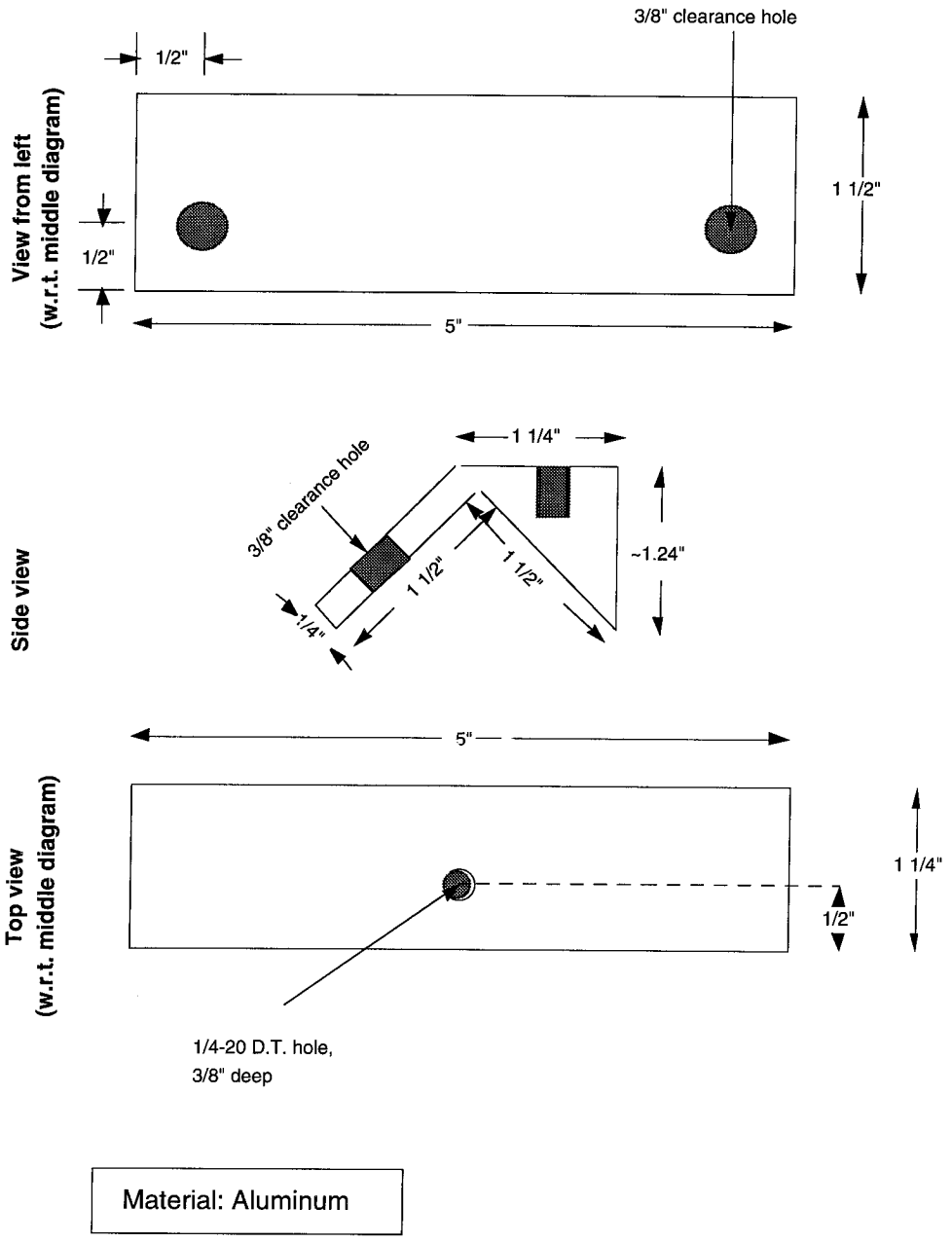

Figure A.5: V-bracket used for mounting the center bar (which runs between the poles of the magnet and supports the sample cell) to the frame of the electromagnet.

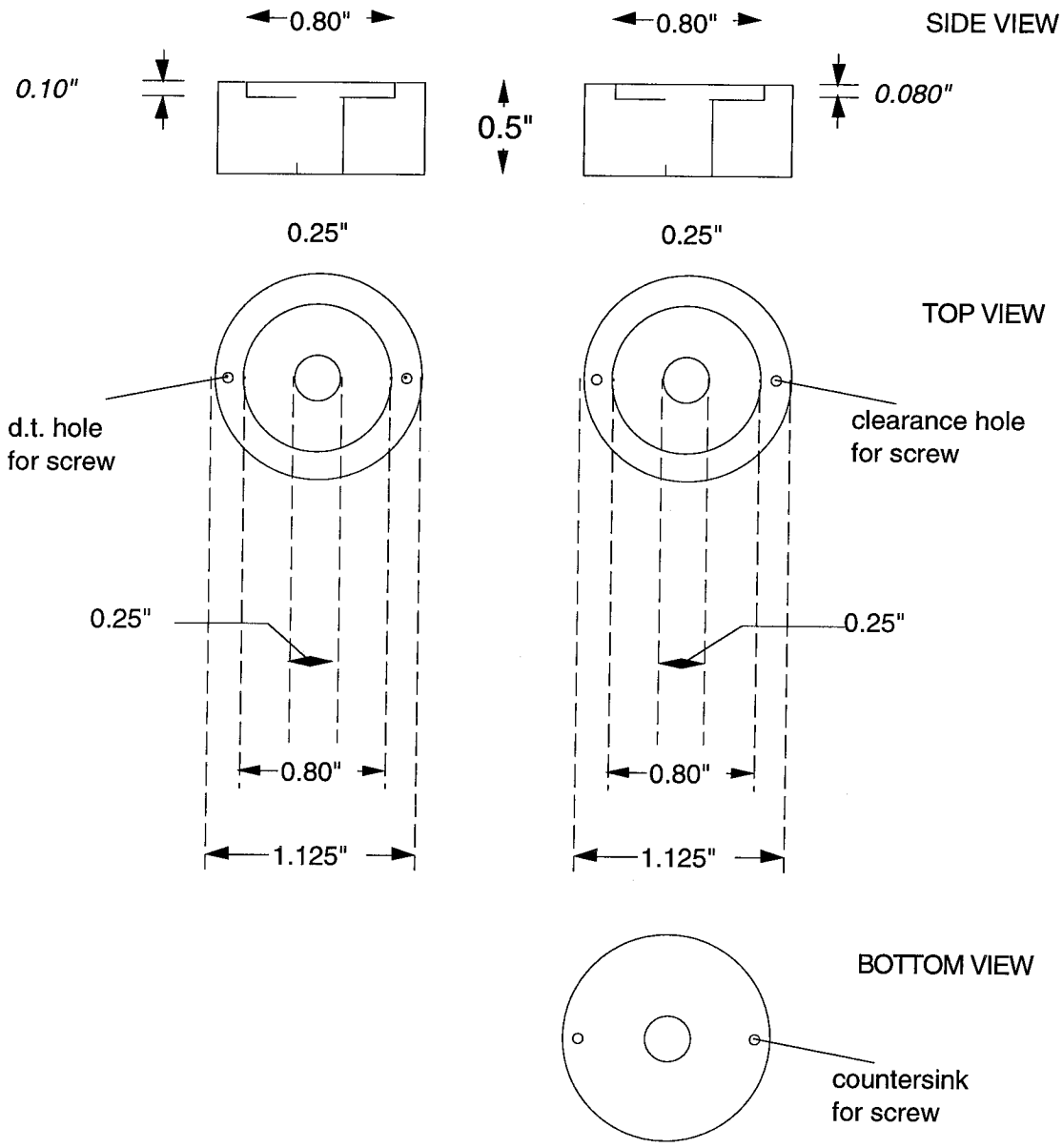

All parts from 6061 Aluminum.

Figure A.6a: Drawings for the cell in which the polymer sandwich is held.

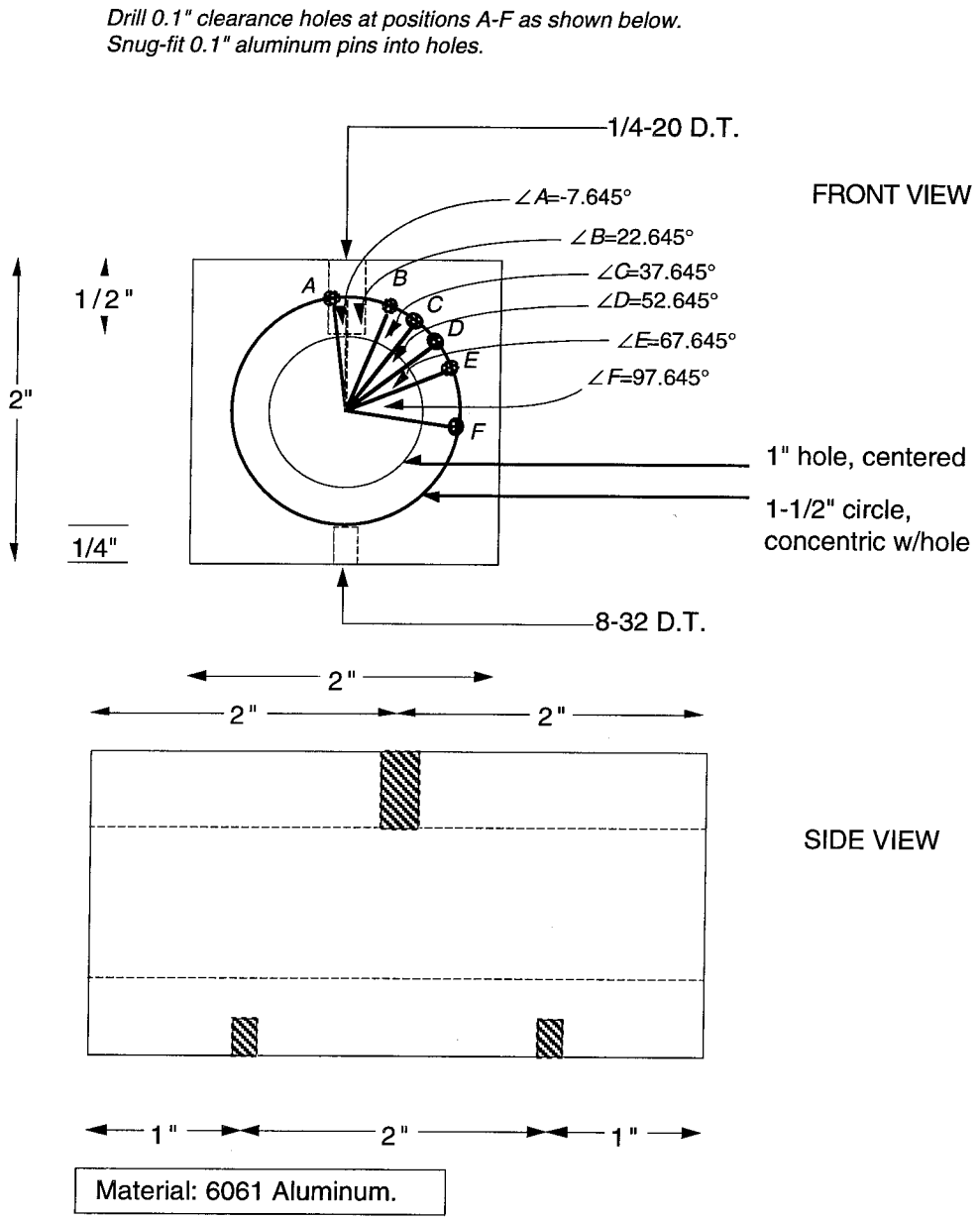

Figure A.6b: Component used to rotate the sample cell in the magnetic field by known angles (using positions A-F).

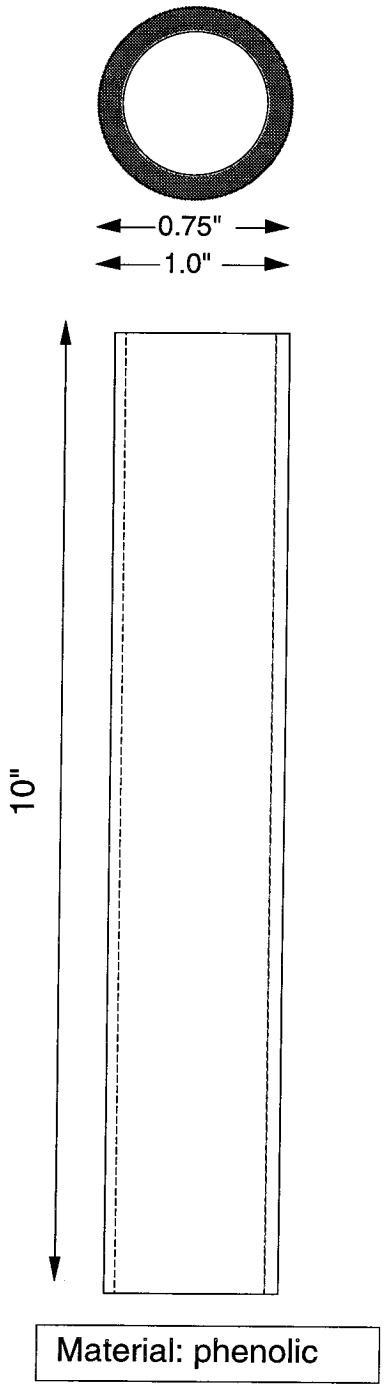

Figure A.6c: Phenolic tube used to handle the sample at elevatied temperatures and when it is within the magentic field.

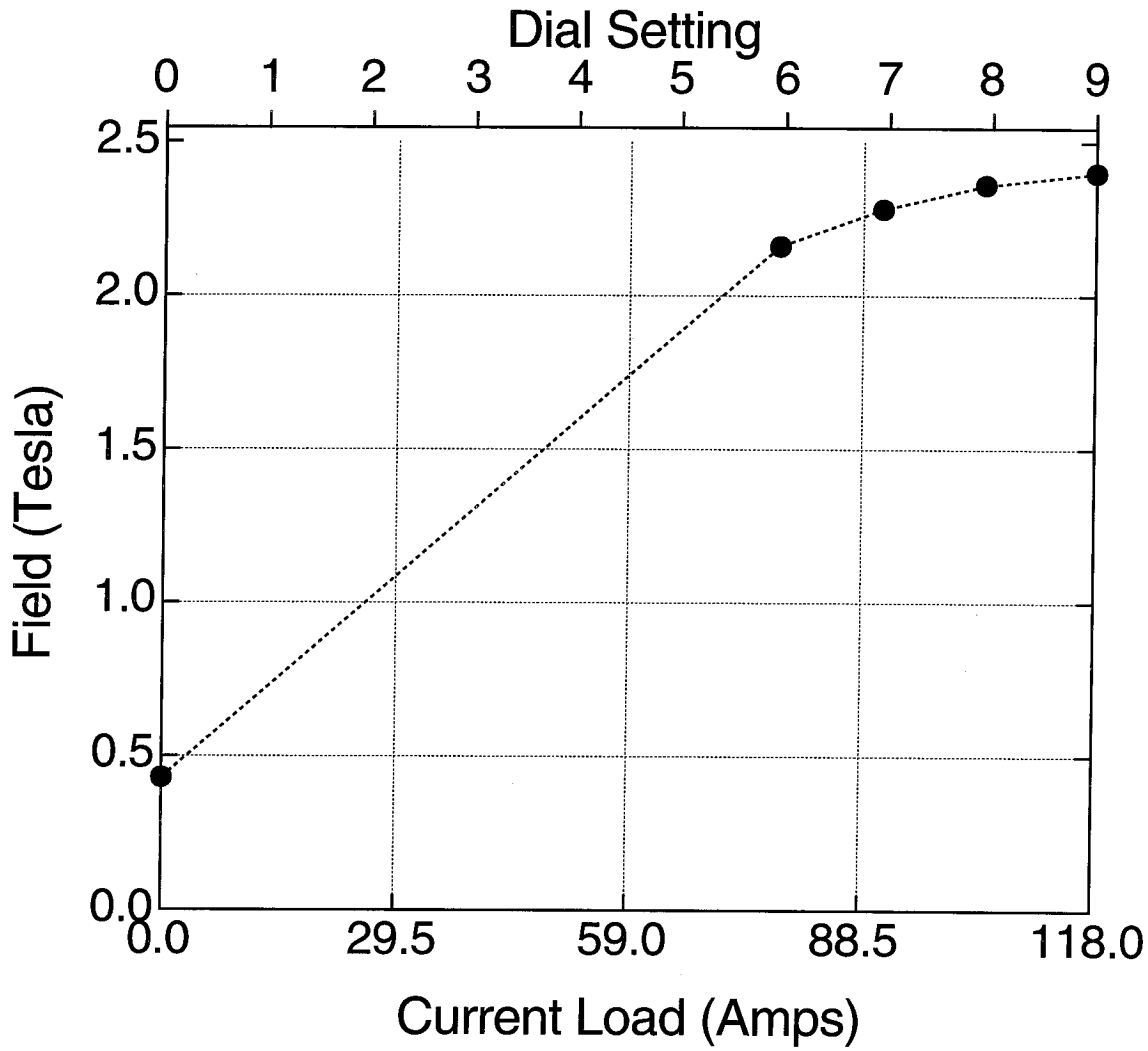

Figure A.7: Calibration curve for the Varian electromagnet.

Bibliography

[1] R. M. Kannan, J. A. Kornfield, N. Schwenk, and C. Boeffel. *Macromolecules*, 26:2050, 1993.

[2] N. Schwenk, C. Boeffel, and H. W. Spiess. *Liq. Cryst.*, 12:735, 1992.

[3] S. Wu. *Polym. Eng. Sci.*, 32(12):823–830, 1992.

[4] S. Wu. *J. Polym. Sci. B. Polym. Phys.*, 27:723–741, 1989.

[5] J. D. Ferry. *Viscoelastic Properties of Polymers, 3rd Ed.* Wiley, New York, 1980.

[6] A. Ciferri, W.R. Krigbaum, and R. B. Meyer. *Polymer Liquid Crystals.* Academic Press, New York, 1982.

[7] C.B. McArdle (ed.). *Side Chain Liquid Crystal Polymers.* Chapman and Hall, New York, 1989.

[8] A. M. Donald and A. H. Windle. *Liquid Crystalline Polymers.* Cambridge University Press, New York, 1992.

[9] V. P. Shibaev and L. Lam (eds.). *Liquid Crystalline and Mesomorphic Polymers.* Springer Verlag, New York, 1994.

[10] P.-G. de Gennes. *The Physics of Liquid Crystals.* Clarendon Press, Oxford, 1974.

[11] S. Chandrasekhar. *Liquid Crystals.* Cambridge University Press, New York, 1977.

[12] G. Vertogen and W.H. de Jeu. *Thermotropic Liquid Crystals, Fundamentals.* Springer-Verlag, New York, 1987.

[13] P. L. Collings. *Liquid Crystals : Nature's Delicate Phase of Matter.* Princeton University Press, Princeton, NJ, 1990.

[14] G.W. Gray and J.W.G. Goodby. *Smectic Liquid Crystals.* Leaonard Hill, Glasgow, 1984.

[15] B. Bahadur. *Liquid Crystals : Applications and Uses.* World Scientific Press, Teaneck, NJ, 1990.

[16] H. Finkelmann, M. Happ, M. Portugall, and H. Ringsdorf. *Makromol. Chem.*, 179:2541, 1978.

[17] H. Finkelmann, H. J. Kock, W. Gleim, and G. Rehage. *Makromol. Chem. Rapid Commun.*, 5:287, 1984.

[18] L. Greene, L. X. Phan, E. E. Schmitt, and J. M. Mohr. *ACS Symp. Ser.*, 520:244, 1993.

[19] R. F. Stewart, J. M. Mohr, E. A. Budd, L. X. Phan, and J. Arul. *ACS Symp. Ser.*, 520:232, 1993.

[20] J.S. Moore and S.I. Stupp. *Macromolecules*, 20:282–293, 1987.

[21] E. J. Kim and O. O. Park. *Mol. Cryst. Liq. Cryst. Sci. Tech. Section, Mol. Cryst. Liq. Cryst.*, 267:41, 1995.

[22] W. Zhou, R. N. Fu, R. J. Dai, Z. F. Huang, and Y. F. Chen. *HRC J. High Resolution Chromatography*, 17:719, 1994.

[23] Y. Ly and Y. L. Chung. *J. Membrane Sci.*, 77:99, 1993.

[24] A. Tadayuki, Y. Shudo, and Y. Fmuio. *CA Selects*, 3:35, 1987.

[25] H. Loth and A. Euschen. *Macromol. Chem. Rapid Commun.*, 8:35, 1988.

[26] F. L. Dickert, G. K. Zwissler, and E. Obermeier. *Ber. Buns. Ges. Phys. Chemie*, 97:184, 1994.

[27] H. Kruger and R. Rubner. 1984. US Patent 4469408.

[28] T. Seki, M. Sakuragi, Y. Kawanishi, Y. Suzuki, T. Tamaki, R. Fukada, and K. Ichimura. *Langmuir*, 9:211, 1993.

[29] T. Seki, R. Fukada, T. Tamaki, and K. Ichimura. *Thin Solid Films*, 243:675, 1994.

[30] G. Attard and C. Imrie. *New Scientist*, May 11:38, 1991.

[31] S. Hvilsted, F. Andruzzi, H. W. Siesler, and P. S. Ramanujam. *Macromolecules*, 28:2172, 1995.

[32] K. Anderle and J. H. Wendorff. *Mol. Cryst. Liq. Cryst. Sci. Tech. Section A: Mol. Cryst. Liq. Cryst.*, 243:51, 1994.

[33] Y. K. Han, D. Y. Han, and Y. H. Kim. *Mol. Cryst. Liq. Cryst.*, 254:445, 1994.

[34] H. Finkelmann, U. Kiechle, and G. Rehage. *Mol. Cryst. Liq. Cryst.*, 94:23, 1983.

[35] R. Zentel and J. Wu. *Makromol. Chem.*, 187:1727–1736, 1986.

[36] R. M. Kannan, J. A. Kornfield, and N. Schwenk. *Advanced Materials*, 6(3):214, 1994.

[37] J. E. Mark, A. Eisenberg, W. W. Graessley, L. Mandelkern, E. T. Samulski, J. L. Koenig, and G. D. Wignall. *Physical Properties of Polymers.* ACS Professional Reference Book, Washington, DC, 1993.

[38] R. M. Kannan. PhD thesis, California Institute of Technology, Pasadena, CA, 1995.

[39] N. H. Hartshorne and A. Stuart. *Crystals and the Polarising Microscope.* Edward Arnold & Co., New York, 1970.

[40] K. Hongladarom, W. R. Burghardt, S. G. Baek, S. Cementwala, and J. J. Magda. *Macromolecules*, 26(4):772, 1993.

[41] R. H. Colby, J. R. Gillmore, G. Galli, M. Laus, C. K. Ober, and E. Hall. *Liq. Cryst.*, 13:233, 1993.

[42] R. M. Kannan, S. F. Rubin, and J. A. Kornfield. *J. Rheol.*, 38:1609, 1994.

[43] P. Fabre and M. Veyssie. *Mol. Cryst. Liq. Cryst. Letters*, 4(2-4):99–105, 1987.

[44] K. F. Wissbrun and A. C. Griffin. *J. Polym. Sci., Polym. Phys. Ed.*, 20:1835, 1982.

[45] R. S. Porter and J. F. Johnson. In F.R. Eirich, editor, *Rheology.* Academic Press, San Diego, 1967.

[46] D. G. Baird. In A. Blumstein, editor, *Liquid Crystalline Order in Polymers.* Academic Press, San Diego, 1978.

[47] S. P. Papkov, V. G. Kulichikhin, V. D. Kalmykova, and A. Y. Malkin. *J. Polym. Sci. Polym. Phys. Ed.*, 12:1753, 1974.

[48] K. A. Koppi, M. Tirell, F. S. Bates, K. Almdal, and R. H. Colby. *J. Phys. II France*, 2:1941, 1992.

[49] R. G. Larson, K. I. Winey, S. S. Patel, and R. Bruinsma. *Rheologica Acta*, 32:245–253, 1993.

[50] S. Wu. *J. Polym. Sci. Polym. B Phys. Ed.*, 25(12):2511–2529, 1987.

[51] S. D. Hudson, A. J. Lovinger, R. G. Larson, D. D. Davis, R. O. Garay, and K. Fujishiro. *Macromolecules*, 26:5643–5650, 1993.

[52] J. H. Rosedale and F. S. Bates. *Macromolecules*, 23:2329, 1990.

[53] K. I. Winey, S. S. Patel, R. G. Larson, and H. Watanabe. *Macromolecules*, 26:2542–2549, 1993.

[54] L. J. Fetters, D. J. Lohse, D. Richter, T. A. Witten, and A. Zirkel. *Macromolecules*, 27(17):4639, 1994.

[55] S. Gotz, W. Stille, and G. Strobl. *Macromolecules*, 26:1520–1528, 1993.

[56] R. G. Kirste and H. G. Ohm. *Makromol. Chem., Rapid Commun.*, 6:179, 1985.

[57] M. Warner, P. Bladon, and E. M. Terentjev. *J. Phys. II France*, 4:93, 1994.

[58] G. J. Kruger, H. Spiesecke, R. Van Steenwinkel, and F. Noack. *Mol. Cryst. Liq. Cryst.*, 40:103, 1977.

[59] E. Hall, C. K. Ober, E. J. Kramer, R. H. Colby, and J. R. Gillmor. *Macromolecules*, 26(15):3764–3771, 1993.

[60] A. Keller, E. Pedemonte, and F. M. Willmouth. *Nature*, 225:538, 1970.

[61] C. Boeffel and H. W. Spiess. *Macromolecules*, 21:1626, 1988.

[62] R. Zentel and M. Benalia. *Makrom. Chem.*, 188:665, 1987.

[63] J. Schatzle and H. Finkelmann. *Mol. Cryst. Liq. Cryst*, 142:85, 1987.

[64] R. G. Larson and D. W. Mead. *Liquid Crystals*, 15:151, 1993.

[65] V. G. Taratuta, A. J. Hurd, and R. B. Meyer. *Phys. Rev. Lett.*, 55:246, 1985.

[66] G. Hadziioannou, A. Mathis, and A. Skoulious. *Colloid Polym. Sci.*, 257:136, 1979.

[67] S. G. Hatzikiriakos and J. M. Dealy. *J. Rheology*, 35:497, 1991.

[68] D. S. Pearson and W. E. Rochefort. *J. Poly. Sci., Poly. Phys.*, 20:83, 1982.

[69] S. G. Hatzikiriakos and J. M. Dealy. *J. Rheology*, 36:845, 1992.

[70] Y-L. Chen, R. G. Larson, and S. S. Patel. *Rheologica Acta*, 33(4):243, 1994.

[71] V. J. Meissner. *Rheologica Acta*, 10:230, 1971.

[72] H. Munstedt and H. M. Laun. *Rheologica Acta*, 20:211, 1981.

[73] T. S. Wilson and D. G. Baird. *J. Non-newton. fluid mech.*, 44:85, 1992.

[74] A. F. Martins, P. Esnault, and F. Volino. *Phys. Rev. Lett.*, 57:1745, 1986.

[75] P. Esnault, F. Volino, A. F. Martins, S. Kumar, and A. Blumstein. *Mol. Cryst. Liq. Cryst.*, 153:143, 1987.

[76] J. P. Casquilho, P. Esnault, F. Volino, M. Mauzac, and H. Richard. *Mol. Cryst. Liq. Cryst. B*, 180:343, 1990.

[77] J. P. Casquilho and F. Volino. *Mol. Cryst. Liq. Cryst. B*, 180:357, 1990.

[78] H. Roth. *Liq. Cryst.*, 11:31, 1992.

[79] E. Hild, A. Kocot, J. K. Vij, and R. Zentel. *Liq. Cryst.*, 16:783, 1994.

[80] M. Winkler, D. Geschke, and P. Holstein. *Liq. Cryst.*, 17:283, 1994.

[81] D. van der Putten, N. Schwenk, and H. W. Spiess. *Liq. Cryst.*, 4:341, 1989.

[82] K. Fuhrmann, Th. Dries, E.W. Fischer, and M. Ballauff. *J. Poly. Sci.: B: Poly. Phys.*, 30:1199, 1992.

[83] A. S. Cherodian, N. J. Hughes, R. M. Richardson, M. S. K. Lee, and G. W. Gray. *Liq. Cryst.*, 14:1667, 1993.

[84] H. Kresse, E. Tennnstedt, and R. Zentel. *Makromol. Chem. Rapid Commun.*, 6:201, 1985.

[85] R. Zentel, G. R. Strobl, and H. Ringsdorf. *Macromolecules*, 18:960, 1985.

[86] F. Z. Bormuth and W. Haase. *Mol. Cryst. Liq. Cryst.*, 153:207, 1987.

[87] R. V. Talroze, S. G. Kostromin, V. P. Shibaev, N. A. Plate, H. Kresse, K. Saher, and D. Demus. *Makrom. Chem., Rapid Commun.*, 2:305, 1981.

[88] H. Kresse, H. Stettin, E. Tennnstedt, and S. Kostromin. *Mol. Cryst. Liq. Cryst.*, 191:135, 1990.

[89] G. S. Attard, G. Williams, G. W. Gray, D. Lacey, and P. A. Gemmel. *Polymer*, 27:185, 1986.

[90] R. B. Findlay. *Mol. Cryst. Liq. Cryst.*, 231:137, 1993.

[91] R. V. Talroze and N. A. Plate. In N. A. Plate, editor, *Structural Transformations of Thermotropic Liquid-Crystal Polymers in Electric and Magnetic Fields.* Plenum Press, New York, 1993.

[92] L. M. Blinov, M. I. Barnik, and A. N. Trufanov. *Mol. Cryst. Liq. Cryst.*, 89:47, 1982.

[93] S. Wenhui, C. Shouxi, J. Yongze, and Q. Renyuan. *Liq. Cryst.*, 19:549, 1995.

[94] F. Lonberg, S. Fraden, A. J. Hurd, and R. B. Meyer. *Phys. Rev. Lett.*, 52:1903, 1984.

[95] C. H. Lin and K. Matyjaszewsky. *Polym. Prepr., Am. Chem. Soc., Div., Polym. Chem.*, 31:599, 1990.